POLITECNICO DI MILANO

DEPARTMENT OF CIVIL AND ENVIRONMENTAL ENGINEERING

SOURCE-RELATED VARIABILITY OF SEISMIC SITE AMPLIFICATION FUNCTION IN NORCIA, CENTRAL ITALY

A DISSERTATION SUBMITTED IN THE PARTIAL FULFILMENT OF REQUIREMENTS FOR MASTER DEGREE IN

CIVIL ENGINEERING

BY

MUHAMMAD SHAKEEL NAZIR

SUPERVISOR: PROF. CHIARA SMERZINI

CO SUPERVISOR: DR. MANUELA VANINI

ACADEMIC YEAR 2019-2020

Acknowledgements

I would like to thank to my supervisor Prof. Chiara Smerzini for providing me this opportunity to complete my thesis under her supervision and for helping me to understand methods and tools used in engineering seismology throughout my thesis work. I also appreciate the help provided by Dr. Manuela Vanini and would like to thank her for her efforts and time to answer my queries and helping me to improve my work.

The recent years at Politenico di Milano have been challenging for me and during this time my friends have been a firm support for me. I would like to thank to all of my local and foreign friends who helped me to live in a new culture and to bring a positive change in all aspects of my life. I am grateful to all of you for your emotional and moral support in my thick and thin and making me to feel at home while being away from home.

A huge credit and appreciation for my parents for their patience, devotion and efforts to keep me motivated towards my goals. I am very grateful to my mother for her unconditional love and countless prayers, to my father who has always been motivating me to achieve my ambitions and supported me in every matter of life and to my siblings who made me to laugh all the time.

At last I am very thankful to all of my teachers who played their part and helped me to improve my knowledge especially Prof. Muhammad Arshad who has been very supportive and helped me to choose best in academia.

Abstract

Study of site amplification caused by earthquake strong ground motion plays an important role in the seismic hazard analysis and risk assessment at regional scale. Standard one dimensional numerical methods available to quantify seismic site response are based on the assumption of vertical propagation of wave and horizontal stratigraphy of soil layers and therefore, neglects the irregular soil profile, buried topographies, 3D complex wave propagation in near source and effect of basin edges. Due to simplified assumptions of 1D numerical methods and to predict more realistic ground response 3D physics based numerical methods are being used however, these method are reliable only in the longer period range typically (above 0.75- 1s) due to posed computational constraints and insufficient knowledge of medium at shorter wavelengths.

In this work case study of Norcia basin effected by the seismic sequences of 2016 Central Italy is considered to illustrate source related spatial variability in site amplification function. To do this, results of 3D physics-based simulations produced by an open source high performance spectral element code called SPEED are used. The SPEED simulations were available for the mainshock M_w 6.5 of October 30, 2016 and for three hypothetical rupture scenarios, with variable magnitude and co-seismic slip distribution. To overcome the limitation associated with the numerical resolution of model and to predict the response spectral ordinates at short periods a novel approach based on trained Artificial Neural Networks (ANNs) is used and Broadband Simulations (BBs) through a MTALB routine were generated. BBs time histories were compared with the BASCO corrected strong ground motions records both in time and frequency domain to validate the reliability of BBs.

After validating BBs results with records spatial variability of Spectral Amplification Function (SAF) was analysed. First, SAF was analysed with respect to same site within the basin (Ideal) and then by considering reference bedrock sites (real) outside of basin for each earthquake scenario. Results point out that BBs prediction were found to have good agreement with the records in both time and frequency domain. Furthermore, some crucial aspects in selecting the reference rock site indicate that the 3D site amplification ratios are strongly affected by the variations in source rupture parameters.

Keywords: *Seismic site amplification, 3D physics-based numerical simulations, Broadband Simulations, Source related 3D site amplification*

Table of Content

List of Figures

List of Tables

1. Introduction

1.1. Background

A recent stat reports that, in the first fifteen years of the new millennium, earthquakes have been, on average, the cause of about fifty thousand deaths per year worldwide. When large scale seismic assessment analyses are carried out, one of the most critical issues concerns the evaluation of the amplification phenomena related to the local geological and geotechnical conditions (Brando et al., 2020). It has long been understood that the geotechnical characteristics of the uppermost soil layers can significantly modify the amplitude and the spectral content of the recorded ground motion induced by an earthquake. This effect is generally referred to as local site effect and it plays a fundamental role in determining the spatial variability of the seismic hazard for a given area (Bindi et al., 2011). As for Italian earthquakes site amplification effects has been recognized as one of the main causes of observed damages and to avoid these structural damages, casualties and an increasing pressure on the growth of economy caused by such catastrophes one should be prepared beforehand to tackle these hazards. Therefore, it is required to study recorded earthquake strong ground motion and extend these studies to the hypothetical scenarios of the most probable earthquakes and to determine scenario dependent spatial variability of amplification function in the study area.

Time domain Analyses in earthquake engineering requires input motions the selection of which is typically based on either artificial accelerograms or records from real earthquakes (Evangelista et al., 2017). Standard methods for hazard assessment, both in a probabilistic and deterministic framework, are based on the use of GMPEs and increasing number of real records contributed to expand research on ground-motion prediction equations (GMPEs) that is, the empirical models providing peak values of ground motion across the entire frequency band of engineering interest, as a function of magnitude, of suitable measures of source-to-site distance, and of site conditions. However, owing to simplicity GMPEs provide (1) only the peak or spectral values whereas the use of nonlinear time-history analyses requiring reliable input motions is becoming more and more relevant within many applications (2) empirical coefficients vary if calibration data set is changed (3) GMPEs considers only generic site conditions (i.e. average shear wave velocity V_{s30}) and (4) the pointwise prediction by GMPEs cannot reproduce the spatial correlation structure of the peak values of motion at multiple sites (Paolucci et al., 2018). On one hand real record are typically insufficient to represent large

magnitude crustal events in near-source conditions, especially if coupled with complex geological and morphological irregularities, as in the case of deep basins or hanging-wall effects while on the other hand artificial accelerograms are generated from a code specified response spectrum and driving signals compatible to that spectrum which may lead to accelerograms not reflecting the real phasing of seismic waves and cycles of motion due to which these methods has less applications.

To effectively cope with such limitations, physics-based source-to-site numerical simulations are becoming a third alternative to produce reliable input motions for earthquake engineering applications, which is worth of investigating (Evangelista *et al.* 2017). Such numerical simulations are based on physical models of the seismic source, the propagation path from the source to the site and local geologic irregularities, and allow one to investigate the dependence of spatial variability on factors, such as magnitude, wave propagation effects, local site conditions, for a variety of "virtual", albeit realistic, conditions (Infantino et al., 2018). SPEED (Spectral Elements in Elasto dynamic with Discontinuous Galerkin) is considered as one of the leading tool to perform 3D physics-based numerical simulations. SPEED is a certified numerical software (http://speed.mox.polimi.it) for 3D elastodynamics problems, that is specifically suited to study seismic wave propagation and dynamic soil-structure interaction problems in complex geological configurations. The code is jointly developed at MOX - Laboratory for Modelling and Scientific Computing of the Department of Mathematics and at the Department of Civil and Environmental Engineering of Politecnico di Milano. The SPEED kernel is based on a discontinuous version of the classical Spectral Element (SE) method, a non-conforming domain decomposition technique combining the flexibility of discontinuous Galerkin finite elements with the accuracy of spectral techniques (R. Paolucci et al., 2016). Deterministic approaches, like the spectral element method rely on the rigorous numerical solution of the seismic wave propagation problem and can provide synthetic ground motion time histories consistent with the 3D model of the seismic source, of the source-to-site propagation path and of local site response (Smerzini 2018). However, due to lack of detailed knowledge to construct a geological model with sufficient details also at short wavelengths, especially for complex configurations. As a result, accuracy achieved by PBS (Physics Based Simulation) is usually bounded up to 1–1.5 Hz. Broadband (BB) waveforms are generally produced by a hybrid (HYB) approach combining low-frequency results from deterministic PBS with high frequency signals from stochastic approaches, typically through either point- or finite-source methods however, these methods show a poor corelation between high frequency

stochastic and low frequency PBS wave form (Paolucci et al., 2018). In the present study a novel approach proposed by (Paolucci et al., 2018) is used to produce BB (Broadband) time histories which couples PBS with the ANN (Artificial Neural Network) predictions and helps to overcome limitations of standard hybrid approaches.

1.2. Scope of Work

The focus of the study presented herein is to evaluate the variability of local seismic site amplification depending on source features. Standard 1D or 2D ground response analysis neglects issues related to the dependency of site amplification on source for a specified soil model. Therefore, detailed 3D soil model with the possibility of introducing different source features plays an important role to overcome limitations associated with the 1D or 2D response analysis models. In this study case study of Norcia earthquake has been considered.

The Norcia earthquake of October 30, 2016 having magnitude M_w 6.5 occurred in the 10km long and 3km wide Norcia basin located in the central Apennin producing severe damage in several small towns including Amatrice, Norcia and Visso. The Norcia mainshock occurred less than 5 km NE from village of Norcia. as a result of upper crustal normal faulting on a nearly 30-km-long, NW-SE oriented and SW dipping fault system known as Mt. Vettore–Mt. Bove (VBFS) (Civico et al., 2019). In addition to real event of 30th October as stated above, three hypothetical scenarios of M_w 6.0, M_w6.5, M_w 5.5 having different hypocentre location and slip distribution were also considered. The PBS of real event of 30th October and hypothetical scenarios were generated by using SPEED in the previous studies while spatial variability of RSR (Response Spectral Ratio) with respect to source was studied in the current work.

Two types of analysis were performed in this study. First of all BB time histories were computed by using MATLAB routine and already trained neural networks for both basin and outcropping bedrock for a certain set of receiver points. Having BB simulations a comparison was made between BB simulated and BASCO corrected recorded time histories in terms of PGA, PGV and PGD for all the stations located in the Norcia. Furthermore, to assess the validity of the numerical model in the frequency domain analysis were performed in terms of FAS (Fourier Amplitude Spectra), RS (Response Spectra) and S_d (Spectra Displacement). In

addition to this spatial variability of peak ground response shake maps were generated by using GIS.

Secondly dependence of 3D ideal SAF (Spectral Amplification Function) on source, magnitude and spatial location will be quantified for the mainshock of October 30, 2016 and for three hypothetical scenarios of earthquake having different magnitude, slip distribution and hypocentre location named as Mw 6.0, M_w 5.5, M_w 6.5_S002 . In order to better understand variability in SAF two cross section named as EW and NS will be considered and variability of SAF for four different periods such as T=0sec, 0.5sec, 1sec and 2 sec will be analysed. In the end variability of SAF with respect to 7 reference bedrock sites will be analysed .

1.3. Organization of Thesis

Chapter 1 is of introduction and explains the need of conducting this study. It explains the vital importance of source related variability of site amplification function in earthquake risk assessment. In addition to this it also explains the available numerical solution to predict 3D site amplification function and their drawbacks and introduces a solution to overcome limitations of numerical methods. At the end of the chapter a brief explanation of the current study is given.

In Chapter 2 the case study of the Norcia Basin is discussed. A brief explanation of geological and tectonic settings of Norcia and of seismic history of the region is presented. It also allow one to understand the concept behind 3D physics-based simulations from the source-to-site (computer code: SPEED), which is the key tool for the simulation of the seismic wave propagation. In addition, the theory behind of a novel method, based on Artificial Neural Network (ANN), with the aim of producing broadband times histories is illustrated in the last section of this chapter.

Chapter 3 devoted to the step-by-step procedure for the construction of numerical models of Norcia basin and explains briefly the hypothetical scenarios and the simulations used in this study.

Chapter 4 provides a comparison between Broadband simulated (BBs) and recorded time histories mainly for the recording station NOR and NRC for the main event of magnitude M_w 6.5 occurred on October 30, 2016. Comparison has been made for the two horizontal (NS & EW), one vertical (Z) and geometric mean of their horizontal components (GMH) component for acceleration, velocity and displacement. Moreover, comparison has also been made

between BBs and recorded data in terms of Fourier Amplitude Spectra (FAS) and Response Spectra (RS). To observe spatial variability in BBs and recorded peak values of earthquake strong ground motion in the study area shake maps were generated by using GIS software (Geographic Information System).

Chapter 5 merely devoted to assess the spatial variability of spectral amplification functions. Two cross sections named as NS and EW were selected in the transversal and longitudinal directions respectively. Variability in 3D ideal SAF along the two cross sections was analysed by taking into consideration four different periods such as T= 0 sec, 0.5 sec, 1 sec and 2 sec for the mainshock of October 30, 2016 as well as for other three hypothetical scenarios of magnitude M_w6.5_S002, M_w 5.5, M_w 6.0. These hypothetical scenarios differ in location of source, magnitude and slip distribution. 3D ideal SAFs have also been analysed for selected receivers along the two cross sections however, only four receivers have been analysed. In the end of this chapter dependency of SAF on the reference bedrock site for all the earthquake scenarios is given and results are compared in terms of their EW, NS, Z and GHM components.

Chapter 6 briefly explains the outcomes of analysis and highlights the concluding remarks about the most relevant aspects of the study.

2. The Case Study: The Norcia Basin, Central Italy

2.1. The Seismic Sequence of central Italy

The 2016 Central Italy seismic sequence consists of a series of moderate-to-large earthquakes which were started in second half of the August and ended in the end of October along a 60-km-long and Apennine normal-fault system. The 10km long and 3km wide Norcia basin located in the central Apennines represents the typical Plio- Quaternary intermontane basins formed during the Apennine chain uplift (Bindi et al., 2011). The tectonic evolution of Norcia basin has been driven by the main fault located along the mountain slope present in the east of the basin. The current seismic sequence of central Italy started in the second half of August 2016 having M_w 6.5 with no previous history of foreshocks. This first main shock having a relatively shallow hypo central depth (around 8Km) was located near the towns of Accumoli and Amatrice resulted in clear horizontal and vertical offset along the Mt. Vettore normal fault outcrop, 299 casualties and considerable damage to the structures in the surrounding region. Subsequently, on October 26, 2016 another mainshock of M_w 6.0 located at 25Km to the north near the town of Visso was observed.

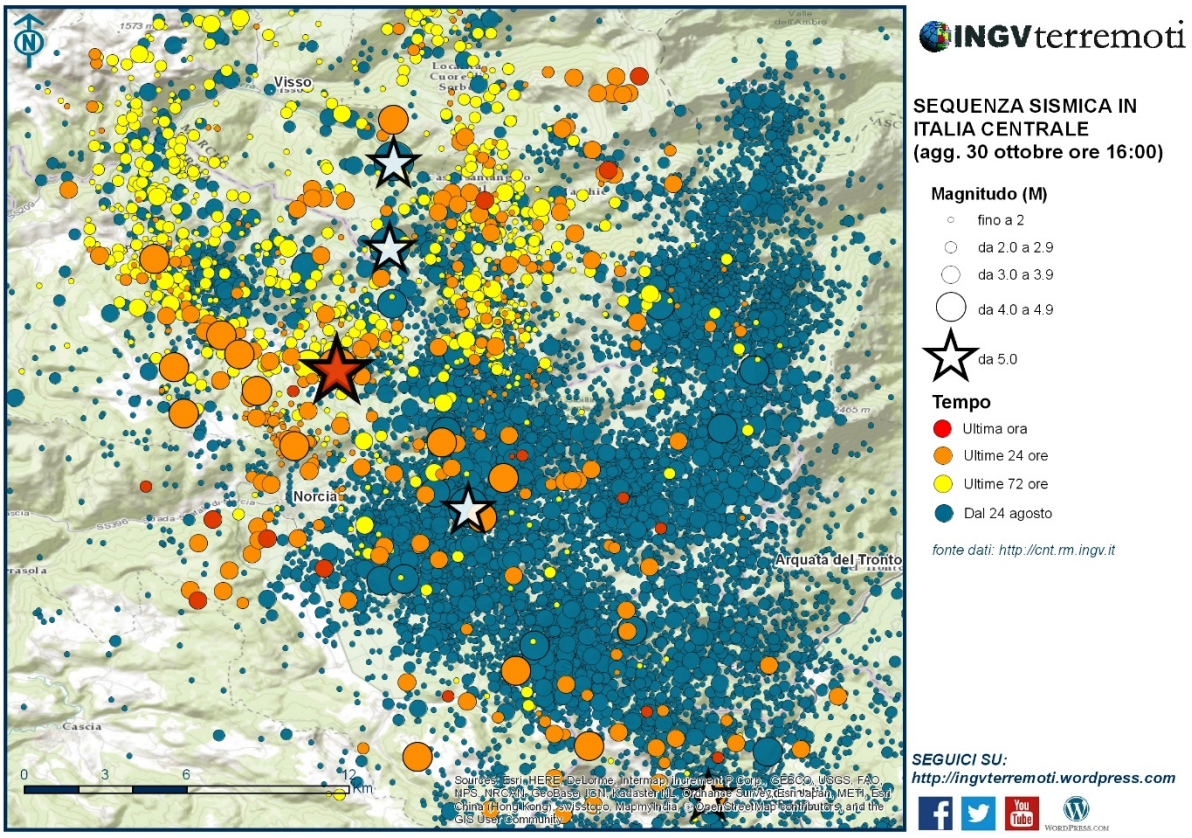

Figure 2-1 Central Italy seismic sequence: Shock distribution Map updated on the 30 October 2016
Source (http://ingvterremoti.wordpress.com/)

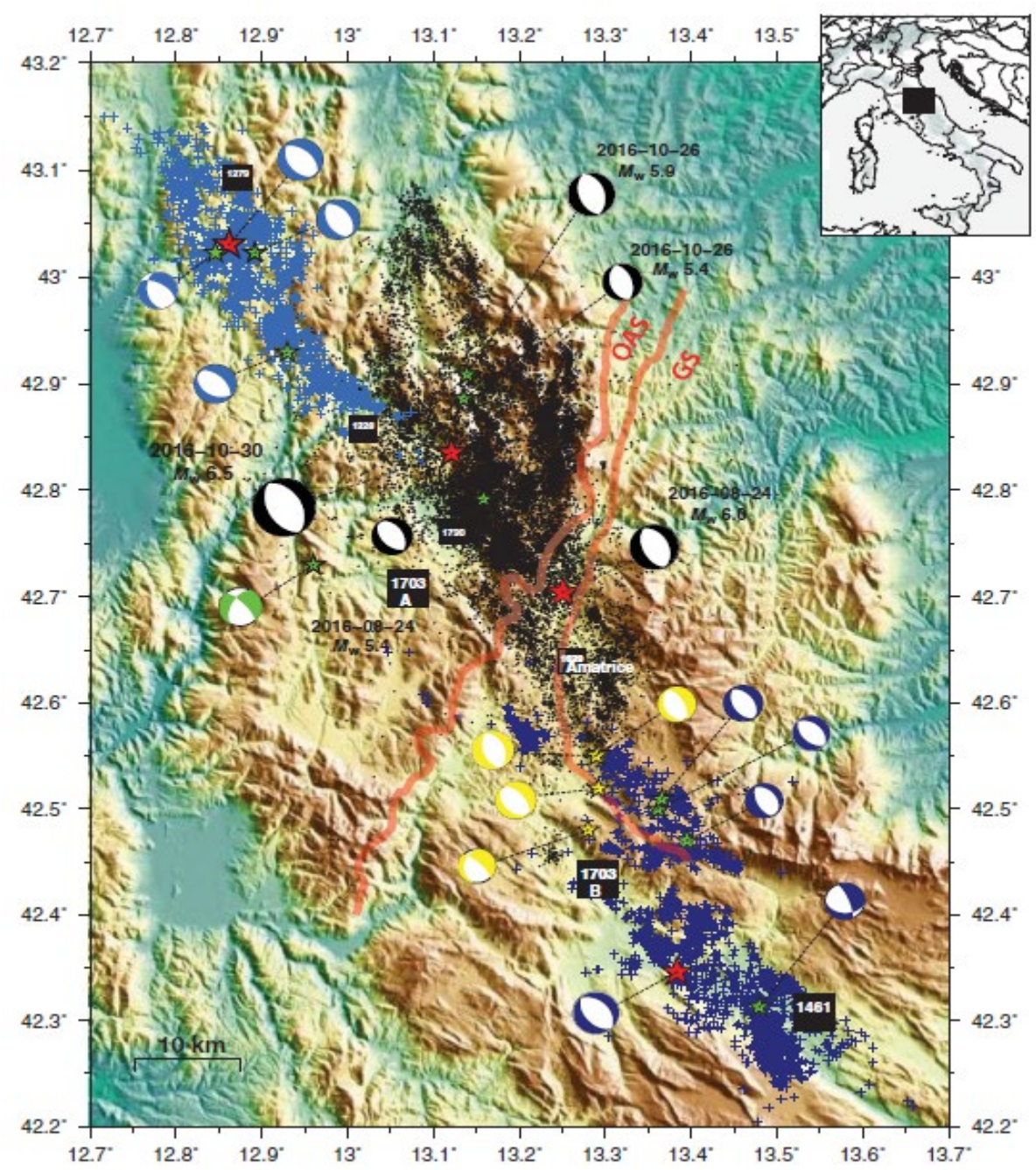

Figure 2-2 Map of the study area. Light blue crosses, Colfiorito seismic sequence earthquakes; dark blue crosses, L'Aquila seismic sequence earthquakes; and black dots, Amatrice–Visso–Norcia seismic sequence earthquakes. For each sequence, green stars, events with Mw ≥5:0; red stars, events with Mw ≥ 6:0; and focal mechanism symbols represent focal mechanisms of the events with Mw ≥ 5:0. Black squares report historical earthquakes. Red lines represent thrust front traces (modified after Centamore and Rossi, 2009) of GS (Gran Sasso) and OAS (Olevano-Antrodoco-Sibillini) thrust fronts. The yellow stars and associated focal mechanisms are related to the four events with 5:0 ≤ML ≤5:5 that occurred on 18 January 2017. Source:(Chiaraluce L et al., 2017) .

This seismic sequences with a major mainshock of magnitude of M_w 6.5 occurred on October 30,2016 located in between the area of previous two events which resulted in the catastrophic damage in Norcia and in the surrounding towns. This catastrophic event was triggered at the depth of around 8Km and was the largest event in the region since the 1980 M_w 6.9 Irpinia

earthquake. Furthermore, this event nucleated at a shallow depth which resulted in the generating of new and larger ruptures at the surface, sometimes exceeding those activated by the first M_w 6.0 shock. This indicates that the event occurred on the same fault system presently reaching about 60 km in length, and a clear overlap with the southern termination of the 1997 seismic sequence faults (Figure 2-1) is observed.

2.2. Geological and Tectonic Settings of Norcia Basin

The continental Norcia basin is located in the inner sector of the Umbria–Marche Apennines The geological setting of this area is particularly complicated by the superimposition of several tectonic events. In particular, the first compressional phases occurred during the late Miocene and involved the Mesozoic and Cenozoic sequence, mainly composed by limestones and marly limestones belonging to the Umbria–Marche pelagic sequence moreover, Norcia basin is a typical intramountainous basin with almost a rectangular shape, having length of 10 km long and width of 4 km, and filled by Quaternary fluvio-lacustrine sediments (Pierantoni et al., 2013). The difference in altitude between the basin and the surrounding reliefs ranges from 600 to 1000 m, due to the activity of the normal faults that control its evolution (Messina et al., 2002). Just like other Apennine tectonic depressions, the formation and the tectonic evolution of Nb has been driven by important Quaternary extensional faults. Due to scarce incision of the basin a few outcrops of deposits are visible in the field. The main deposits are characterized by gravels belonging of uplifted and faulted alluvial fans, outcropping the northern sector, topped by alluvial terraces.

Additional information on subsoil can be obtained from a down-hole test (DH), performed in the eastern part of the plain (Bindi et al., 2011), close to the Norcia city centre and from the recent micro zonation studies (MZS Norcia, 2018). The velocity profile of the DH shows a clear inversion of Vs with depth, from 700 m/s in the uppermost 48 m to 500 m/s down to 60 m. The first layer corresponds to the cemented deposits of the alluvial fan, as outcropped in the NE part of Nb, which overlay the silts and clays of the lacustrine deposits never outcropped in the basin. A recent geological survey in Norcia basin showed that the main deposits are characterized by faulted and uplifted cemented gravels in the northern-eastern sector of the basin, representing the oldest deposits. A map of geological survey done by (Di Giulio et al., 2020) is given in the Figure 2-3.

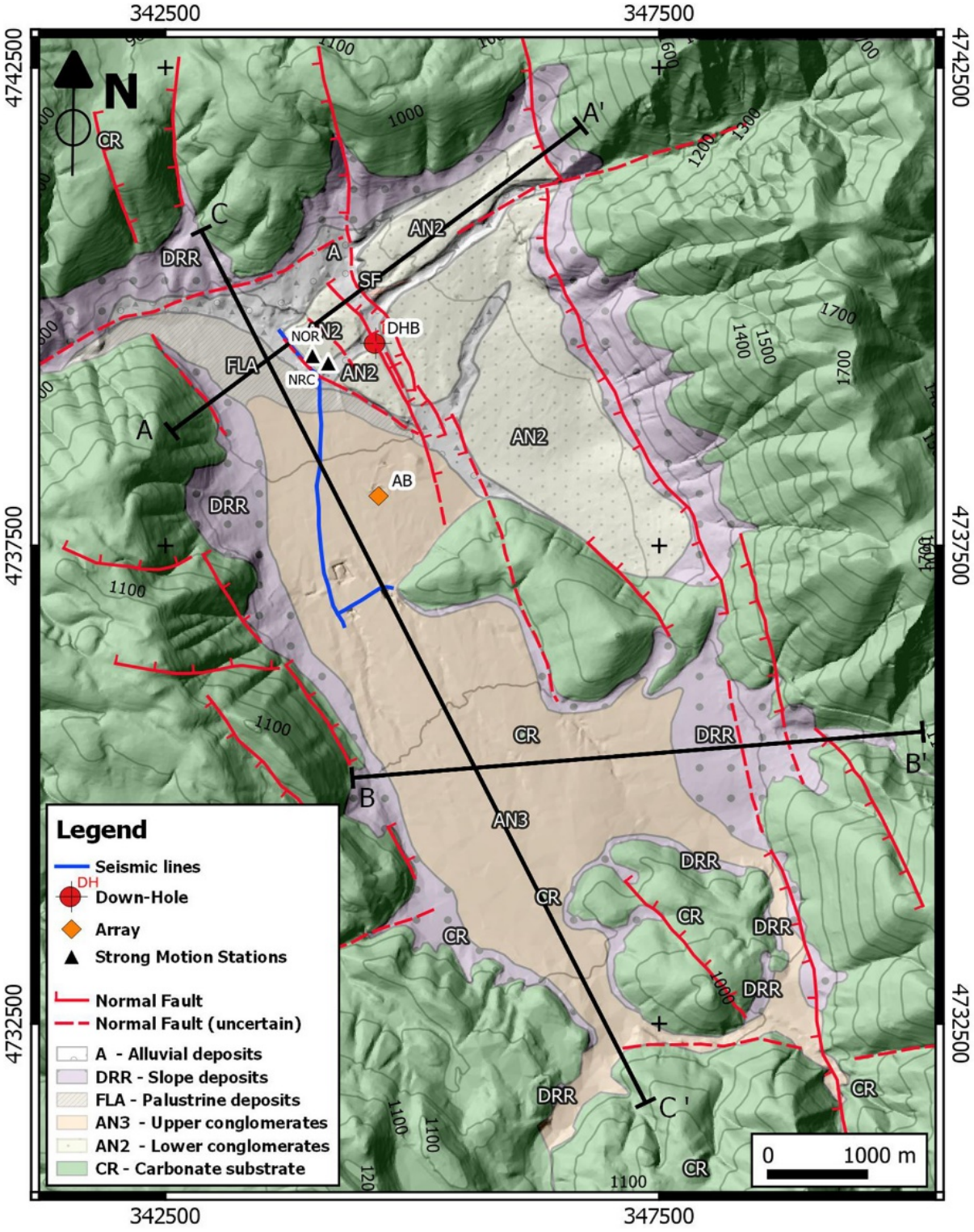

Figure 2-3 Geological Map of Norcia Basin

2.3. 3D Physics Based Simulation and Generation of Broadband

Physics-based numerical modelling of the seismic response of arbitrarily complex earth media has gained major relevance in recent years, owing, on one side, to the ever-increasing progress

in computational algorithms and resources, and, on the other side, to the growing interest towards the development of deterministic scenarios as input within seismic hazard and risk assessment studies. In the last 20 years there has been an impressive progress worldwide towards the development of high-order numerical methods for the simulation of seismic wave propagation under realistic tectonic and geomorphological conditions.

Typically, PBSs are based either on a kinematic description of the coseismic slip distribution model or on a spontaneous dynamic rupture process. They provide a realistic level of complexity of the generated seismic wavefield and enhance its frequency content within physical constraints from seismological observations. However, due to lack of detailed knowledge to construct a geological model with sufficient details also at short wavelengths, especially for complex configurations. As a result, accuracy achieved by PBS (Physics Based Simulation) is usually bounded up to 1–1.5 Hz. To overcome this limit Broadband (BB) waveforms are generally produced by using a hybrid (HYB) approach combining low-frequency results from deterministic PBS with high frequency signals from stochastic approaches, typically through either point- or finite-source methods however, these methods show a poor corelation between high frequency stochastic and low frequency PBS wave form (Paolucci *et al.* 2017).

A novel approach proposed by (Paolucci et al., 2018) is used to produce BB (Broadband) time histories which couples PBS with the ANN (Artificial Neural Network) predictions and helps to overcome limitations of standard hybrid approaches. The 3D PBS are obtained from a spectral element code called SPEED (SPectral Elements in Elastodynamics with Discontinuous Galerkin). The main steps involved to obtain Broadband time histories from 3D PBS simulations by using ANN (Artificial Neural Networks) can be briefed as follows and will be explained in the upcoming section of ANN2BB procedures.

i. Generation of Earthquake Scenario
ii. Training of an ANN
iii. Computation of Response Spectral Ordinates
iv. Frequency Enrichment
v. Initiation of an Iterative Procedure

2.3.1. 3D Physics Based Simulation (PBS)

In the framework of the joint research activity between Politecnico di Milano and re-insurance industry Munich RE, the SPEED[1] code (SPectral Elements in Elastodynamics with Discontinuous Galerkin) was developed by the Department of Mathematics and the Department of Civil and Environmental Engineering of Politenico di Milano, as an open-source numerical code suitable to address the general problem of elastodynamics in arbitrarily complex media (Mazzieri et al. 2013).

SPEED is designed for the simulation of large-scale seismic wave propagation problems including the coupled effects of a seismic fault rupture, the propagation path through Earth's layers, localized geological irregularities such as alluvial basins and topographic irregularities. Some examples of applications with the additional presence of extended structures, such as railway viaducts, can be found in the SPEED web site. (Paolucci et al, 2014; Paolucci et al. 2018)

Treating numerical problems with such a wide range of spatial dimensions is allowed by a non-conforming mesh strategy implemented through a Discontinuous Galerkin (DG) approach (Antonietti et al. 2012). Numerical Algorithm can be briefed in the following steps:

- Selection of an heterogeneous 3D medium
- Discretization of computational domain by keeping in consideration the structure and material involved.
- Discretization of spectral element in each sub domain
- Enforcement of continuity of numerical at the interface by considering DG algorithm which defined a penalty function for jumps in displacement (De Basabe et al. 2008).

SPEED permits one to use non-conforming meshes (h-adaptivity) and different polynomial approximation degrees (N-adaptivity) in the numerical model. This makes mesh design more flexible (since grid elements do not have to match across interfaces) and permits to select the best-fitted discretization parameters in each subdomain, while controlling the overall accuracy of the approximation.

Particularly the numerical mesh may consist of smaller elements and low-order polynomials where wave speeds are slowest, and larger elements and of high-order polynomial where wave speed is relatively high. Moreover, since the DG approach is applied only at a subdomain level, the complexity of the numerical model and the computational cost can be kept under control,

avoiding the proliferation of unknowns, a drawback that is typical of classical DG discretizations (Paolucci et al. 2014).

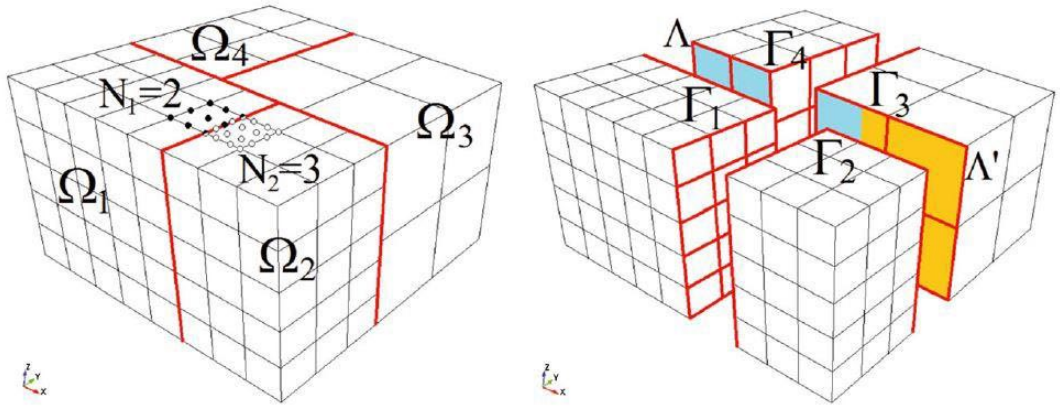

Figure 2-4 3D example of non-conforming domain decomposition. The whole domain is composed of different non-overlapping polygonal subdomains, made by hexahedral elements.Discontinuous Galerkin discretization allows to deal with a nonuniform polynomial degree distribution (N_adaptivity, e.g., N1 = 2 in Ω1 and N2 = 3 in Ω2), as well as a locally varying mesh size (h_adaptivity between subdomains Ω1, Ω2, Ω3 and Ω4). The surface between two neighboring subdomains Ωk and Ωi , then may not be a complete side of Ωk or Ωi (e.g., Λ and Λ').(Mazzieri et.al 2013)

2.3.2. Training of an ANN (Artificial Neural Network) Model

ANNs are generally used to estimate the nonlinear relationship between a highly populated vector of input variables and a vector of output unknowns, for the correlation of which fast- and closed-form rules cannot easily be applied. In fact, under mild mathematical conditions, any problem involving a continuous mapping between vector spaces can be approximated to arbitrary precision (i.e., within an error tolerance) by feed-forward ANNS, which are the most often used type (Cybenko, 1989). The purpose of the use of Artificial neural networks (ANN) here in is to relate between long period spectral ordinates selected for $T \geq T^*$, being T^* the threshold period corresponding to the range of validity of PBS, with short period spectral response ordinates for $T < T^*$. The main steps involving ANN2BB conversion are as follow:

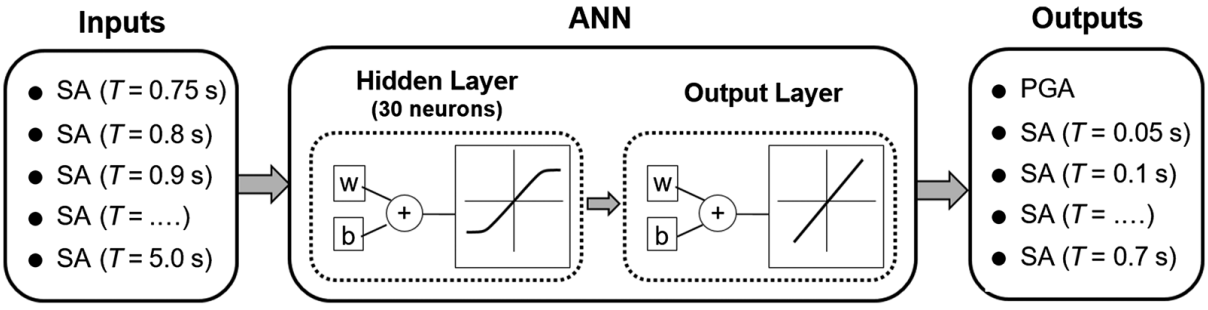

Figure 2-5 Logic scheme of the ANN training patterns: the long-period spectral ordinates (in this case T= 0:75 s) represent the teaching inputs, whereas the short-period ones are the outputs predicted by the ANN.

A high-quality strong ground motion dataset (denoted in the following by SIMBAD was used for training. SIMBAD consists. The SIMBAD database (Selected Input Motions for displacement-Based Assessment and Design) was created by assembling records from different strong ground motion databases worldwide, with the main objective of providing records of engineering relevance for the earthquakes, at epicentral distance Repi approximately less than 35 km, with moment magnitude, MW, ranging from 5 to 7.3, were considered. These are the conditions generally governing seismic hazard throughout Italy, for most return periods of practical interest. For the scope of this study, the selected records should be accurate at long periods. In fact, most records (about 90%) included in the database are from digital instruments, while a limited number of analog records was retained, typically from large magnitude earthquakes, for which a good signal to noise ratio at long periods could be achieved. In general, raw acceleration time histories were processed according to the procedure devised by Paolucci et al. (2011) and applied to the Italian Accelerometric Archive (ITACA, http://itaca.mi.ingv.it). One of the features of the aforementioned procedure is that single and double integration of processed acceleration records provides velocity and displacement waveforms without non-physical baseline trends, and no further correction is required. For each record, the same filter band was selected and applied to the three spatial components. Except for a few exceptions, records were included in SIMBAD only if the high-pass filter frequency was not larger than 0.15 Hz (Smerzini et al., 2014).

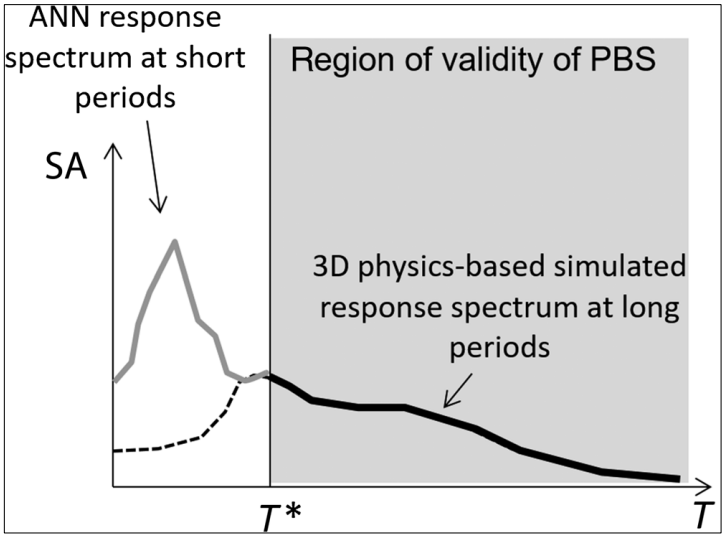

Figure 2-6 Sketch illustrating the idea behind the proposed Artificial Neural Network (ANN)-based approach to generate broadband (BB) ground motions: for a given ground motion, response spectral ordinates at short periods, that is, for periods $T \leq T^*$, in which T^* is the minimum period of validity of the physics-based numerical model, are computed from the 3D physics-based simulated response spectral ordinates at long periods. SA, spectral acceleration; PBS, physics-based numerical simulation.

2.3.3. ANN to Broad Band Procedure

A summary of steps involved in the ANN2BB procedures are given in the Figure 2-7.

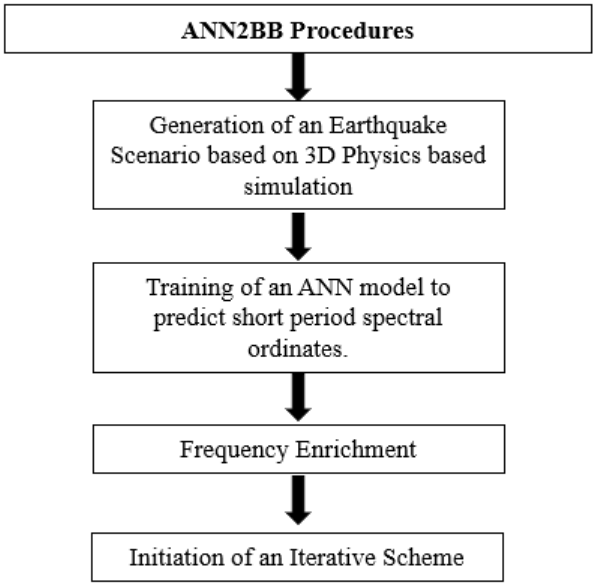

Figure 2-7 Summary of ANN2BB Procedures

2.3.3.1. Generation of Earthquake Scenario

An earthquake ground-motion scenario is produced based on 3D PBS, for which the accuracy in terms of response spectral ordinates is limited to $T \geq T^*$, owing to mesh discretization issues as well as to limited information on the geological models.

2.3.3.2. Training of an ANN

This has been explained in the section 2.3.2. An ANN is trained based on a strong-motion record data-set to predict short-period spectral ordinates ($T<T^*$) based on long-period ones ($T \geq T^*$). Different ANNs may be trained for different values of T^*, related to the frequency resolution of the numerical model (in this application, $T^*= 0{:}75$ s is considered). This allows one to compute, for all PBSs with range of validity $T > T^*$, a site-specific ANN-based BB response spectrum ANN2BB as well as maps of peak values of short-period ground motion. Whereas, for $T<T^*$, they are obtained from the ANN. Both horizontal and vertical components can be obtained, although with a lower level of accuracy for the vertical case. At this stage, such BB response spectrum ($T<T^*$) does not correspond to a specific waveform. The corresponding spectral ordinates, for $T \geq T^*$, coincide with the simulated ones,

2.3.3.3. Frequency Enrichment

The simulated low-frequency waveform is enriched in the high-frequency waveform by a stochastic contribution, characterized by the magnitude and source-to-site distance of the scenario earthquake under consideration.

2.3.3.4. Initiation of Iterative Scheme

The HYB PBS stochastic waveform (STO) is iteratively modified in the frequency domain, with no phase change, until its response spectrum matches the target ANN2BB spectrum.

In order to obtain BB time histories from the ANN2BB spectra, a spectral matching approach is used, similar to those adopted in the engineering practice to adapt a real accelerogram to a prescribed target spectrum in which the record is iteratively scaled either in the frequency domain or by wavelet trans-forms with no phase change, until its response spectrum approaches the target within a given tolerance. In our case, instead of a recorded accelerogram, we consider the time history resulting from the PBS and, as a target, the ANN2BB spectrum. In this work, the scaling in the frequency domain is performed, but other spectral matching procedures can obviously be used.

The difficulty, with respect to the standard spectral matching approach, comes from the low-frequency band-limited nature of the simulated time history, which implies that the high-frequency content of the waveform, essentially consisting of numerical noise, is not usable for scaling. To overcome this issue, before spectral matching to the desired target ANN2BB spectrum, the high-frequency portion of the simulated waveform was enriched by a stochastic component, by gluing the low- and high-frequency parts with the procedure described in Smerzini and Villani (2012). For high-frequency signals, they successfully tested both the Sabetta and Pugliese (1996) and the Boore (2003) approaches, the latter implemented in the code EXSIM (Motazedian and Atkinson, 2005), and selected the result providing the best fit to the target ANN2BB spectrum. Because spectral matching is achieved by scaling only amplitudes, the high-frequency random phases generated in the HYB step are maintained.

3. Numerical Model for Seismic Response in Norcia

Once that the topographical, geotechnical and geological information are collected, the 3D geological model can be constructed combining: (a) the digital elevation (and, if needed, bathymetry) model; (b) the crustal structure generally described in form of a layered model of S and P wave velocity, V_S and V_P, and (c) the local shallow geological structure with a model of V_S and V_P variable both in the horizontal and vertical direction, and possibly including the corresponding models for internal soil damping and local variation of shear modulus and damping as a function of shear strain (or, in 3D, of the second invariant of the strain tensor). Such a model is then combined with the source one based on seismotectonic knowledge (INFANTINO et al., 2018).

The 3D numerical simulations for the event of October 30, 2016 of magnitude M_w 6.5 need as input two basic information which are as follow;

i. 3D Depth-Velocity Model

ii. Kinematic Source Model

- Definition of the kinematic slip distribution along the causative fault
- Definition of crustal velocity model

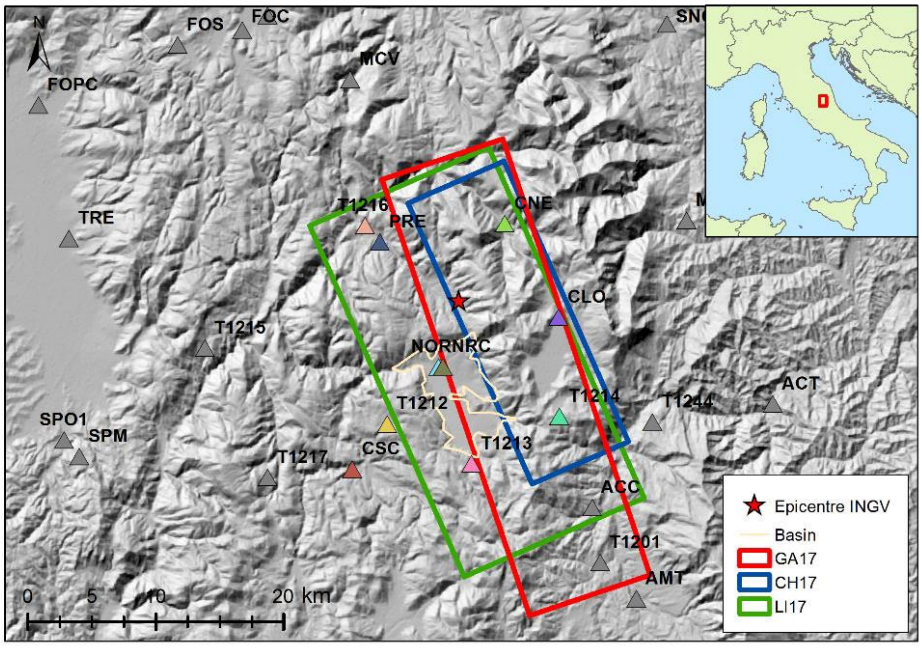

Figure 3-1 Comparison between the fault geometry solution of Gallovic (GA17, from Pizzi et al. 2018), Liu et al. (2017, LI17) and Chiaraluce et al. (2017, CH17)

An accurate depiction of the seismic source is essential for the numerical prediction of reliable strong ground motions in the vicinity of faults. Initial fault plane solutions for the event mainshock of M_w 6.5 occurred on October 30, 2016 were consistent with predominantly normal faulting mechanisms striking northwest–southeast.

i. 3D Depth- Velocity Model

3D depth-velocity model of Norcia basin is constructed by assembling 9 cross-sections obtained through geological and geophysical methods (i.e. 2 seismic reflection sections from Böhm et al., 2011; 5 gravimetric profiles from Aringoli et al., 2014; 2 geologic sections from Motti, 2017), 83 H/V tests at various locations (i.e. 48 from Angeletti et al., 2018; 20 from Porreca et al., 2018; 15 from Bindi et al., 2011), 42 Vs-depth profiles (i.e. 39 from Angeletti et al., 2018; 2 from INGV-Milano; 1 from Bindi et al., 2011), 3 VP-depth profiles (i.e. 2 from Angeletti et al., 2018; 1 from Bindi et al., 2011), 3 boreholes associated with SPT measurements (i.e. all from Angeletti et al., 2018), and 4 boreholes associated with geotechnical laboratory tests (i.e. all from Venanti et al., 2018). After the proper harmonization of the data, a single idealized VS-depth model is generated for whole basin and by using the idealized VS-depth relation, 3D sediment thickness model is generated by making use of the spatial interpolation schemes of MATLAB 2016b (Özcebe et al., 2019).

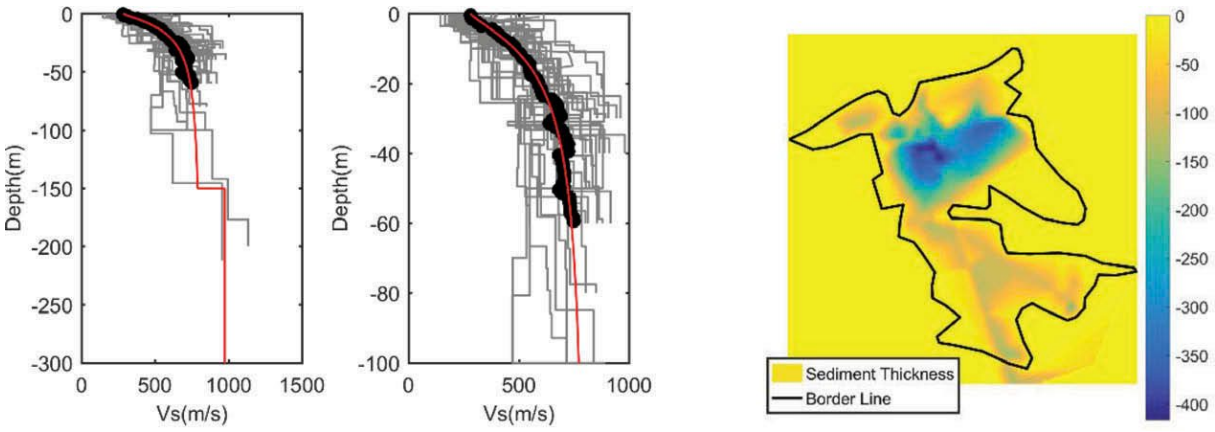

Figure 3-2 Idealized mathematical model of Norcia basin. Left: Shear-wave velocity (in m/s)-depth (in m) relation. Right: sediment elevation from ground surface (in m) *(*Özcebe et al., 2019).

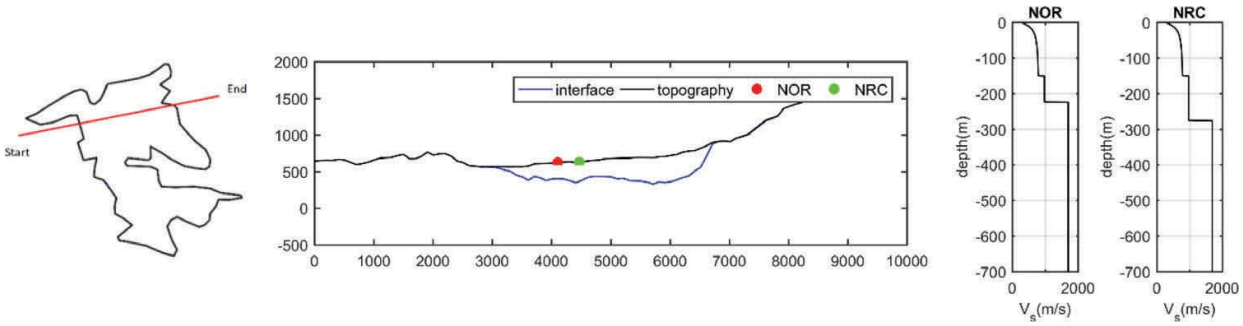

Figure 3-3 Left: Choosen section that crosses the northern Norcia basin and passes nearby two seismic stations (NOR and NRC). Center: Combined topography and depth of basin for the extracted section. Right: VS-depth plots for NRC and NOR. All length units are in meters (Özcebe et al., 2019).

A 2D finite difference model created for chosen cross section Figure 3-3. It has an angle (CCW) of 12.66° with E-W direction.

ii. Kinematic Source Model

Results of three published fault inversion studies (i.e. Chiaraluce et al., 2017; Liu et al., 2017; Pizzi et al., 2018) as given in Figure 3-1 compared through preliminary analyses using the analytical method proposed by Hisada and Bielak (2003), based on the asymptotic integration of dynamic Green's functions in a linear viscoelastic layered half-space showed that the best agreement between the observations and simulations is obtained through the choice of the source slip distribution model proposed by Pizzi et al. (2018), together with the corresponding hypo central location and fault geometry. The remaining parameters are calibrated through series of sensitivity analyses carried out using the codes of SPEED and Hisada (Özcebe et al., 2019). Parameters considered to be used in SPEED code for the crustal model defined according to Pizzi et al. (2017) are reported in Table 3-1.

Table 3-1 z: thickness, ρ: density, VS: shear wave velocity, QS: quality factor for S-waves, VP: P-wave velocity, QP: quality factor for P-waves

z (> $z_P^{(i)}$) (m)	ρ (kg/m^3)	V_S (m/s)	Q_S	V_P (m/s)	Q_P	Damping Type
-1000	2500	1700	200	3160	400	freq-prop
-2000	2840	2600	200	4830	400	freq-prop
-5000	2940	3100	200	5760	400	freq-prop
-21000 (Model Base)	3150	3500	200	6510	400	freq-prop

The numerical model of the Norcia basin expands over an area of 40×50×21 km3, having more than 350,000 spectral elements of 3rd order and is capable of propagating seismic waves up to maximum frequency of 1.5 Hz.

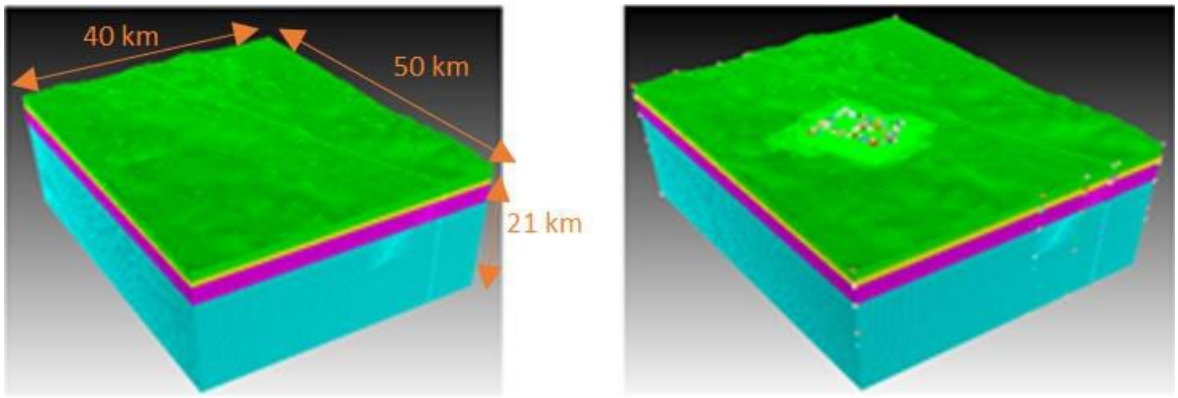

Figure 3-4 3D Numerical Model of Norcia
Left: Out cropping bedrock Right: Out cropping bedrock and Basin

Basin model considers nonlinear viscoelastic response of the shear wave velocity model, discussed based on the material degradation. Material nonlinearity of the basin material has taken into account by fitting a modulus degradation and damping curves.

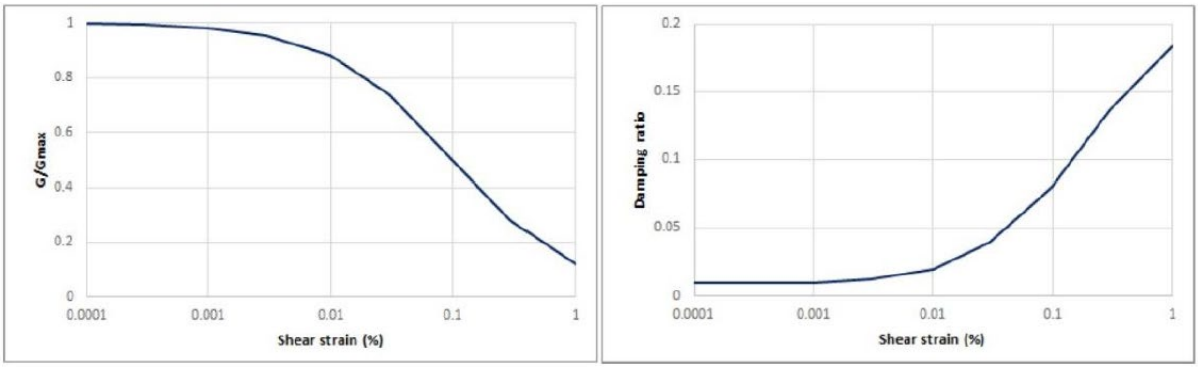

Figure 3-5 Left: Modulus degradation Curve Right: Damping Ratio

The model for Norcia basin and the information regarding concerning input data have been taken from the previous studies conducted by a student of Civil Engineering in his master thesis at Politecnico di Milano, Italy.

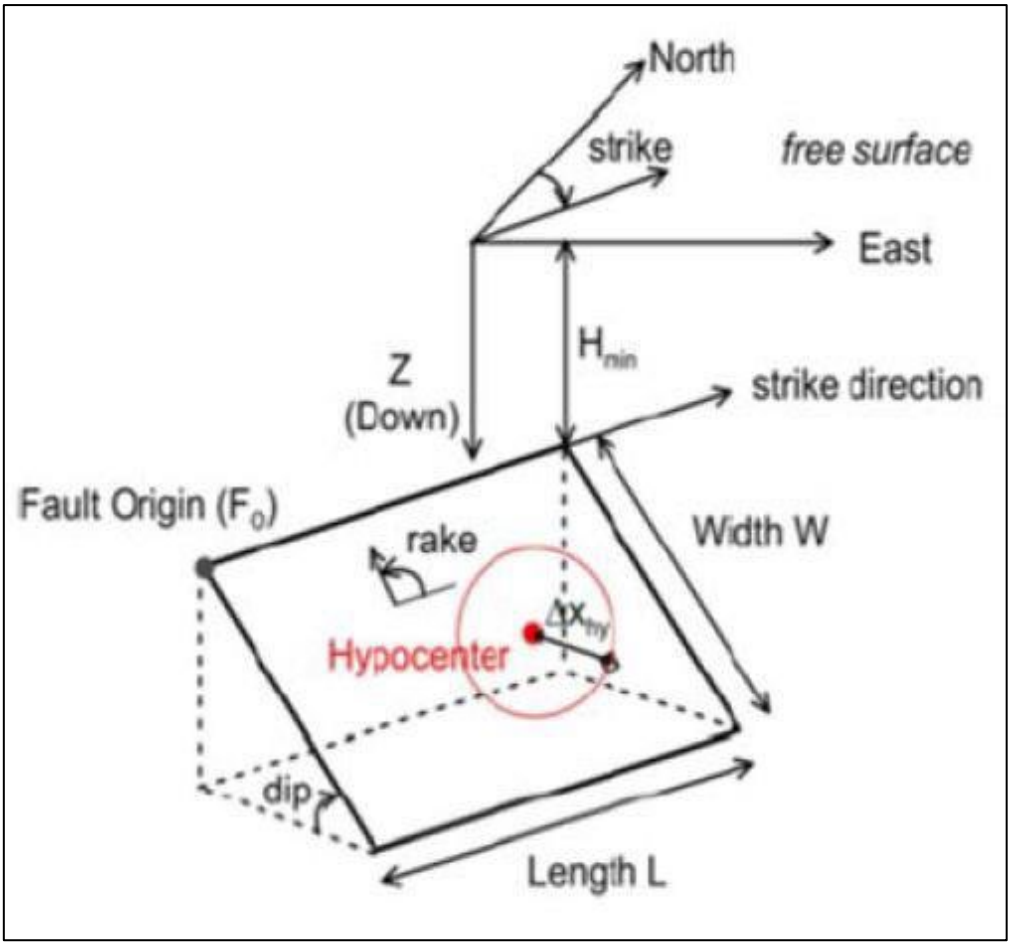

Figure 3-6 Fault Geometry

In Table 3-2 information about hypocentre depth and magnitude is given along with other geological information. Figure 3-6 illustrates the geometry of fault and corresponding elements in a fault system. It is evident from the information reported in the Table 3-2 that all the earthquake scenarios have same strike, length , width rake and dip angle.

Table 3-2 Geometric Information of fault system in earthquake scenarios

Event	Magnitude (Mw)	Strike (^{0})	Dip (^{0})	Rake (^{0})	L_{max} (Km)	W_{max} (Km)	Epicentre [Lon;Lat]	Hyp Depth (Km)
30-10-2016	6.5	160	40	36	36	13	42.85;13.11	-7
Hypo.	6.5_S002	160	40	36	36	13	42.85;13.11	-7
Hypo.	6.0	160	40	36	36	13	2.76;13.15	-7.3
Hypo.	5.5	160	40	36	36	13	42.89;13.07	-8.4

3.1. Summary of Simulations

For each earthquake scenario simulations were performed for both basin and outcropping bedrock. A total of 4 earthquake scenarios, out of which 3 are hypothetical scenarios varying in magnitude, hypo central location and slip distribution and one is the main shock of M_w 6.5 occurred on October 30, 2016 is considered in this study. The three hypothetical scenarios are named as M_w 5.5_S001, M_w 6.0_S001 and M_w 6.5_S002, the former also referred to as M_w 5.5 and M_w 6.0 respectively. It is worth noting that the outcropping bedrock simulations were performed in order to have ideal rock material, and hence to estimate the amplification functions within the alluvial basin. The SAF (Spectral Amplification Function) computed by considering spectral response at a site in basin with respect to the same site but considering it as an ideal bed rock is named as 3D Ideal SAF while the SAF computed at a site in basin with respect to another site located at real bedrock is termed as real SAF here in after.

Table 3-3 Summary of simulated scenarios (Gallovic-based: Pizzi et al., 2017 – HB94: Herrero and Bernard et al., 1994)

Earthquake Scenario	**Magnitude (M_w_ ID)**	**Soil Model**	**V_{rup} (m/sec)**	**Rise Time τ (sec)**	**Source**
30-10-2016	6.5	OB[1]	1700	Randomized around 0.7	Gallovic Based
		Basin (NL[2])			
Hypothetical	6.5_S002	OB	1700	Randomized around 0.5	HB94
		Basin (NL)			
Hypothetical	6.0_S001	Basin (NL)	1700	Randomized around 0.5	HB94
		OB			
Hypothetical	5.5_S001	OB	1700	Randomized around 0.5	HB94
		Basin (NL*)			
1 :Outcropping Bedrock , 2: Non liner Elastic					

A summary of all the earthquake scenarios and the set of simulations performed are reported in the Table 3-3 while, effective fault area for all the scenarios along with the location of their hypocentre is reported in the

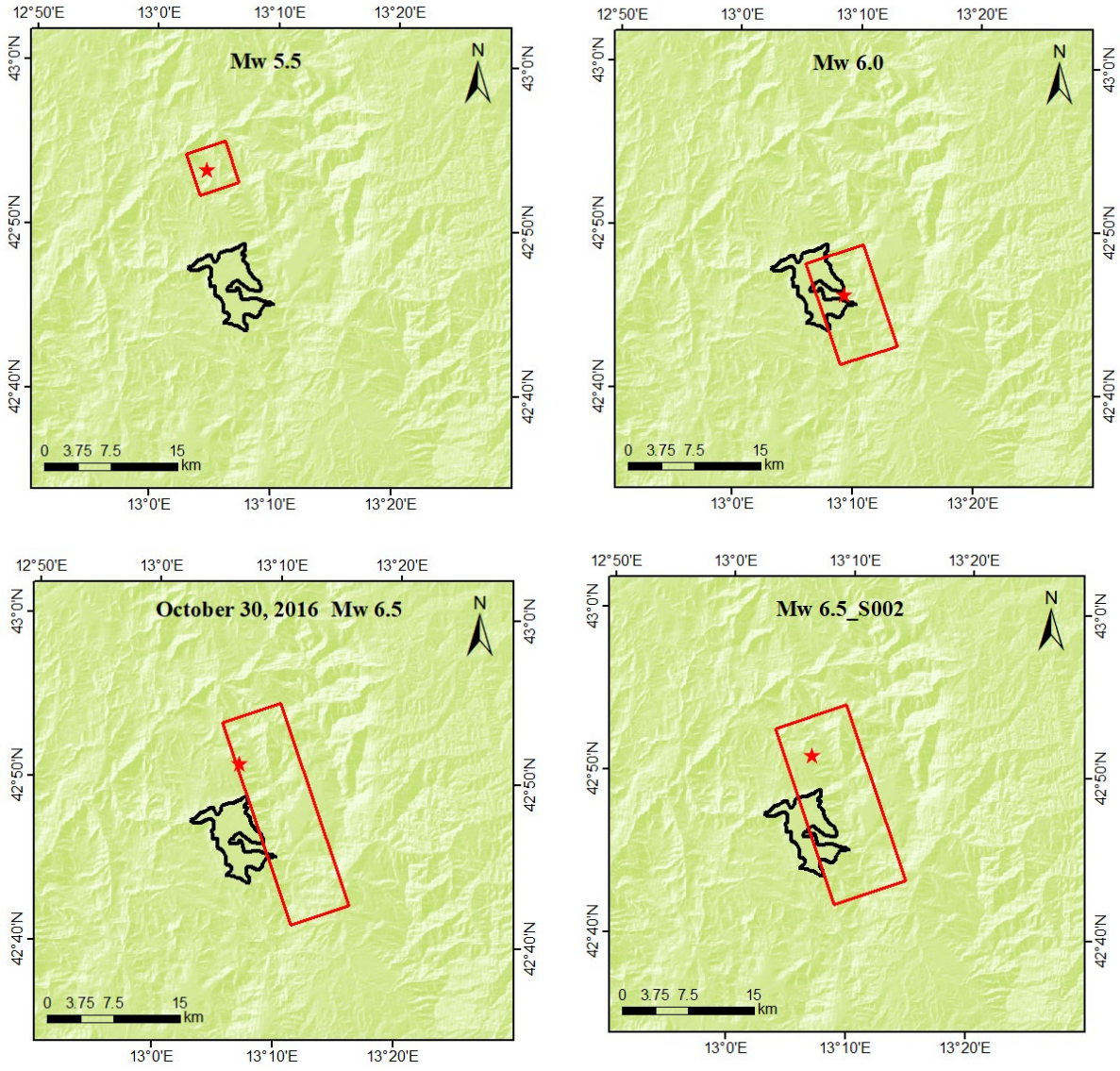

Figure 3-7 Effective fault area and location of hypocentre for different earthquake scenarios.
Top Left: Hypothetical scenario of M_w 5.5_S001 (M_w 5.0) ; Top Right: Hypothetical scenario of M_w 6.0_S001 (M_w 6.0)
Bottom Left: Mainshock of October 30, 2016 M_w 6.5 ; Top Right: Hypothetical scenario of M_w 6.5_S002

4. Comparison between BB Simulations and Recordings

In this chapter a comparison has been made between the results obtained from Broadband simulations (BBs) and those recorded at real stations. The time histories recorded at real monitoring were already corrected for baseline correction using BASCO procedures. The baseline correction procedure is used to remove long-period noise combined with the records (Maini, 2015). The aim of this correction is to recover as much physically plausible velocities and displacements as possible and to obtain results in terms of permanent displacement. In addition to what is stated above a comparison will also be discussed between recorded and simulated time histories in terms of Fourier amplitude spectra (FAS), Response Spectra (RS) in terms of pseudo spectral acceleration (PS_a) and Spectral displacement (Sa).The comparison is performed by taking into consideration main event of magnitude Mw6.5 occurred on October 30, 2016. A total of 16 recording stations are considered in this analysis and focusing on the results obtained at the stations closer to the hypocenter. These stations and their position is shown in Figure 4-1and a summary of their characteristics is shown in Table 4-1 results of acceleration, velocity and displacement in terms of two horizontal EW, NS and vertical component Z however, for simplicity only NOR, NRC, CNE and CLO will be focused as they lie within the 8km from the hypo centre . For the other stations complete set of results can be found in the appendix.

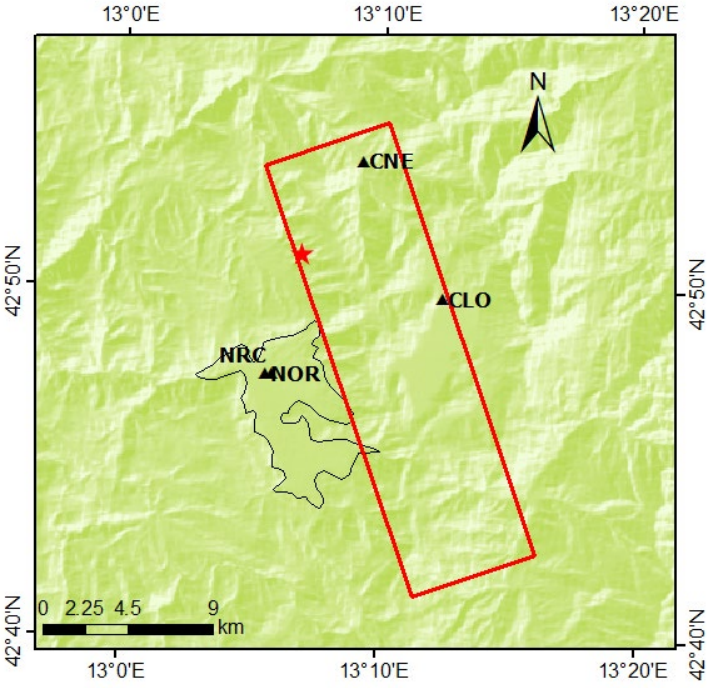

Figure 4-1 Recording Stations (Black triangles) considered in in analysis; Effective fault and source are in red ; Contour represent Basin

Table 4-1 Ground type and Epicentral distance of recording stations

Station	Soil Type EC8	Epicentral Distance R_{ep} (Km)
CLO	A*	7.798
CNE	C*	7.719
NRC	B*	4.55
NOR	C*	4.662

In Figure 4-1 recording stations present in the study area along with the effective fault is shown while in Table 4-1 soil type and distance from epicentre to the corresponding recording station is reported. Symbol ∗ in the soil classification means that soil class is inferred from geological considerations, rather than being based on direct measurements of the shear wave velocity.

4.1. Comparison between time histories

4.1.1. EW Components

In Figure 4-2 a comparison between BB simulated (in red) and recorded time histories (in black) has been made for 4 selected stations in terms of Acceleratio, Velocity and displacement for EW component. It can be observed that there is reasonable agreement between simulated and recorded peak response especially in terms of PGA and velocity at almost all the four stations however, broadband results tends to underpredict residual permanent displacement. Both CLO and CNE stations are located in outcropping bedrock and have almost equal distance

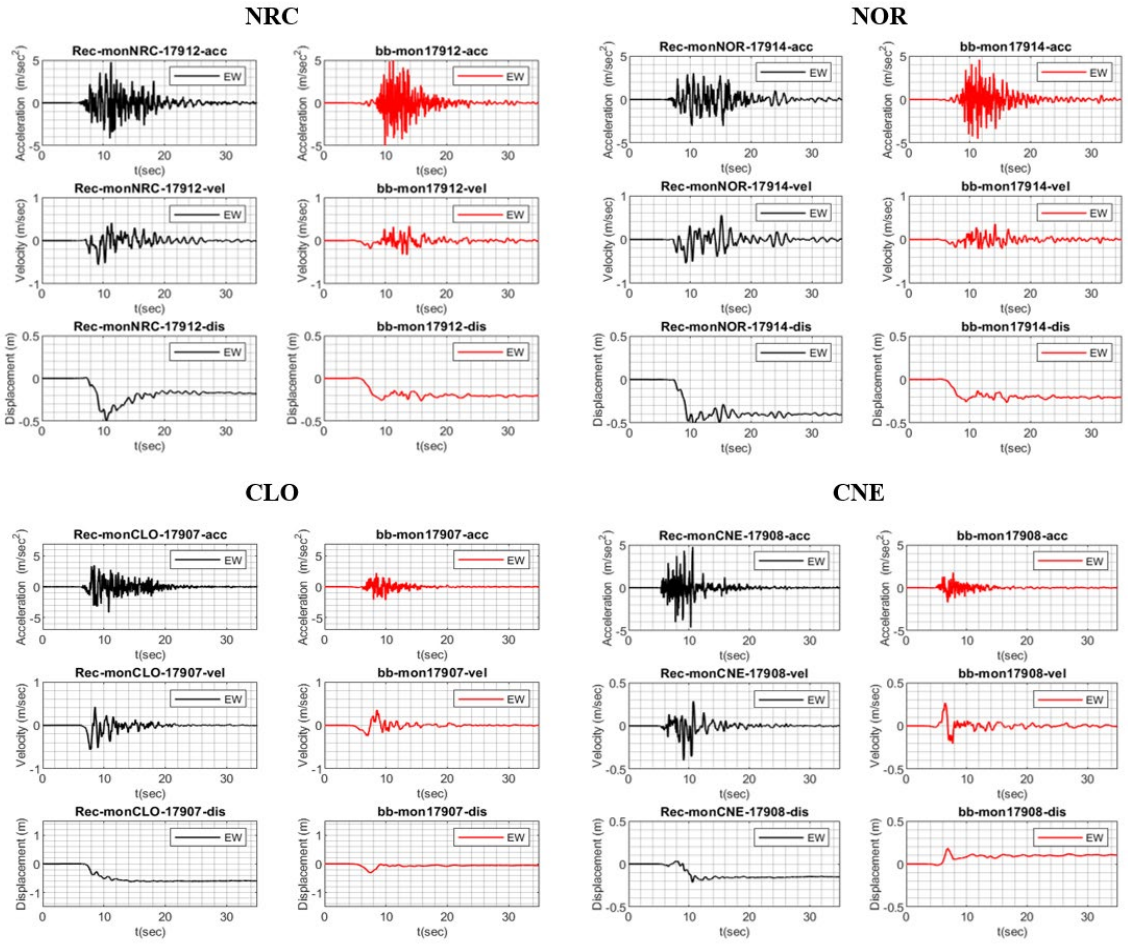

Figure 4-2 Acceleration, Velocity and Displacement for each station in terms of EW Component
Red : BB Simulations ; Black: Recordings

of 8 Km from hypocenter.

CNE and CLO stations show peaks before 10 sec while NRC and NOR stations show amplification between 10 and 20 seconds and this is due to the fact that CLE and CNO are located in the bedrock due to which they have higher velocity of propagation as compared to NOR and NRC which are located in basin.

4.1.2. NS Components

In **Figure 4-3** a comparison between BB simulated (in red) and recorded time histories (in black) has been made for 4 selected stations in terms of Acceleration, Velocity and displacement for NS components. It is evident that numerical model tends to underpredict permanent displacemet.

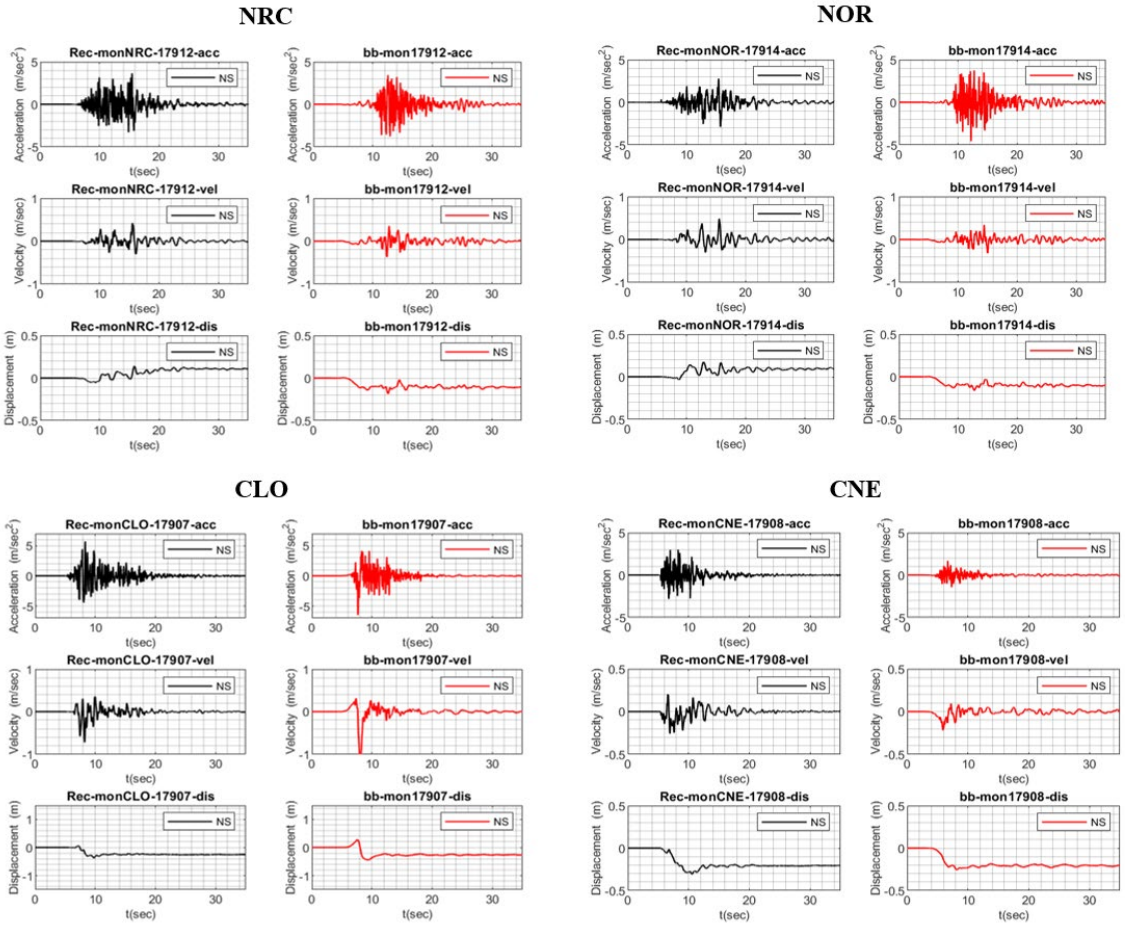

Figure 4-3 Acceleration, Velocity and Displacement for each station in terms of NS Component
Red : BB Simulations ; Black: Recordings

4.1.3. Z Components

In Figure 4-4 a comparison between BB simulated (shown in red) and recorded time histories (shown in black) has been made for 4 selected stations in terms of Acceleration, Velocity and

displacement for vertical components. We see a good agreement between simulated and recoded data.We see that CLO station located in the northern part results in higher permanent displacement as compared to CNE station which is located in the nothern part relative to the CLO station as can be seen in the Figure 4-4. In addition to this we see both NOR and NRC

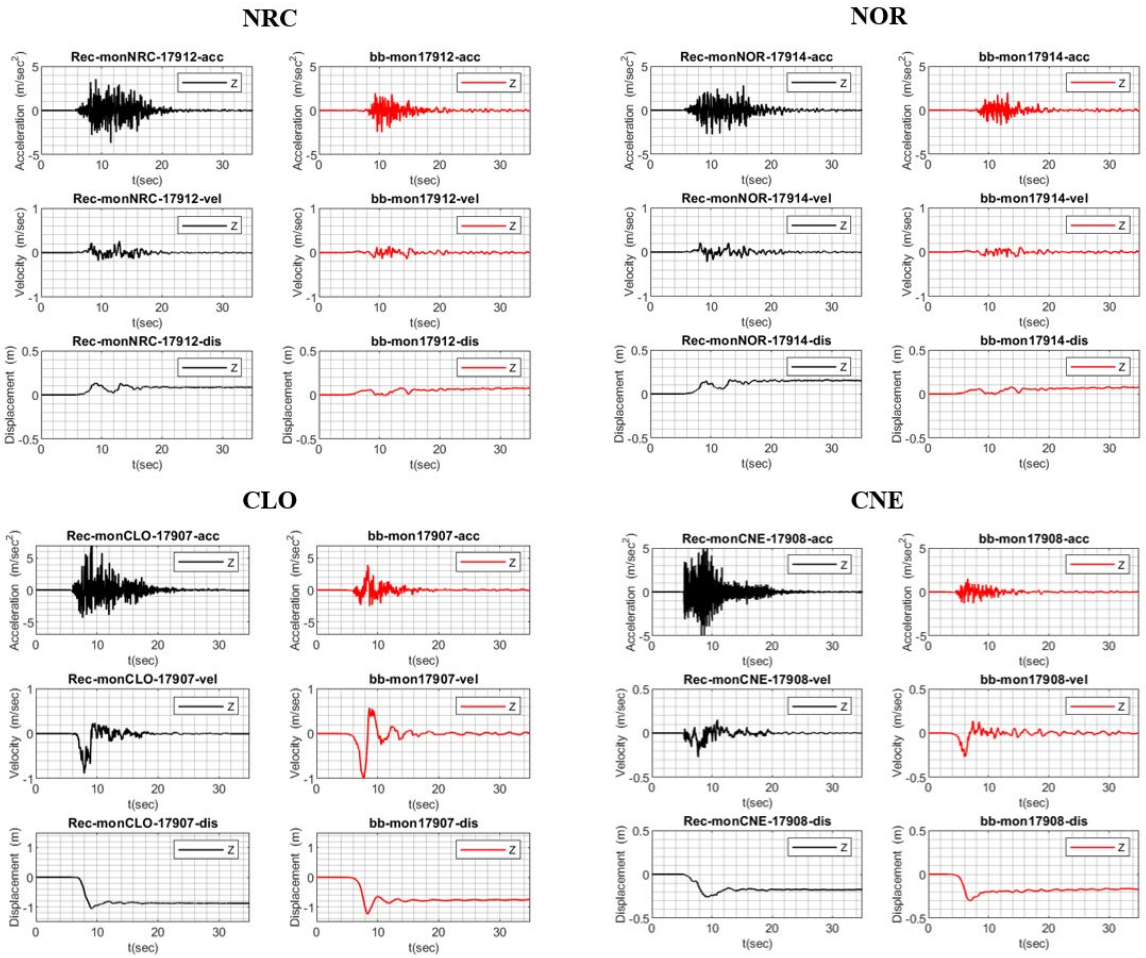

Figure 4-4 Acceleration, Velocity and Displacement for each station in terms of Z Component
Red : BB Simulations ; Black: Recordings

stations show almost same value of permanent displacement.

We can conclude that within the basin horizontal componets results in higher values of permanent displacement however, outside of the basin on the outcropping bedrock vertical component shows larger value of permnanent displacement. It is reasonable to say that BB results tend to predict more or less similar response as of recording station although model tends to underpredict permanent displacement at some location and this is the most critical point when physics based simulation are compared to the real earthquake observations in the near source region. Near source records are related to the details of source slip mechanism however, due to insufficient complexity of geological model, strong presence of non-vertical

incidence angles simulated results are different than real records (Smerzini, 2018). As we move away from the epicentral region these details becomes less relevant.

4.2. Fourier Amplitude Spectra (FAS)

In Figure 4-5 comparison of FAS (Fourier Amplitude Spectra) between BB (in red) and recorded time histories (black) is shown for 4 selected stations for EW, NS and Z components.

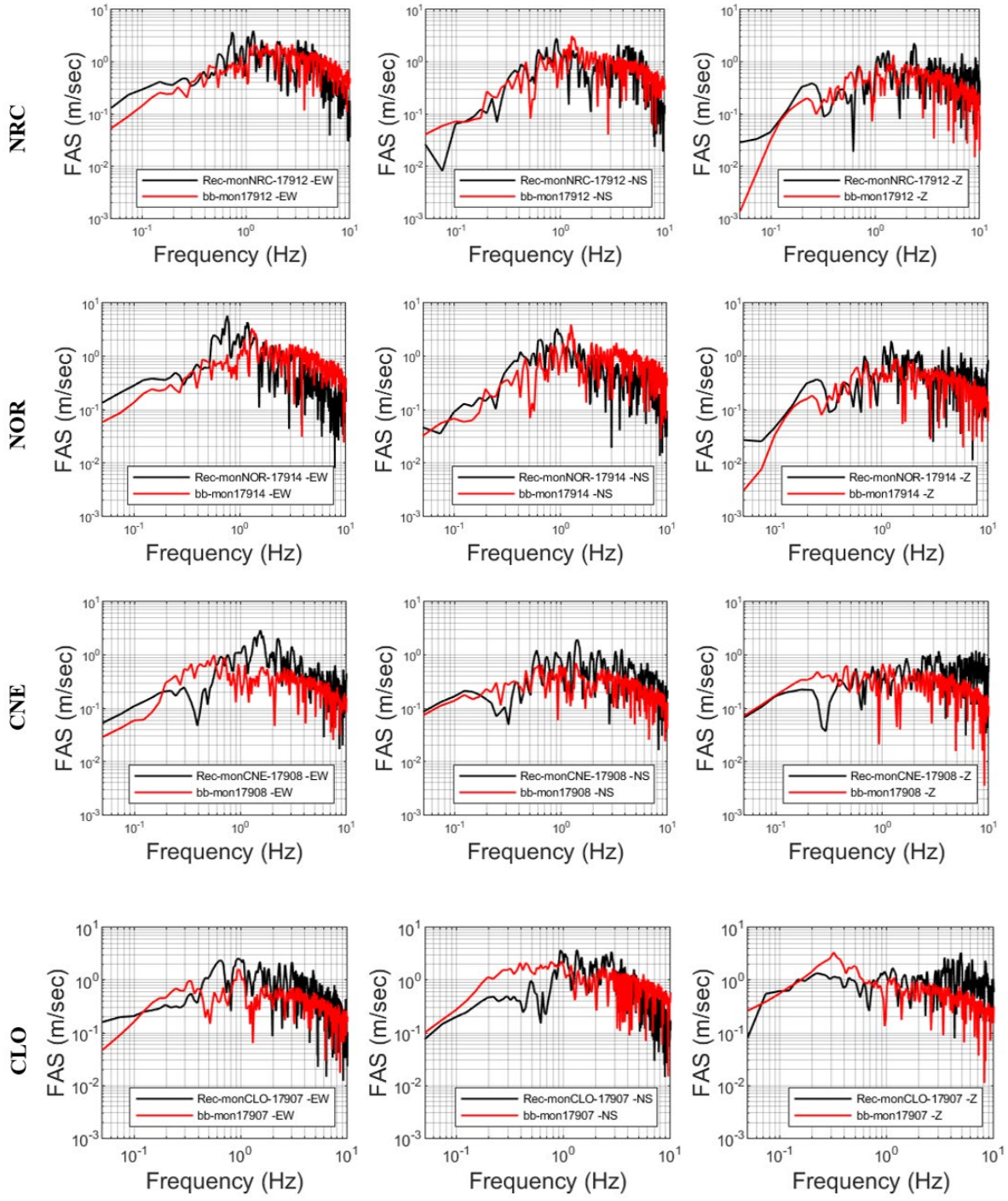

Figure 4-5 Comparison of FAS between BB Simulated and recorded data
Left to right: Components EW, NS and Z ;Red: BB Simulation; Black: Recordings

It can be inferred that both recorded and BB simulated results hold a good agreement upto 1.3Hz which is validity limit of these physics based simulations however, it is worth noting that above 1Hz BB simulations enriches wave form by keeping the low frequency wave form practically invariant and BB predicts almost same amplitude as of recording stations only at NOR and NRC station which lie within the basin and are more prone towards complex 3D wave propagation effects . This shows that the validity of BB simulation achieved seems better in the low frequency range. Moreover, peaks in FAS can be seen at around 1.3Hz which corresponds to the fundamental frequency of the basin. It is evident that peak response is higher inside basin as compared to at outcropping bedrock stations due to the amplification caused by the presence of loose sediment in the basin. Furthermore, the peak response with in the basin is governed by the horizontal components.

4.3. Response Spectra

Response spectra of observed time histories in terms of 5% damped pseudo spectral acceleration and spectral displacement is computed and compared with the numerical predictions. The displacement response spectra is computed by using Equation 3-1.

$$PS_a = w^2 S_d \qquad \text{Equation 3-1}$$

Where;

w is the angular frequency, S_d is the spectral displacement and PS_a is the pseudo spectral acceleration.

4.3.1. Pseudo Spectral Acceleration (PSA)

In Figure 4-7 a comparison of PSA (Pseudo Spectral Acceleration) between BB simulated (in red) and recorded time histories (in black) has been made for 4 selected stations for EW, NS and Z components.

It is evident that the model predicts more or less same response as of recording stations for NOR and NRC stations at lower periods below 1 sec which is the limit of physics based simulations. Peak response of NRC station is higher as compared to NOR station due to greater thickness of sediments under NRC station we have higher amplification. In contrast to this the numerical model underpredict spectral response for outcropping bedrock stations and this could be due to the complex wave propagation in the near source region and insufficient detailed geological information of the complex geology of the basin.

In general as it is evident that within the basin peak response is governed by horizontal components because of NW-SE oriented and SW dipping fault system. It is worth nothing that above period of 2 sec agreement between simulated and recorded data improves representing the validity of numerical model for T>T* (T* =0.75sec).

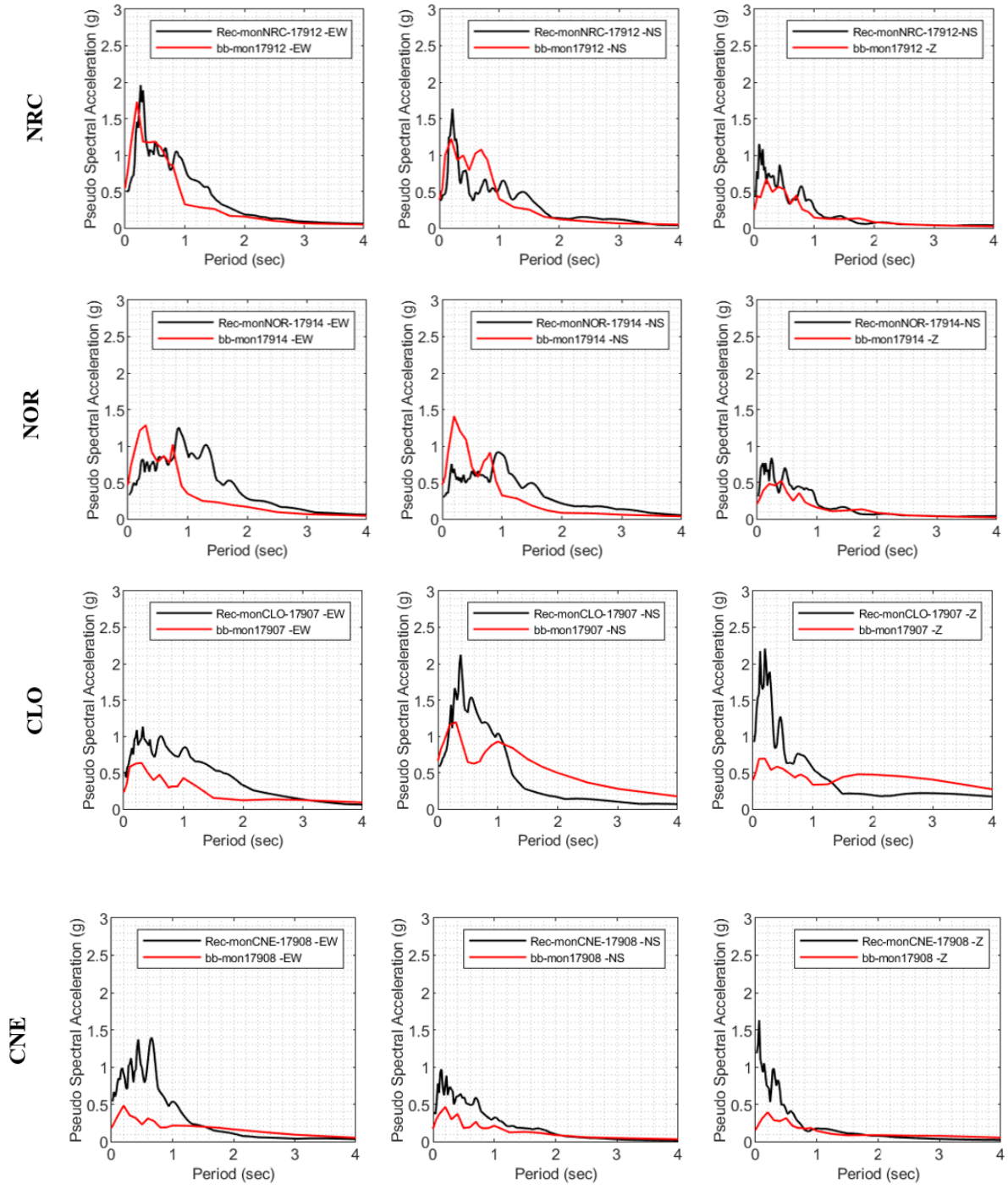

Figure 4-6 PSA Comparison between BB and recoded data
Left to right: Components EW, NS and Z ; Red: BB Simulation; Black: Recordings

4.3.2. Spectral Displacement (S_d)

In Figure 4-8 and Figure 4-9 a comparison of S_d (Spectral Displacement) between BB simulated and recorded time histories has been made for the 4 selected stations for EW, NS and Z components. It can be inferred that for periods up to 1 sec both recording and numerical model show a good agreement. However, between T= 2-3sec numerical model predictions do not coincide with the recordings this aspect is more clear in CLO and NOR station.

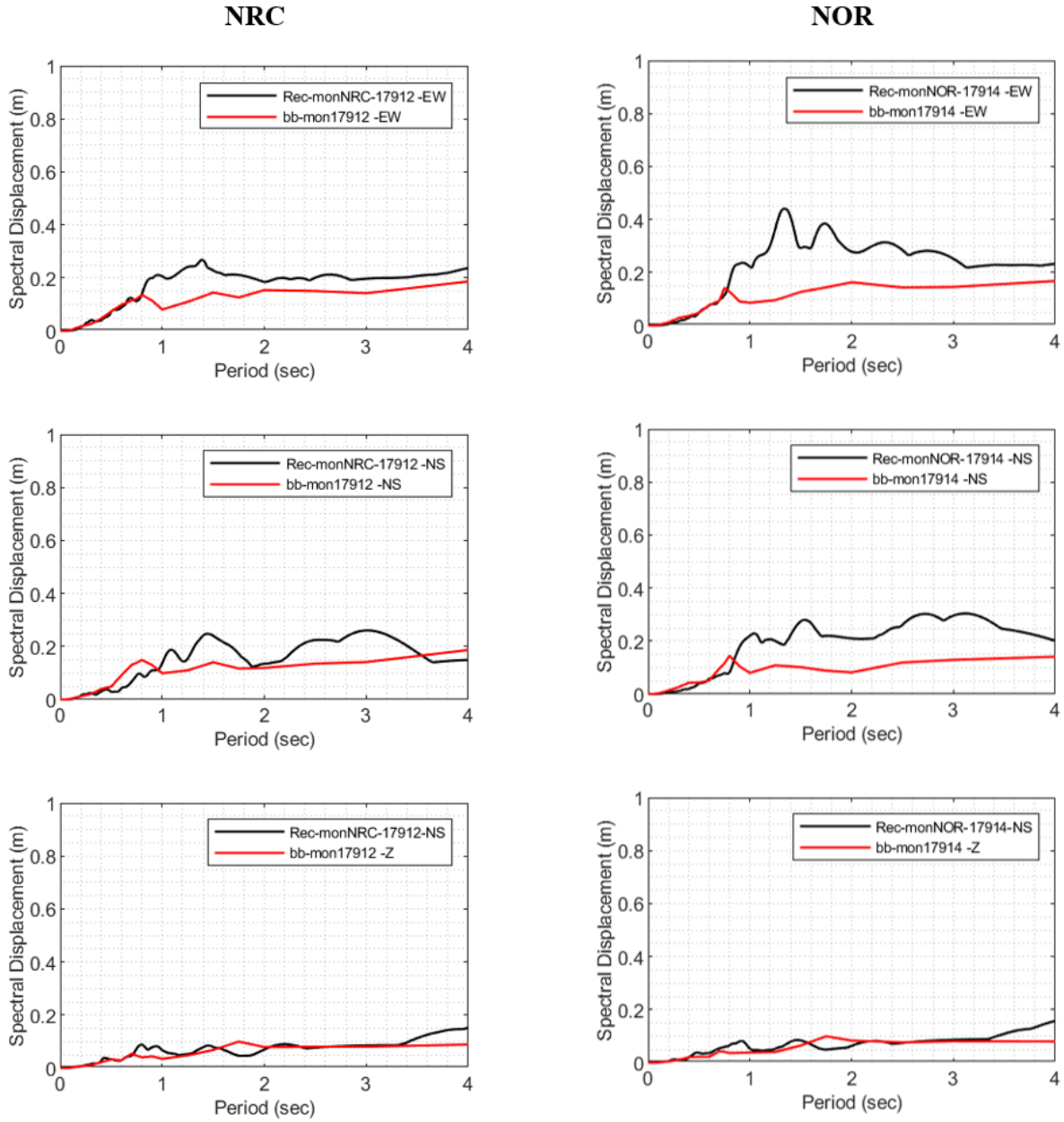

Figure 4-7 Spectra Displacement (S_d) Comparison between BB simulated and recordings
Top to Bottom: Components EW, NS and Z Red: BB Simulation; Black: Recordings

At NRC and CNE station we can see that the numerical model predicts results which are similar to recording stations. Moving forward, it is also evident that for longer periods such as T=4 sec BB simulation tends to have nearly similar displacements as compared to recordings except in the case of CLO station in agreement of what has been shown with histories in Figure 4-2 to Figure 4-4. The tendency of numerical model to preserve peak ground displacement with reasonable accuracy at the longer periods points out the reliability of the kinematic source model.

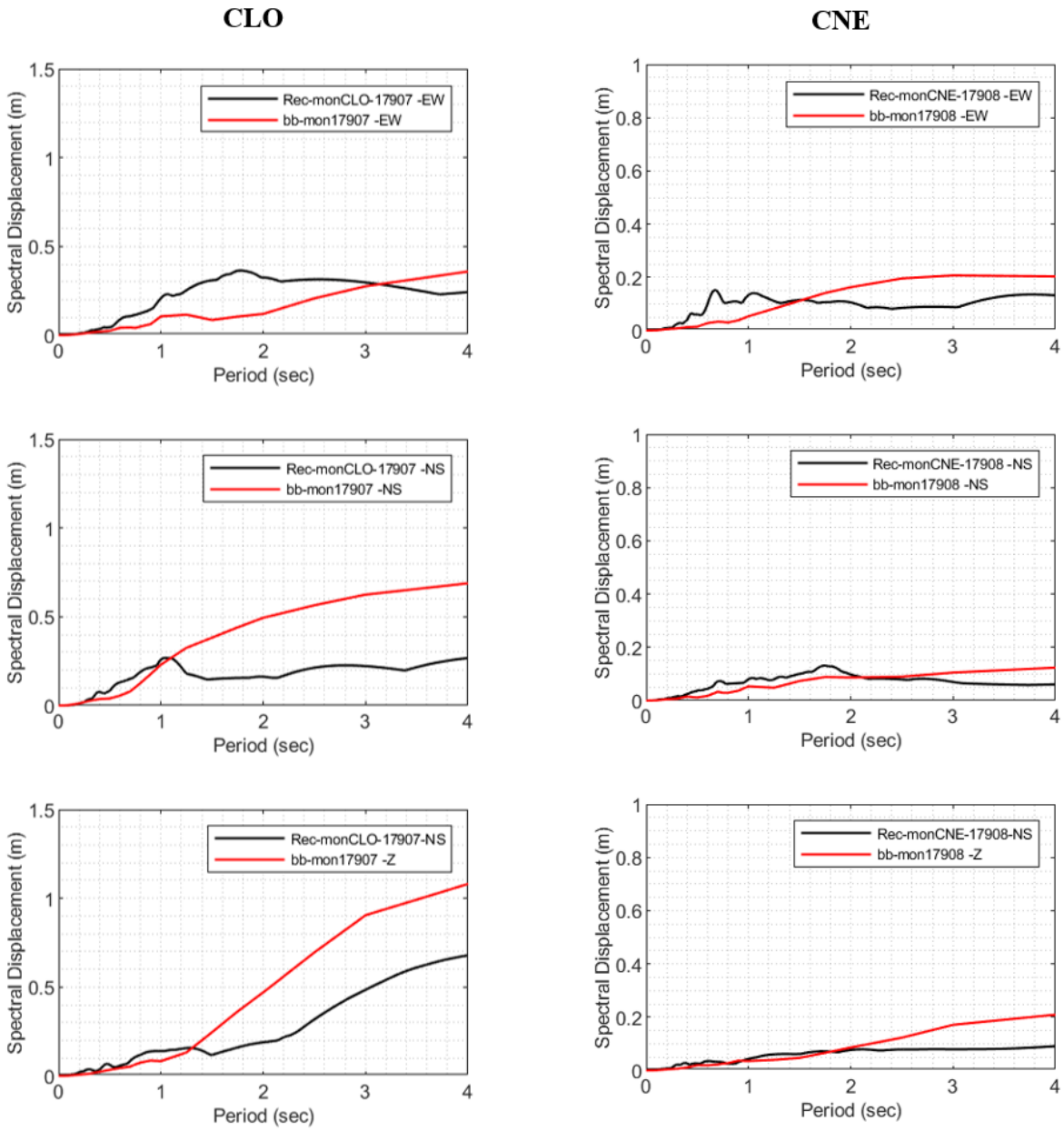

Figure 4-8 Spectra Displacement (S_d) Comparison between BB simulated and recordings
Top to Bottom: Components EW, NS and Z ; Red: BB Simulation; Black: Recordings

4.4. Ground Shaking Maps

Maps of simulated time histories are created by using GIS (Geographic Information System) software and compared with the peak ground values of acceleration, velocity and displacement recorded at the real recording stations. This is very useful to predict the spatial agreement between simulated and recorded peak ground response and hence spatial validity of numerical model can be quantified. The comparison was made for the main event of Mw 6.5 that occurred on October 30, 2016 in Norcia. Mpas in terms of PGA, PGV and displacement are given in the Figure 4-10 to Figure 4-12

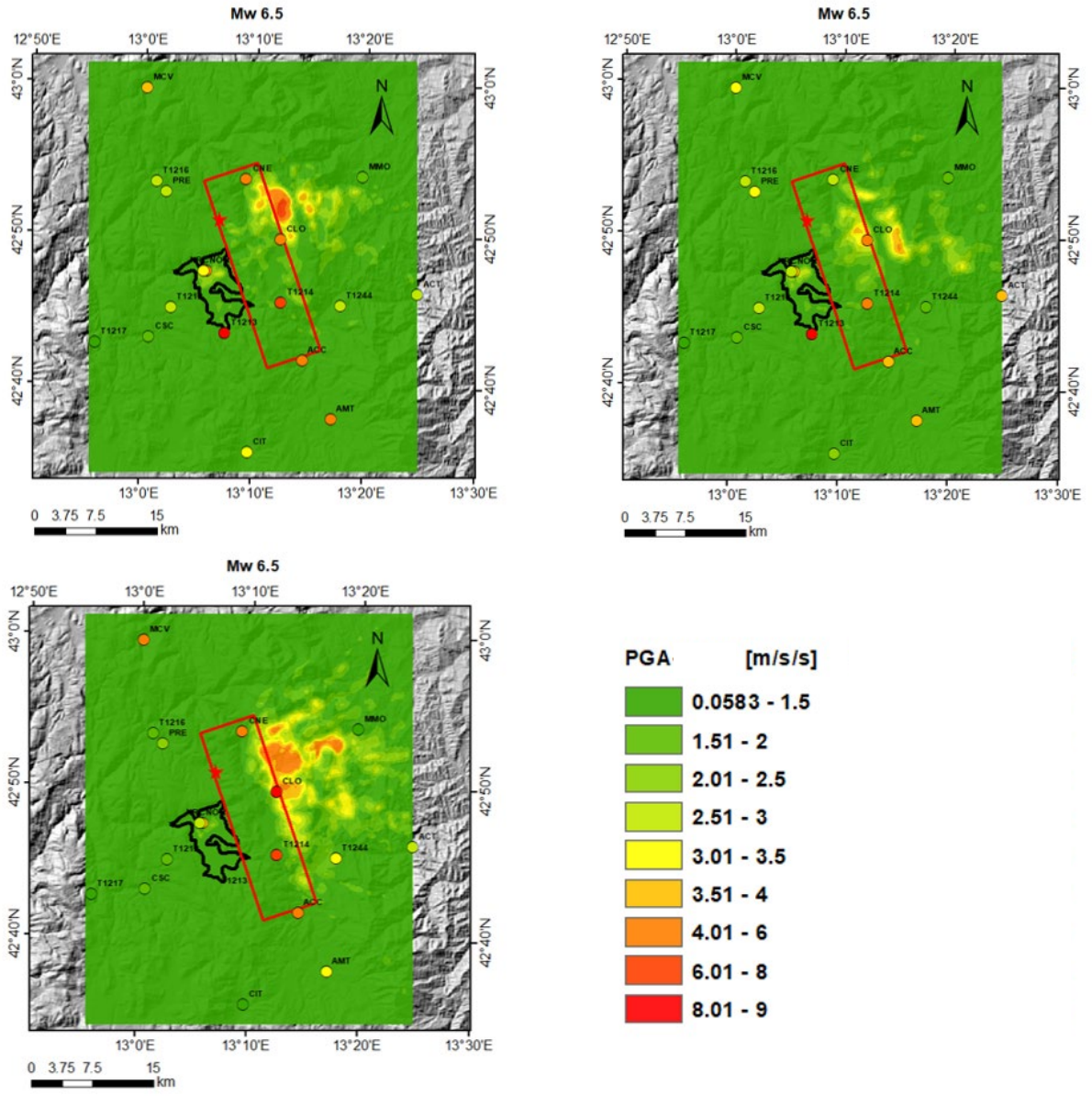

Figure 4-9 Comparison between PGV BB simulated and peak values recorded at recording stations
Top left: EW Component , Top right: NS component, Bottom left: Z Component

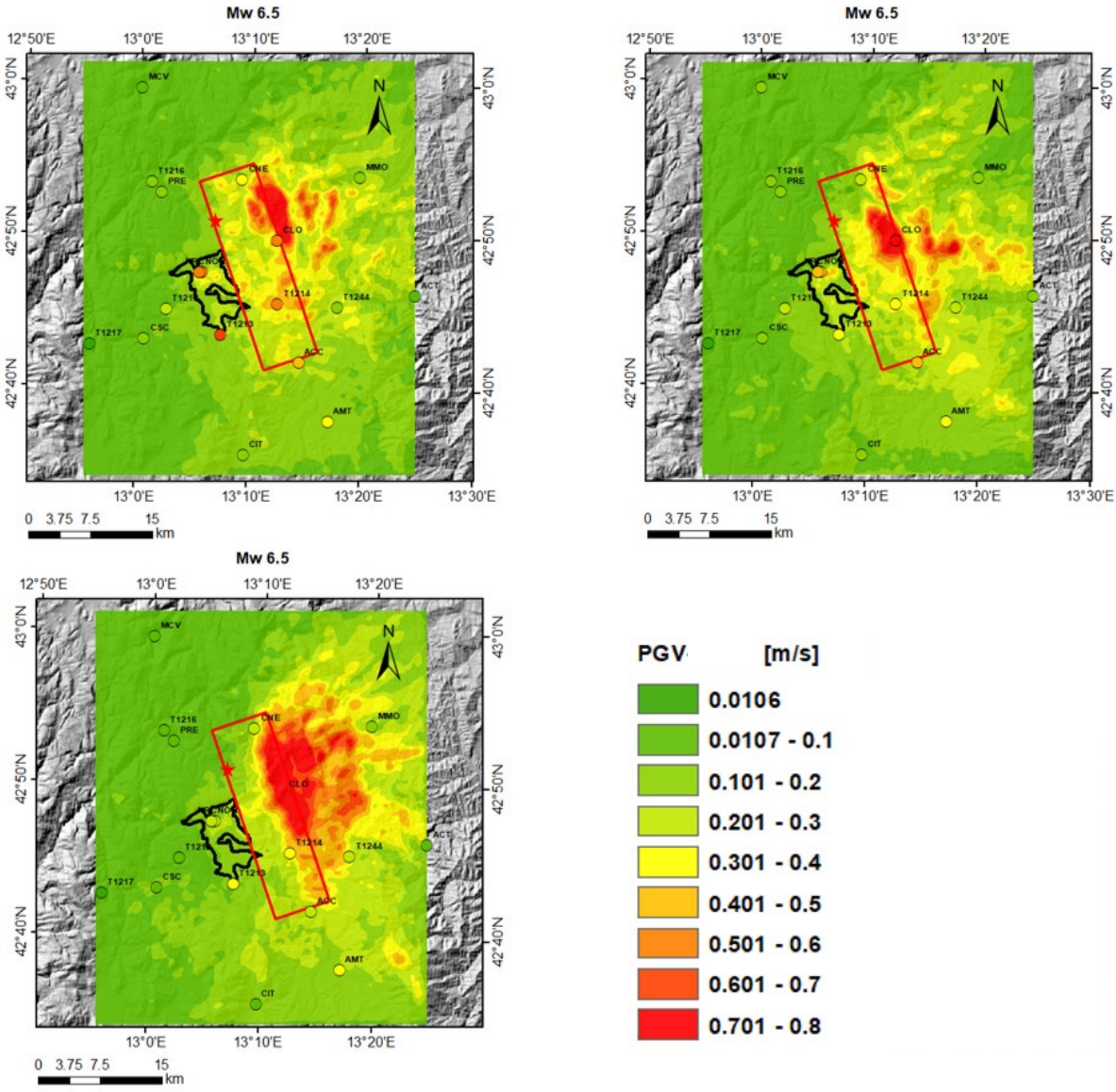

Figure 4-10 Comparison between PGV BB simulated and peak values recorded at recording stations
Top left: EW Component , Top right: NS component, Bottom left: Z Component

In general there is a reasonable agreement between the recorded and the simulated values although simulated values underestimate results at some locations such as at the station AMT, T1219, T1213, T1214 and this could be due to complex wave propagation, diffraction of S waves at the basin edges and lack of detailed knowledge about complex geological features in basin and outcropping bed rock. However, station NRC and NOR reflect good comparison with the recorded data. In addition to this in Figure 4-11 we can observe a rather good relation between simulated and recorded data of NS and Z component in terms of PGV especially in the near source region. In Figure 4-12 we can see that simulated and recorded permanent displacement are well correlated in the near source region especially in EW and Z component of NOR and NRC and CLO station. We can conclude that globally there is a reasonable

agreement between simulated and recorded values of PGV, PGA and permanent displacement however, results of simulation tends to underpredict at some station which could be due to 3D site complexities, uncertainty in the 3D wave propagation, diffraction of S waves at the basin edges and lack of detailed knowledge about complex geological features.

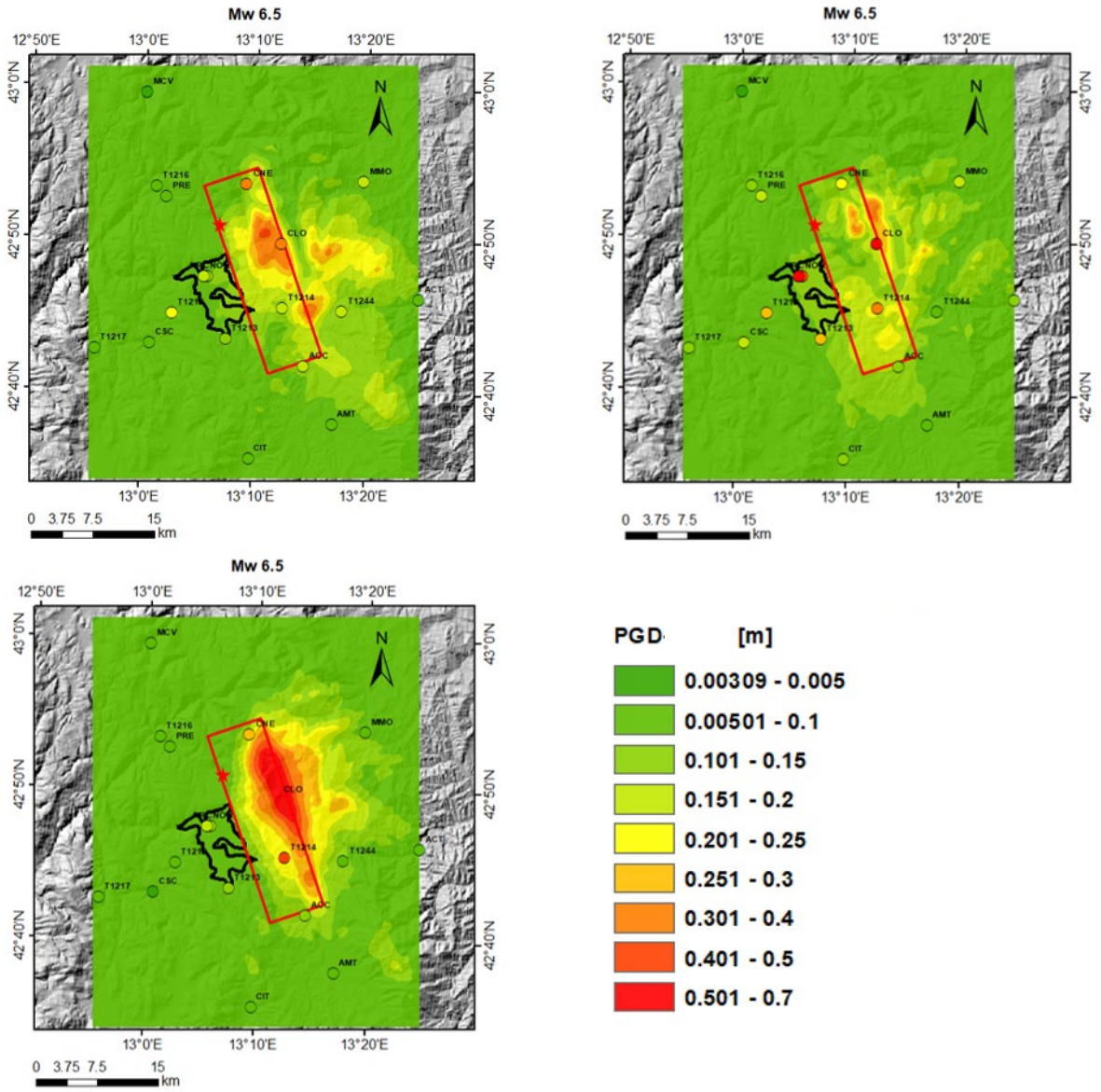

Figure 4-11 Comparison between PGV BB simulated and peak values recorded at recording stations
Top left: EW Component , Top right: NS component, Bottom left: Z Component

5. Analysis of Response Spectral Ratios (RSR)

In this chapter the main focus is to study the seismic site effects which are related to the amplification of seismic waves in superficial geological layers. The surface ground motion may be strongly amplified if the geological conditions are unfavourable (e.g. sediments). Therefore, the study of local site effects plays a crucial role in the assessment of strong ground motions and hazard assessment.

Amplification functions are often quantified as the ratio of the ground motion at the soil surface to the ground motion at a rock site at the same location however one can also determine the amplification of a certain location with respect to a refence bedrock site and study how amplification function varies by changing reference sites . In this chapter we have both cases the former of which being called here in after Ideal case where amplification function is computed with respect to the same site by considering it as bedrock. In general amplification functions can be defined for any ground motion parameter herein they are performed for acceleration response spectral values at different vibration periods.

$$SAF = \frac{S_{a\ (5\%\ damped)\ BASIN}}{S_{a\ (5\%\ damped)\ BEDROCK}}$$

3D numerical models need a certain number of physical parameters which are poorly constrained for future earthquakes because of the lack of knowledge (epistemic uncertainty) on the physical phenomenon itself. For example, the distribution of co-seismic slip, the earthquake hypocentre and geological setting at the site of interest are features that are difficult to determine a priori. For this reasons, the input parameters should be varied within a physically realistic range rather than fixed to default values (*Smerzini et al., 2010*). Furthermore, a proper characterization of the fault rupture process, in terms of source parameters, such as slip pattern, rupture velocity and focal mechanism might have a crucial role for the evaluation of seismic input, especially in the near-source earthquakes.

The main focus of this part of thesis is to assess the spatial variability of 3D site amplification function within the basin by taking into consideration original event of Mw 6.5 occurred on October 30, 2016 and some hypothetical scenarios of Mw 5.5, Mw 6.0 and Mw 6.5. These hypothetical scenarios have different slip distribution and hypocentre location. The analysis is performed for the following:

i. 3D ideal SAF (Spectral Amplification Function) which is computed as the ratio of spectral acceleration ($S_{a\,(BASIN)}$) at a site in the basin to the spectral acceleration at the same site by considering it as a outcropping bedrock ($S_{a\,(BEDROCK)}$). We compared SAF for all earthquake scenarios to determine how SAF varies by changing magnitude of earthquake, slip distribution and the source.

ii. Spatial variability of 3D SAF computed with respect to a real bedrock (reference bedrock) is analysed and compared with the 3D ideal case for two horizontal EW, NS and a vertical component Z.

iii. Two cross sections named as transversal and longitudinal which are approximately in NS and EW directions respectively within the basin are considered and 3D ideal SAF is compared for four different time periods for all the earthquake scenarios.

5.1. Analysis of 3D Ideal Site Amplification Function (SAF)

Two cross sections named as longitudinal and transversal are considered inside basin and SAF have been computed for selected receivers. Since site amplification function is directly related to the topography and superficial depth of sediments therefore, In order to reasonably analyse spatial correlation of SAF only those receivers were considered along the cross section having relatively different depth of sediments from each other. We analysed a total of 6 and 5 receiver points from transversal and longitudinal sections respectively however, only 2 real stations such as NRC, NOR and 2 receiver points named as 153 and 373 will be focused here as they have relatively different sediment thickness so, the effect of SAF can be analysed in a good manner. Complete set of results for the other receiver points can be found in appendix 1.

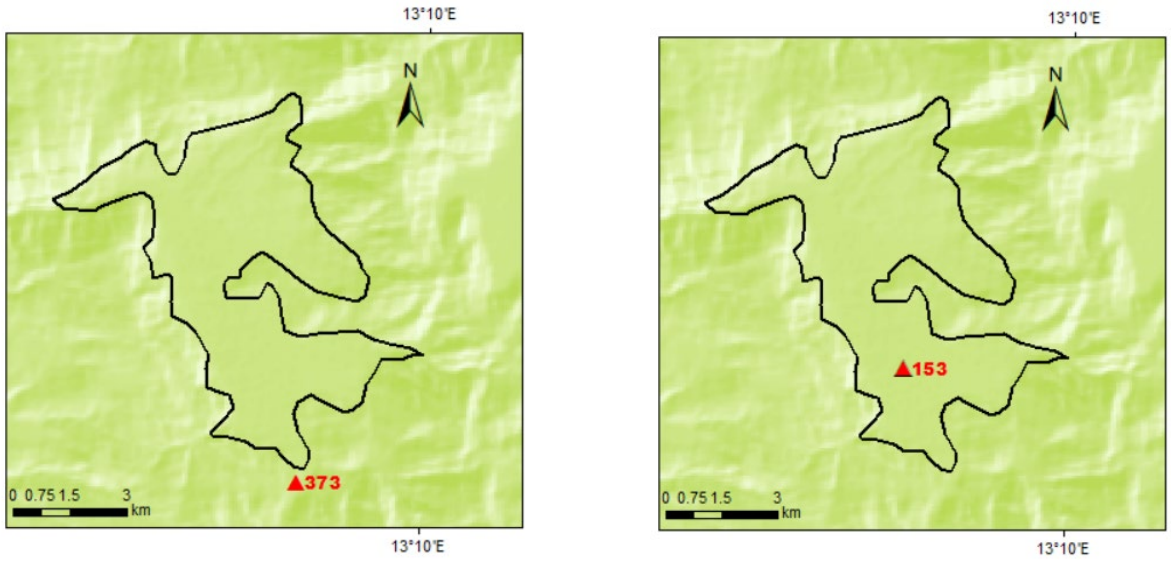

Figure 5-1 Receiver Points Locations
Left: Receiver Point 373 ; Right: Receiver Point 153

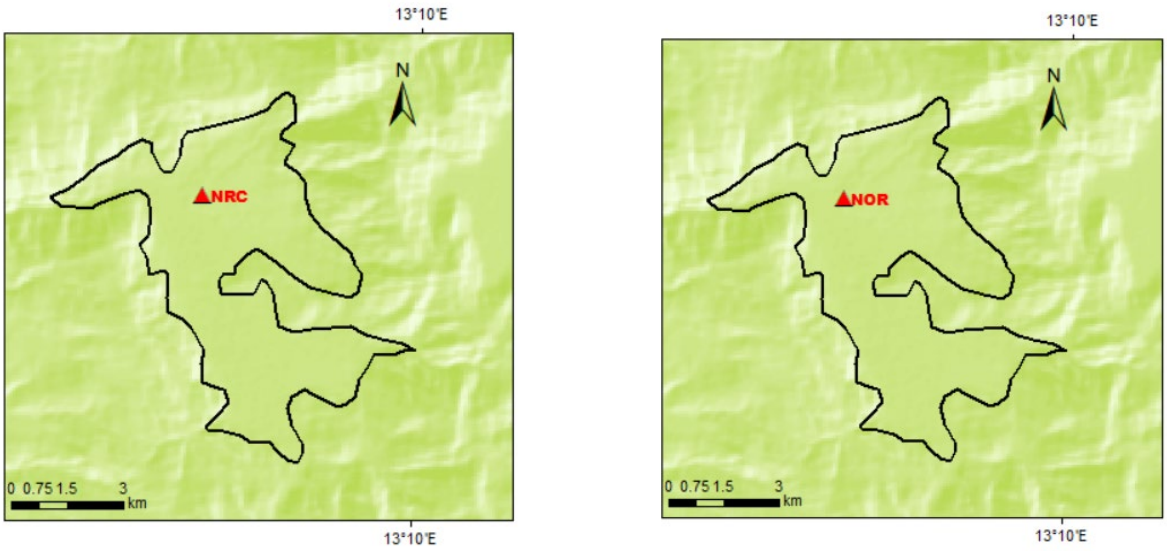

Figure 5-2 Station Locations
Left: Station NRC ; Right: Station NOR

The location of the stations and the receivers points used in this study are shown in Figure 5-1 and Figure 5-2.

In Figure 5-3 selected cross section and the corresponding receiver points are shown. Furthermore, some reference sites around the basin have also been marked.

Local site amplification effects can be originated by several mechanisms. For station installed in alluvial basins, the site amplification effects can be related not only to the reduction of the seismic impedance of the layers from the bedrock to the free surface (1D site effect) but also to diffraction phenomena and wave conversions taking place at the edges of the basin as well as the trapping and focusing of energy within the soil volume (2D–3D site effects). The multiple reflection of energy and the propagation back and forth of the basin induced surface waves can lead to a dramatic increase of damage due to amplification of ground motion and the extension of its duration (Bindi D et.,al 2011)

In Figure 5-4 to Figure 5-5 a comparison between NOR, NRC, 153 and 373 has been made in terms of SAF for different earthquake scenarios. It can be inferred that both NOR and NRC show resonance at around 0.75-0.8 sec which corresponds to the fundamental frequency (f_0 =1.3Hz) of a soil column beneath the NRC station (Pourshayegan, 2016). Furthermore, EW components of NRC and NOR station show an amplification factor of 11 and 7 respectively for the M_w 6.5 event. This difference in the peaks of amplification factor for the two stations is due to depth of sediments beneath the stations which allows the trapping and focusing of energy within the soil volume and the phenomenon usually referred to as 2D-3D site effect . NRC and

NOR stations have depth of sediments 276 m and 205m respectively. It is evident that at both NRC and NOR stations and two other receiver points peak response is governed by EW components. Moreover, generally moving towards south from the NRC station we observe a decay in the peaks of amplification.

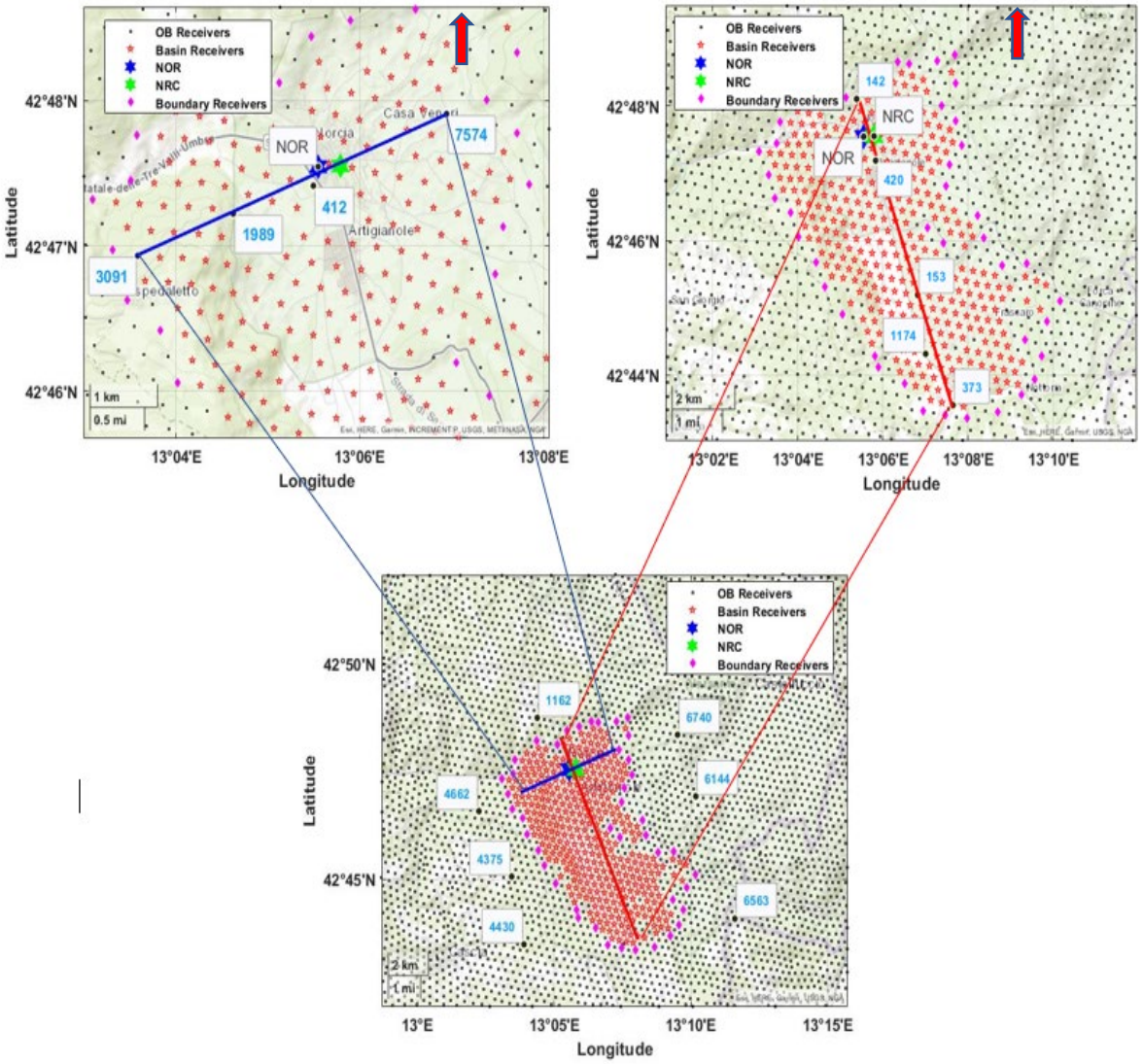

Figure 5-3 Top Left: It describes receiver points chosen along the EW cross section and only NOR station discussed here in**; Top Right:** It shows receiver points chosen along the NS cross section and only 153, 373 and NRC Station discussed here in **; Bottom:** It shows 7 reference sites considered in the analysis

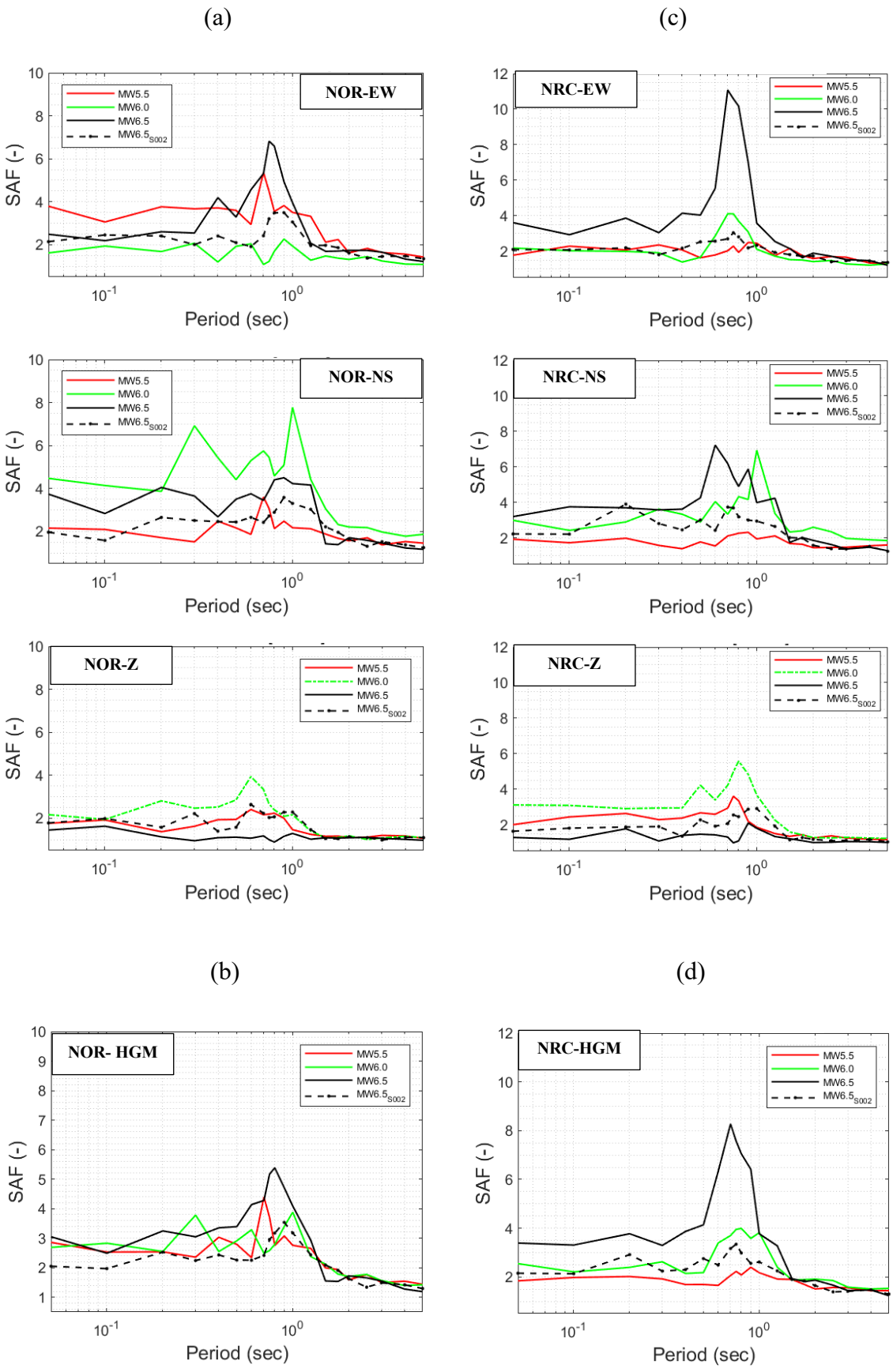

Figure 5-4 Spectral Amplification Function (a, b): NOR Station (c, d) NRC Station
Top to Bottom (a,c): EW,NS,Z component (b,d): HGM Component

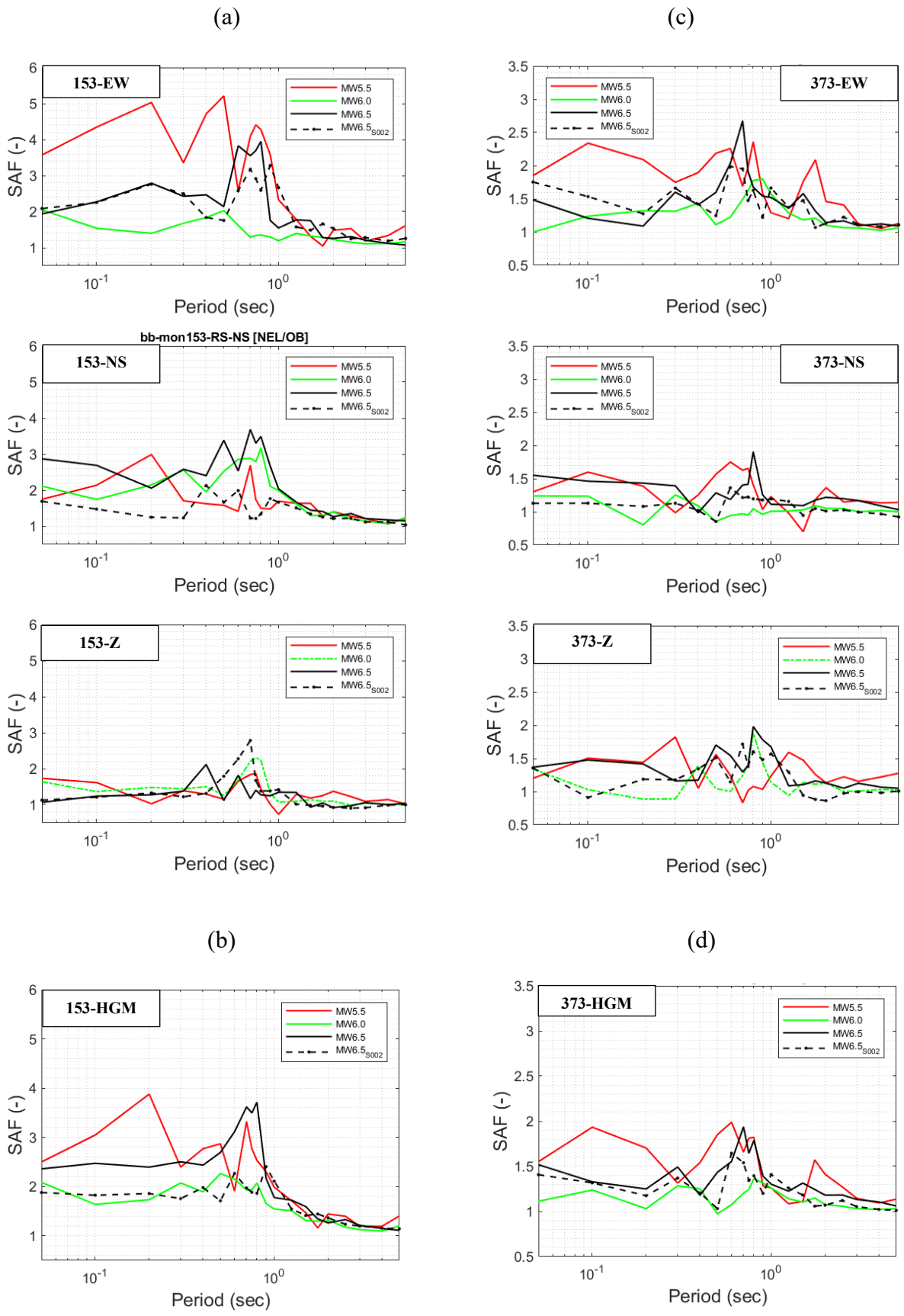

Figure 5-5 Spectral Amplification Function (a, b): receiver 153 (c, d) receiver 373
Top to Bottom (a,c): EW,NS,Z component (b,d): HGM Component

Effect of source and magnitude can be observed especially in EW and NS components. We can observe from Figure 5-4 that for the main event of October 30, 2016 and hypothetical scenario of M_w 5.5 and M_w 6.5_S002 source is located in the north of the basin while for the scenario M_w 6.0 it is located in the SE direction from the NRC station. It is clear from the Figure 5-4 and Figure 5-5 that EW component is more amplified for scenarios M_w 6.5, M_w 5.5 and M_w 6.5_S002 while, in case of M_w 6.0 having source in the SE direction we observe that the NS component shows higher amplification. Comparison in terms of geometric mean of the two horizontal components EW and NS depicts the similar trend of decay in the peaks of SAF from north to south in the basin in the period range of 0.7sec-0.9sec. In order to observe detailed effect of variability of SAF along the two cross sections we have analysed spatial variability of SAF in terms of EW, NS,Z and GMH components for four different periods such as 0.5sec, 1 sec, 2 sec and 3 sec .

Two cross sections named as transversal and longitudinal cross sections were considered as shown in Figure 5-6 and all the receiver points along these two cross sections were analysed. The length of longitudinal cross section is about 3133m while the transversal cross section has a length of about 8694m. It can be considered that both longitudinal and transversal cross are representative EW and NS sections of the basin therefore, they will be named as EW and NS section here in after respectively. Furthermore, profile of depth of sediments along the two cross sections is also given in the Figure 5-7.

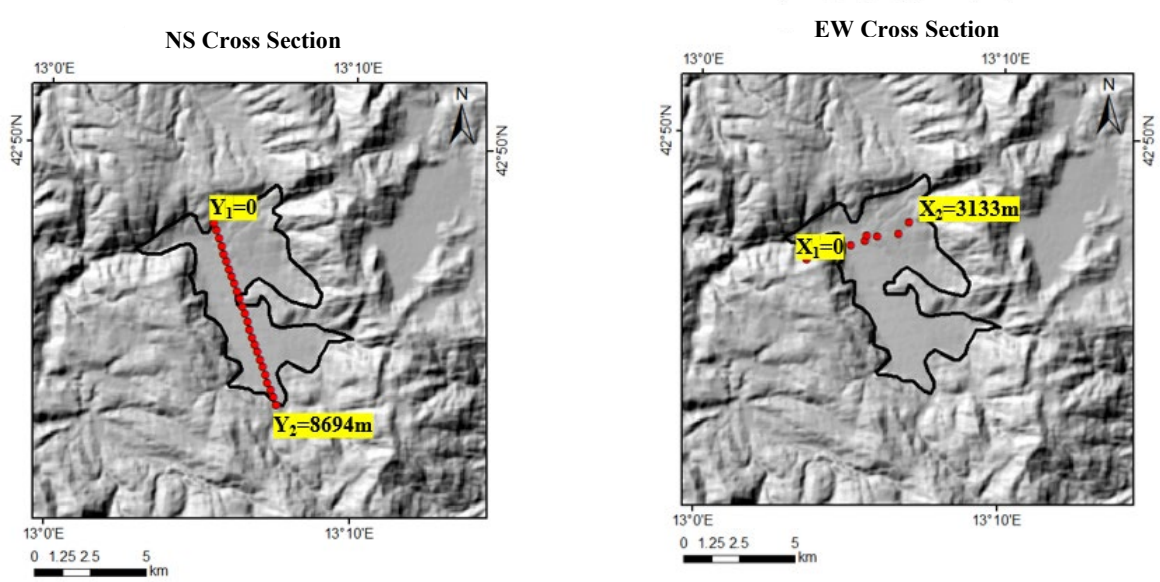

Figure 5-6 Representative Cross Sections
Left: NS Cross section of length 8694m Right: EW Cross section of length 3133m

The result along the two cross section are given in the proceeding sections.

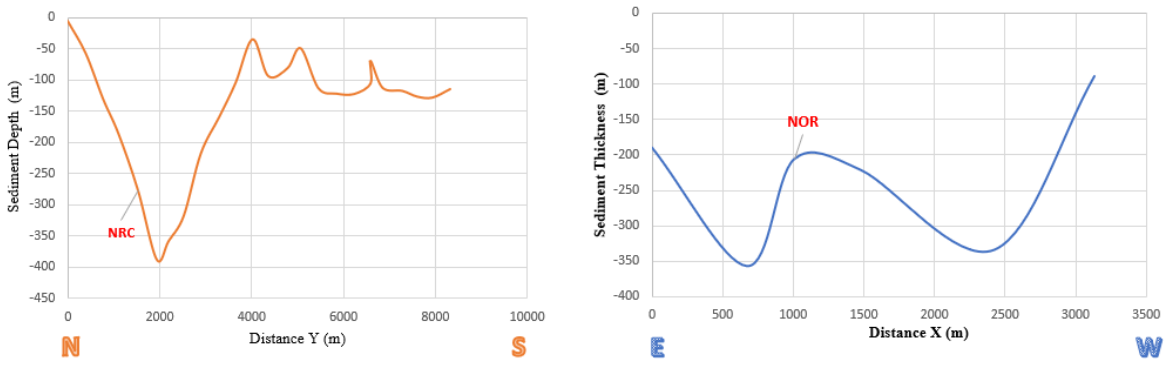

Figure 5-7 Sediment profile along representative cross sections Left: NS Cross Section; Right: EW Cross Section

5.1.1. NS Cross Section

a)

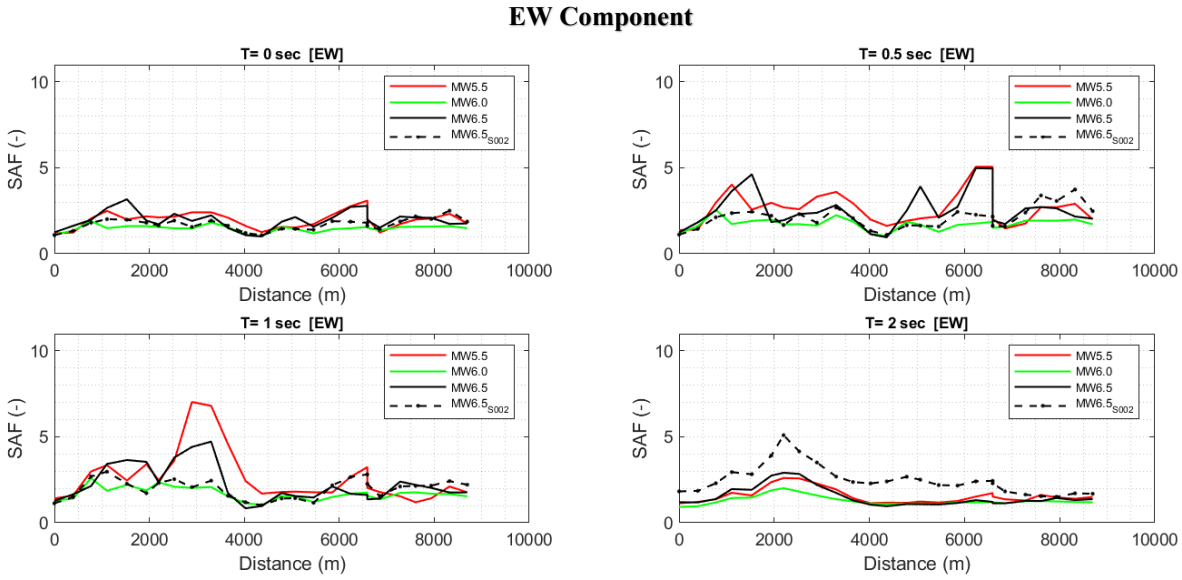

b)

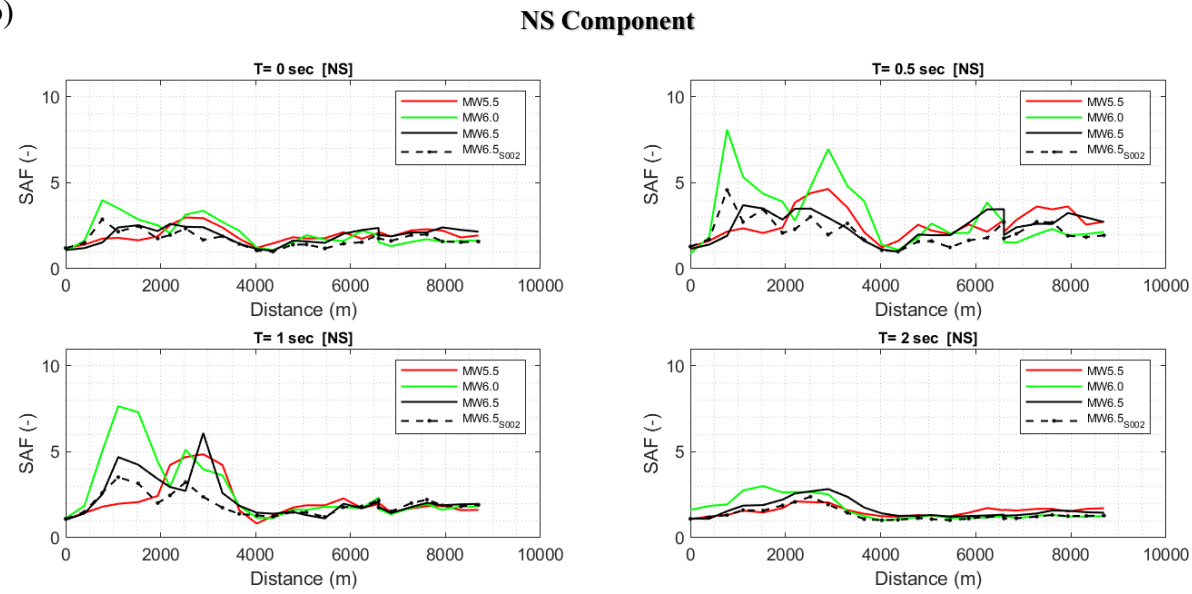

Figure 5-8 3D Ideal SAF a) EW Component, b) NS Component

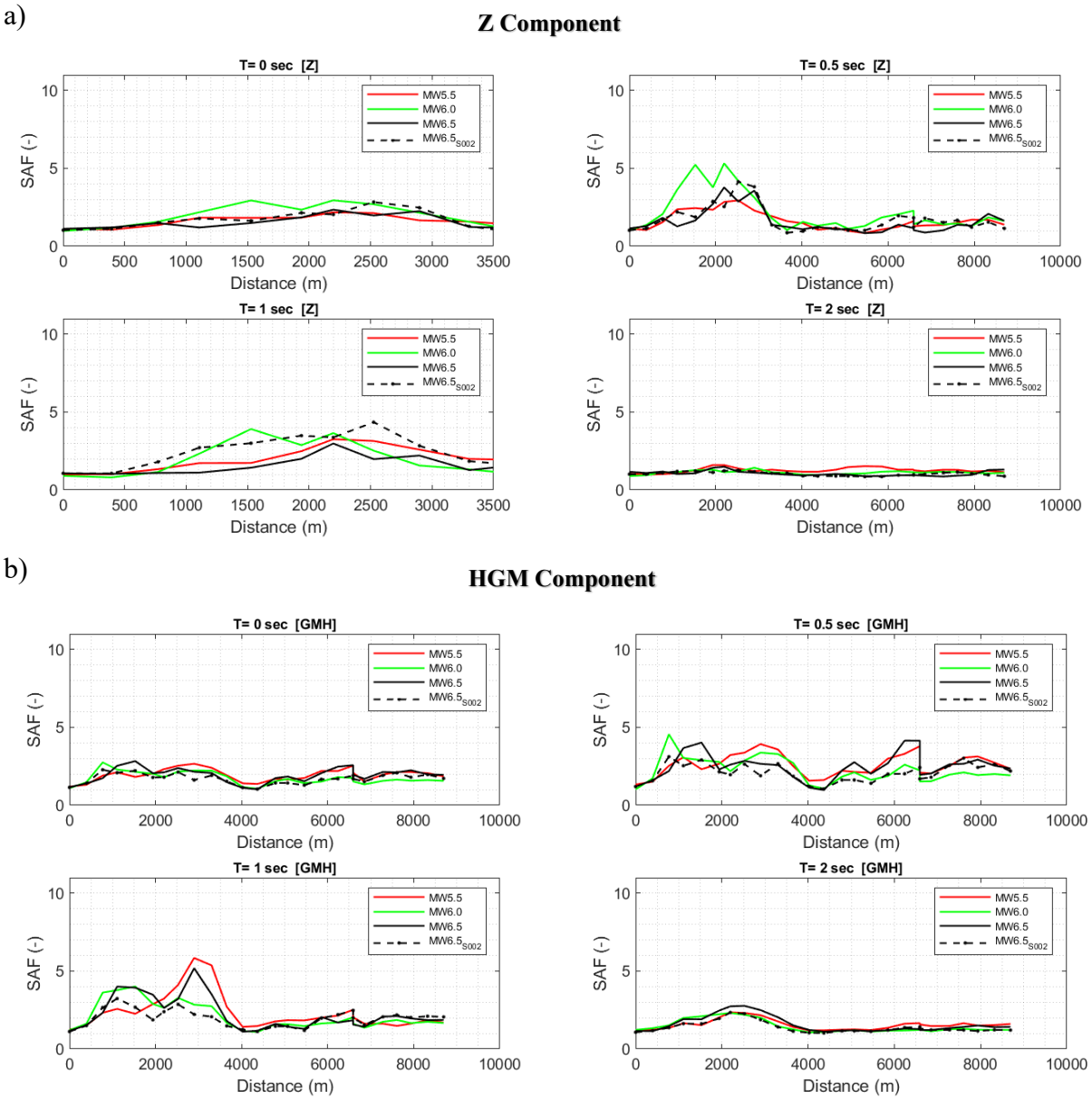

Figure 5-9 3D Ideal SAF a) Z Component , b) HGM Component

It can be seen in Figure 5-8 and Figure 5-9 that in general moving from north toward south there is a decay in the peaks of SAF in all the three components such as EW, NS and Z. It can also be observed that the amplification peaks of SAF are more pronounced in the first 4000m of the section which have higher sediment thickness while in the other part from 4000m to 9000m we don't see such peaks especially in NS and Z component. Moving forward, role of earthquake scenarios is obvious in the EW and NS components however, Z component doesn't show marked difference in the SAF for different magnitudes. It is clear that by changing the source location from north (M_w 6.5, M_w 6.5_S002 and M_w 5.5) to the south (M_w 6.0) of the basin the relevance of SAF shifts from EW components to the NS component so directivity effects comes at paly. SAF of PGA at T= 0 sec shows more or less same amplitude in all the

three components however, a marked difference in the SAF can be seen in the period range of 0.5sec- 1sec sec while for period greater than 2 sec effect on SAF is not so relevant especially in NS and Z components. This can also be evident by looking at the GMH components which show significant amplification in the period range of 0.5sec to 1 sec and in the first 4000m of the cross section. We can conclude that:

i. Effect of period on SAF is more relevant in the period range of 0.5sec-1 sec.

ii. SAF amplitude decreases from north to south in the basin.

iii. By changing the source from north to south relevance of SAF shifts from EW to NS component however, Z component doesn't show marked variation in the SAF for a certain period.

5.1.2. EW Cross Section

a)

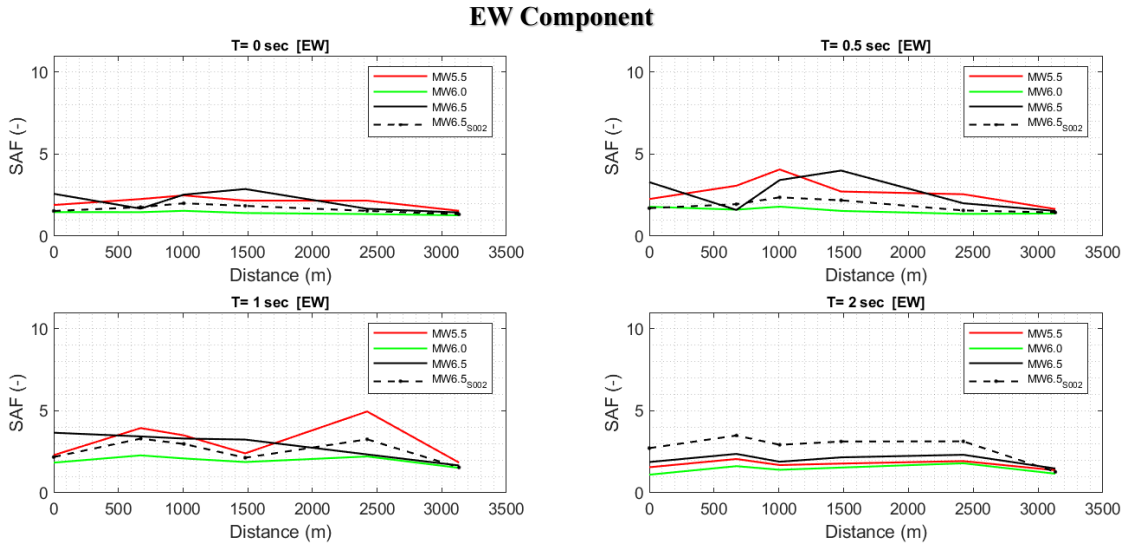

b)

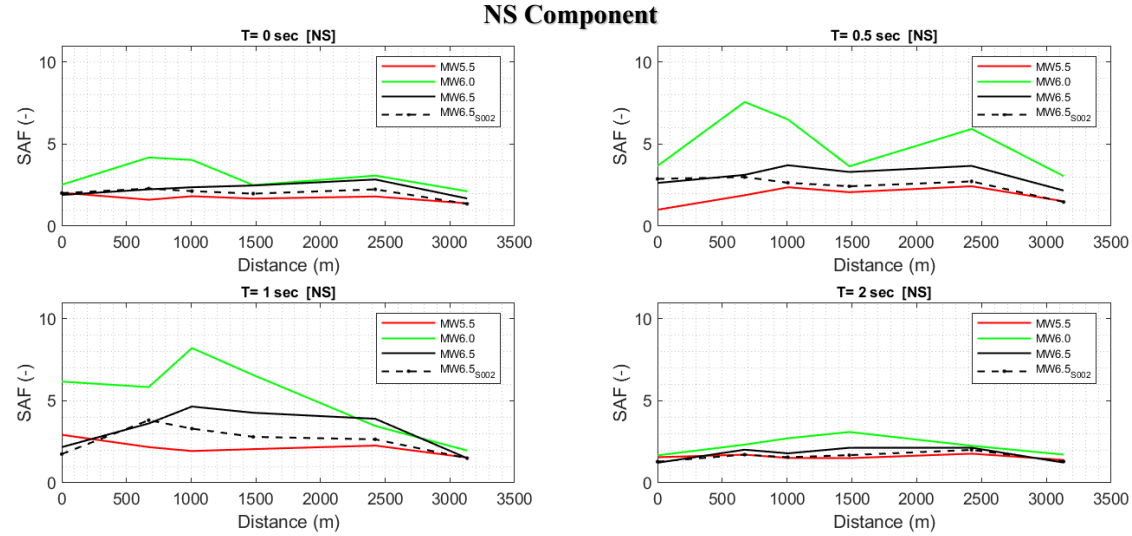

Figure 5-10 3D Ideal SAF a) EW Component, b) NS Component

a)

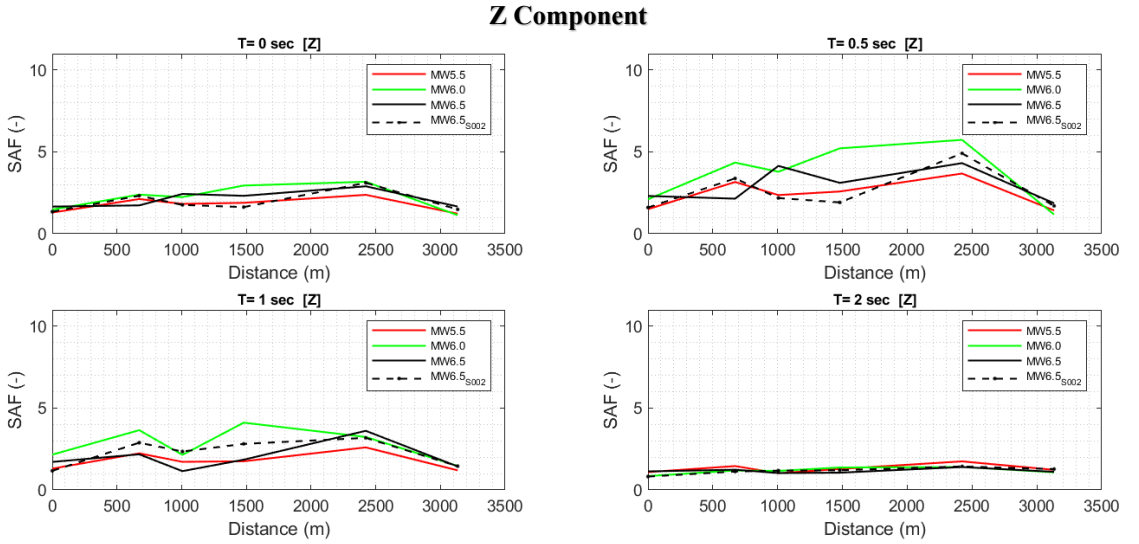

b)

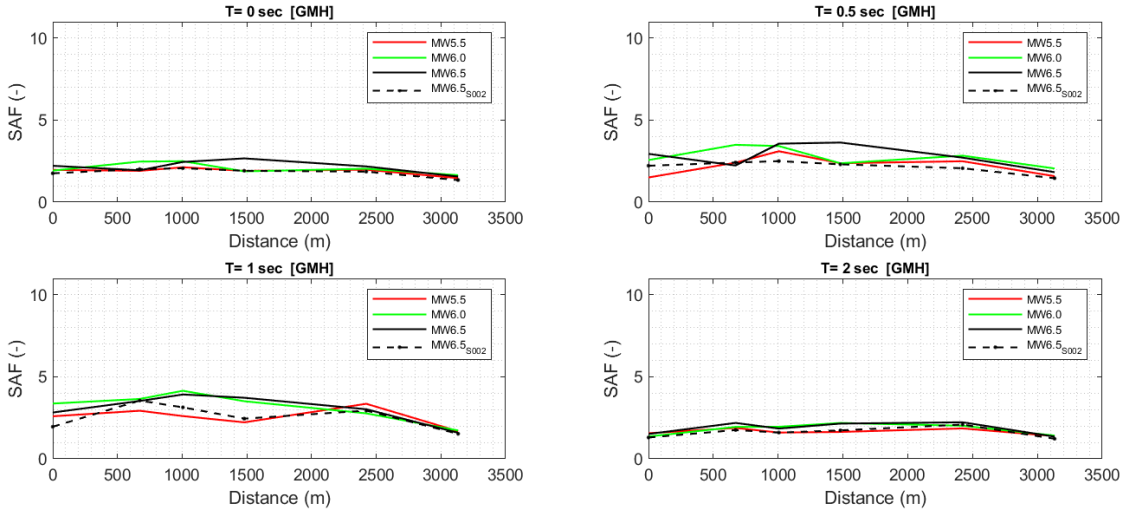

Figure 5-11 3D Ideal SAF a) Z Component , b) GMH Component

It can be seen in Figure 5-10 and Figure 5-11 that in general moving from west toward east the response of SAF is varies according to the soil profile characteristics shown in Figure 5-7. In general we have peaks in the SAF at deeper depth of sediments such as at 672m and 2423m .The response of NOR station which is located at one third of the EW cross section at about 1000 m shows similar SAF to the one observed at NRC station in the NS cross section in Figure 5-8 and Figure 5-9. As it has been stated in the previous section and it can be observed here too that by changing the source from northern part of basin to the south the relevance of SAF shifts from EW to NS and Z components. The period between 0.5sec-1sec is most relevant to observe scenario dependency of SAF. Moreover, it can also be inferred that there is least dependency of SAF on magnitude for the period T= 2 sec. From this discussion we can

reasonably determine the dependency of SAF on source , local site conditions and magnitude of earthquake so, we can conclude that:

i. The more relevant amplifications are shown in the period range of 0.5sec-1 sec.

ii. SAF varies from west to east depending on the local site conditions and peaks can be observed where the thickness of sediments is larger.

iii. By changing the source from north to south dominanacy of SAF shifts from EW to NS component however, Z component doesn't show marked variation in the SAF for a certain period.

5.2. Variability of 3D SAF with Reference Site

The comparison made in the previous section has been proven useful to predict spatial variation in SAF with respect to source, earthquake scenario and local site condition however, the SAF computed in this way is an ideal case as the same site and same simulation is considered as reference bed rock and to predict SAF in a more realistic way it is necessary to evaluate SAF by taking into consideration a real bedrock as reference site therefore, in this section we have considered some reference bedrock sites outside of the basin and dependency of SAF [NEL/OB_{Ref}] on reference bedrock is analysed for each site for the different earthquake scenarios.

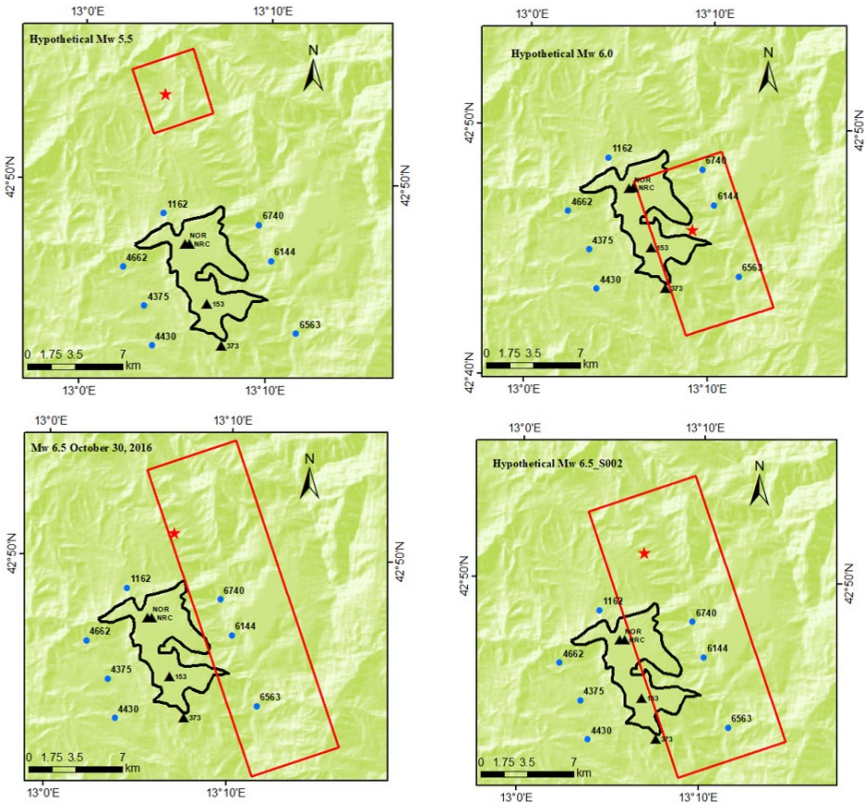

Figure 5-12 Reference Sites considered for the different earthquake scenarios

5.2.1. NRC Station

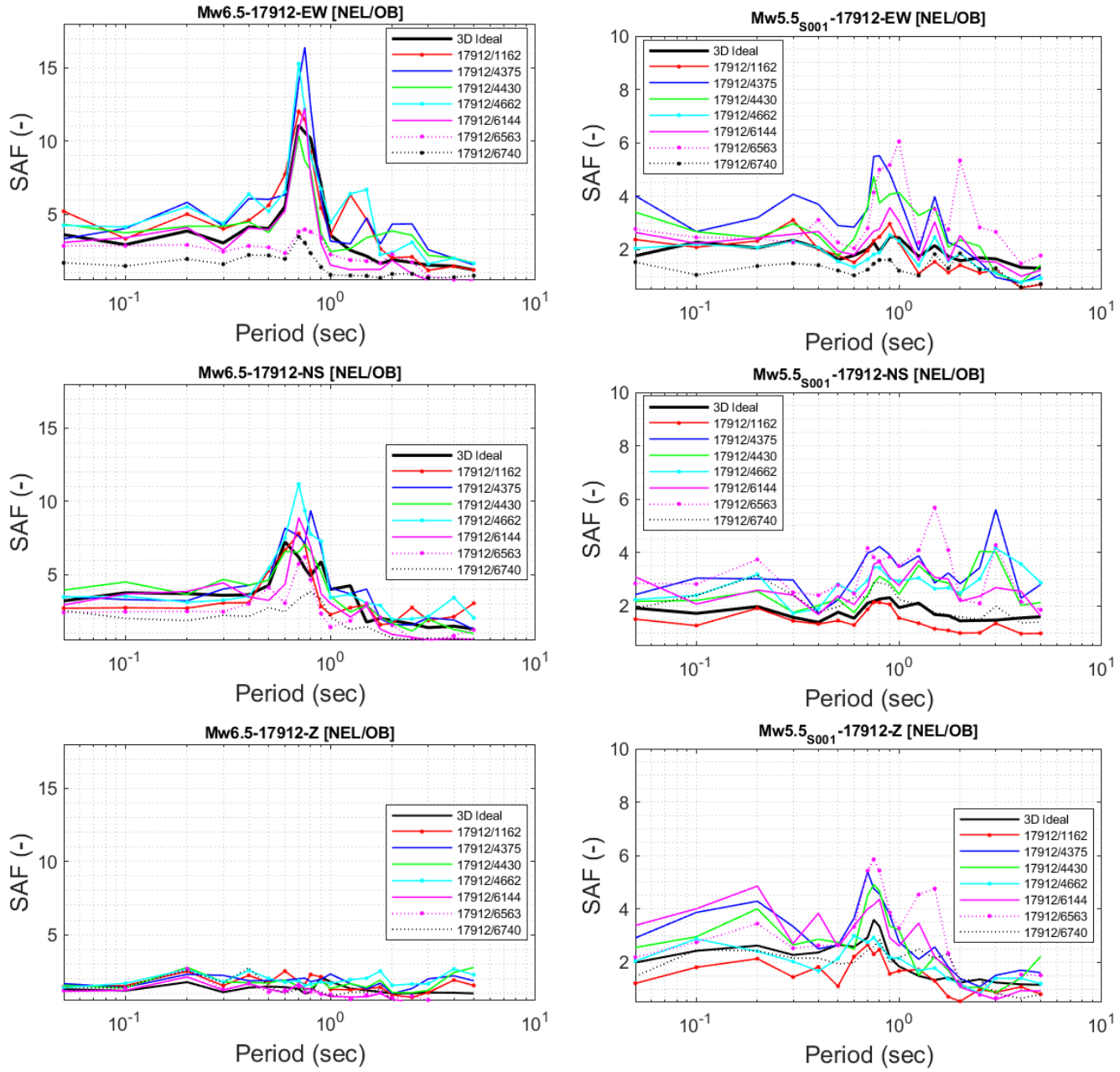

Figure 5-13 SAF dependency on reference site for NRC station in terms of EW, NS and Z components Left: October 30, 2016 Mw 6.5; Right: Hypothetical Scenario Mw5.5; Top to Bottom: Components EW, NS, Z

The selected reference sites are shown in Figure 5-12 and it can be seen that a total of seven reference sites have been selected in this study around the basin.

Analysis was performed for 6 sites along NS cross section and 5 sites along EW cross section however, for the sake of simplicity only NOR, NRC, 153 and 373 will be shown here in .

A comparison of different earthquake scenarios to assess the dependency of SAF on the reference bed rock sites have been made in terms of three components named as EW, NS and Z and compared with 3D ideal SAF in Figure 5-13 and Figure 5-14.

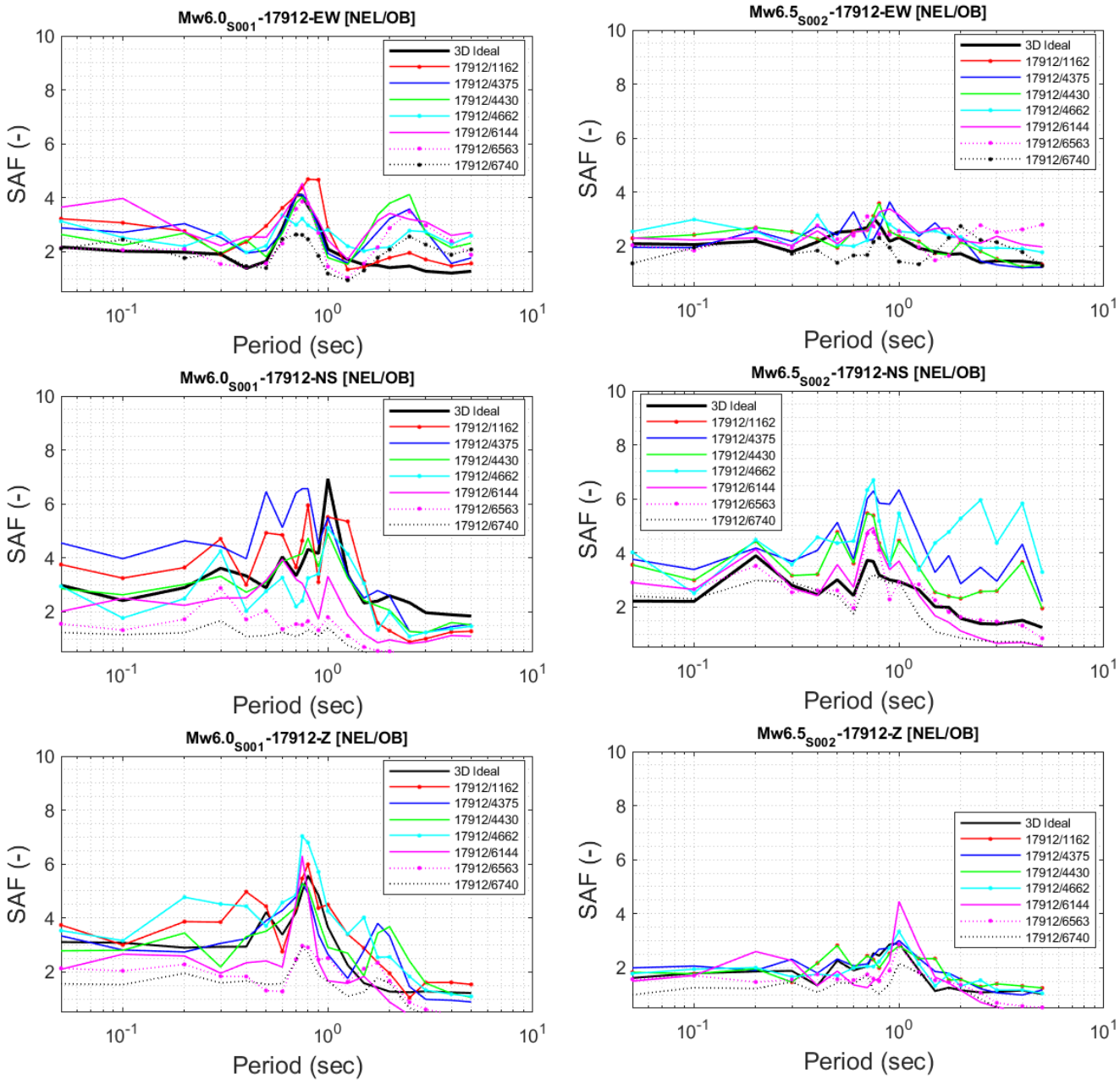

Figure 5-14 SAF dependency on reference site for NRC station in terms of EW, NS and Z components Left: Hypothetical Scenario Mw 6.0_S001; Right: Hypothetical Scenario Mw6.5_S002; Top to Bottom: Components EW, NS, Z

It is evident from the Figure 5-13 and Figure 5-14 that resonance occurs at around 0.75sec which is fundamental frequency of the site in the vicinity of the NOR station (Pourshayegan, 2019) in all the scenarios except the one with M_w 6.5_S002 where it occurs at around 0.9sec-1 sec especially in the Z component and after a period of 1 second we observe decay in the peak

in most of its components. In general we can observe that 3D ideal SAF is lower than real SAF in all the earthquake scenarios due to simplified assumption of considering basin as an outcropping bedrock except for M_w 6.0 where 3D ideal SAF is more or less similar to real SAF. It is evident that the SAF is highly dependent on source and magnitude of earthquake as by changing scenario we have amplification even in the vertical component which is not so relevant in the real event of M_w 6.5. It is obvious what has already stated in the previous section that for all the scenarios peak response of SAF is governed by EW component except in the case of M_w 6.0 where highest amplification is governed by NS component. The vital role of slip distribution in the spectral amplification can be predicted from M_w 6.5_S002 and M_w 6.5 which have same hypocentre but there is considerable difference between the SAF. In a more broader way we can observe that the sites on the left side (western part) of surface projection of fault show higher amplification as compared to those on the right side (eastern part) although this aspect appears to be wrong especially in the case M_w 5.5 where reference site 6563 results in same amplification as of site 4375 located o the left side. Such sensitivity of SAF towards site could be due to 3D complex wave propagation phenomenan.

5.2.2. NOR Station

A comparison of different earthquake scenarios to assess the dependency of SAF on the reference bed rock sites have been made in terms of three components named as EW, NS and Z and compared with 3D ideal SAF in Figure5-15 and Figure 5-16. It can be observed that resonance occurs at a frequency of about 0.75sec which is the fundamental frequency of the local site in that area. In comparison to NRC station we can see that the EW component is less amplified as compared to EW component of NRC however, NS component is more or less same. The difference in the amplification could be related to the thickness of sediments under the two station, NRC station having higher thickness of sediments results in to higher SAF while NOR station has lower thickness of sediments therefore, the SAF is relatively lesser in the case of NOR.

In addition to this it also evident that the reference sites on the left side of the surface projection of fault results into higher amplification as compared to those on the right side. It is worth noting that in case of M_w 6.0 the difference between 3D ideal and real SAF is not so considerable and the dependency of SAF on site is also not so pronounced especially in EW and Z component moreover, the peak value of SAF is governed by NS component. In general

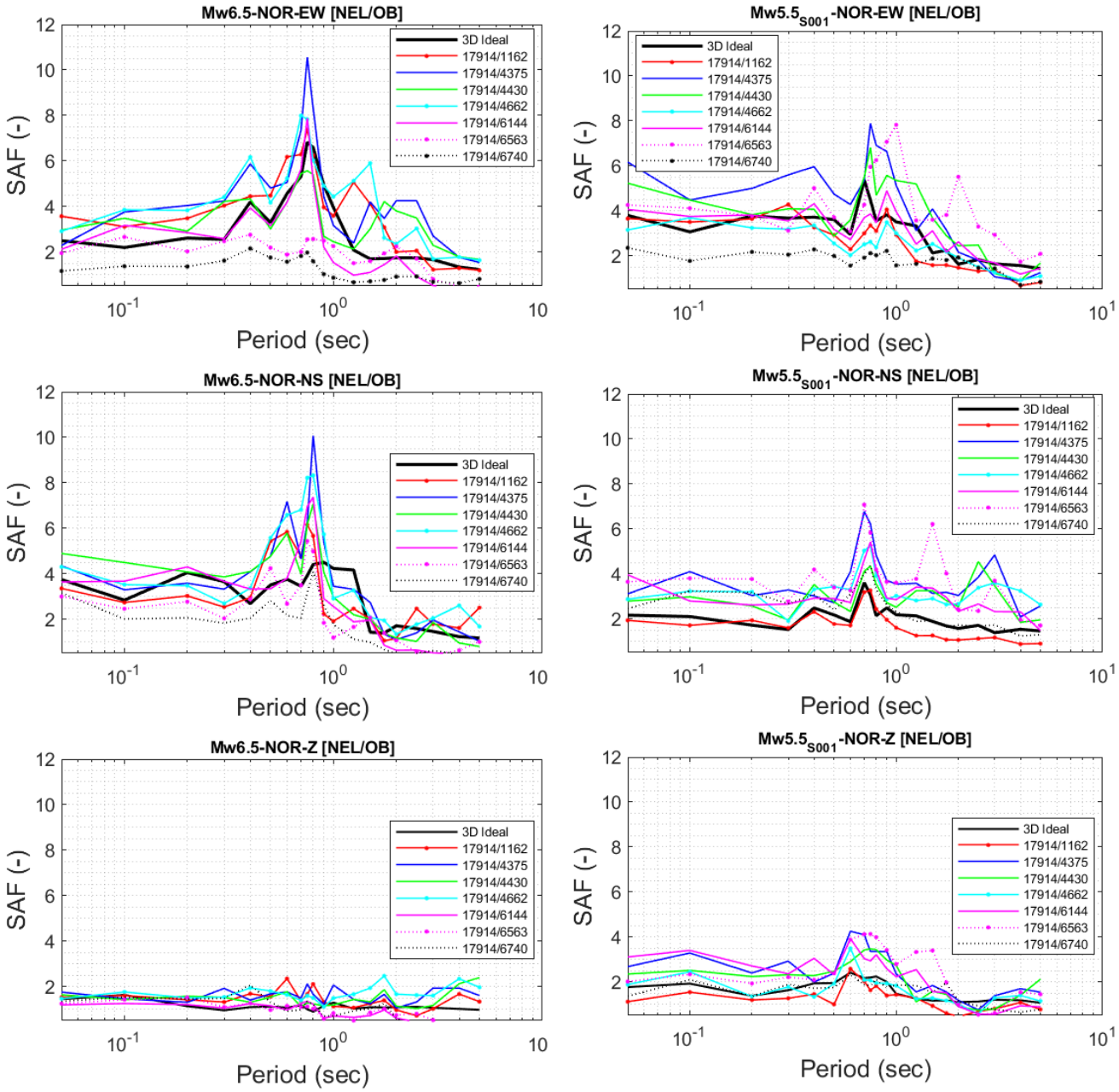

Figure 5-15 SAF dependency on reference site for NOR station in terms of EW, NS and Z components Left: October 30, 2016 Mw 6.5; Right: Hypothetical Scenario Mw5.5_S001; Top to Bottom: Components EW, NS, Z

SAF peak response is at NOR station is governed by horizontal components and role of vertical component is rather limited especially in case of M_w 6.5, M_w 6.5_S002 and M_w 5.5.

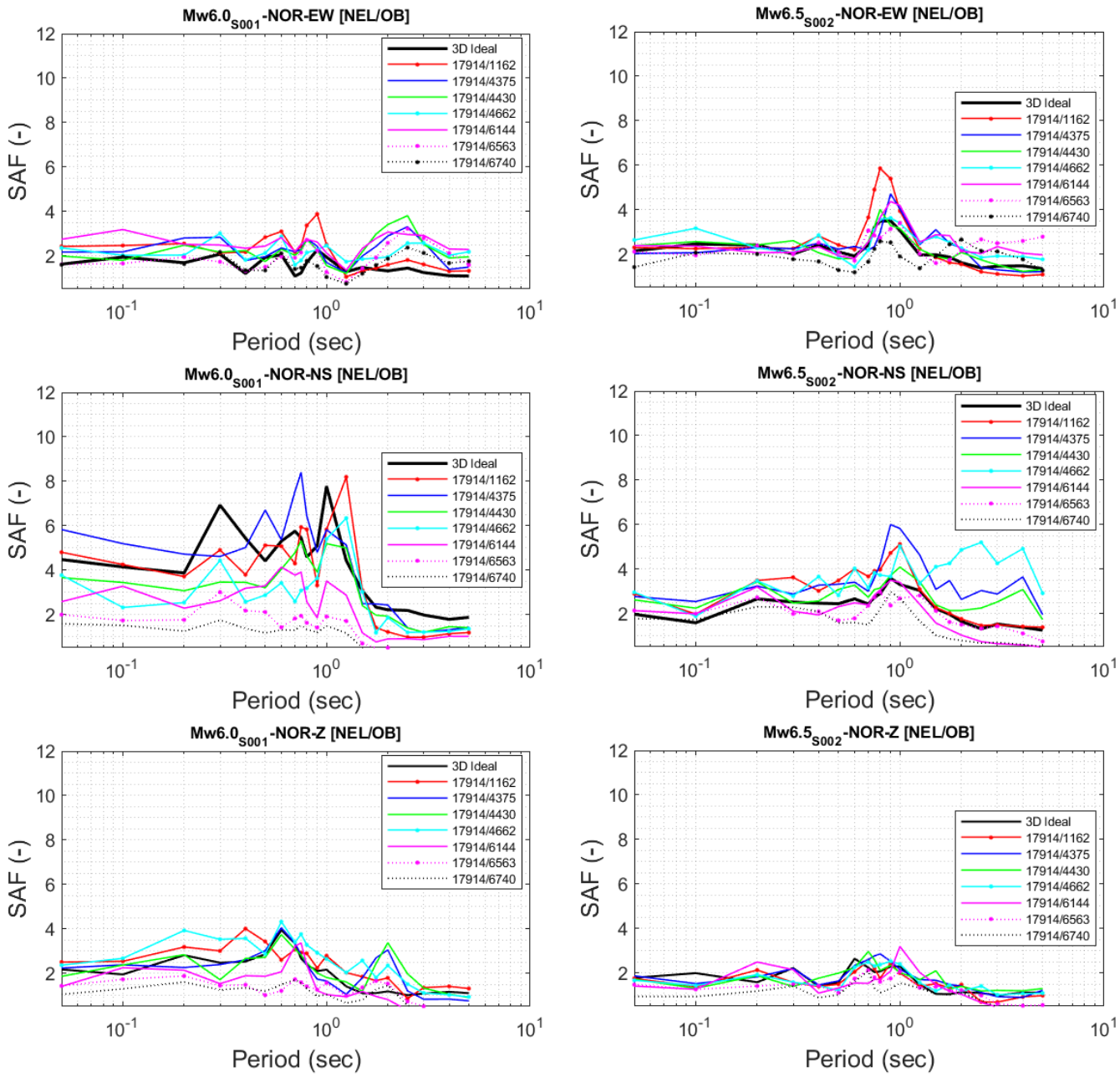

Figure 5-16 SAF dependency on reference site for NOR station in terms of EW, NS and Z components Left: Hypothetical Mw 6.0_S001; Right: Hypothetical Scenario Mw6.5_S002; Top to Bottom: Components EW, NS, Z

5.2.3. Receiver 153

A comparison of different earthquake scenarios to assess the dependency of SAF on the reference bed rock sites have been made in terms of three components named as EW, NS and Z and compared with 3D ideal SAF in Figure 5-17and Figure 5-18. It is inferred from the trends that peak response of SAF is observed around 0.75sec-0.9sec. Moreover, the 3D Ideal SAF tends to be lower than the real SAF in horizontal components of all the earthquake

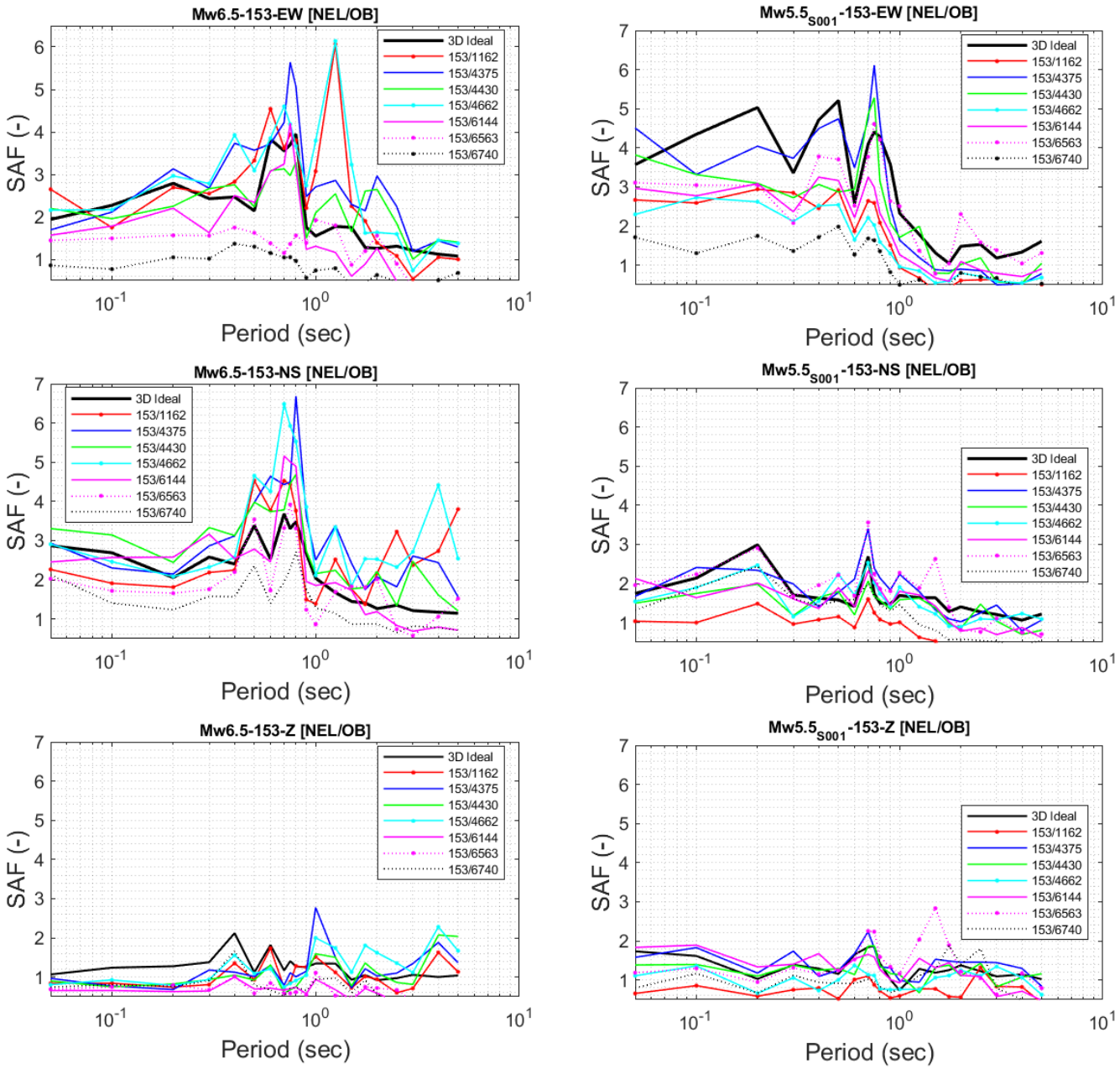

Figure 5-17 SAF dependency on reference site for receiver point 153 in terms of EW, NS and Z components Left: October 30, 2016 Mw 6.5; Right: Hypothetical Scenario Mw5.5_S001; Top to Bottom: Components EW, NS, Z

scenarios however, peak response in vertical component of all the scenarios is more or less similar in both ideal and outcropping bedrock case. It is worth noting that 153 located towards south of the basin and we can clearly observe a decay in the peak response of SAF as compared to NOR and NRC station. This aspect is more dominant in the horizontal components of M_w 6.5 and M_w 5.5. Effect of position of source on the SAF is also relevant and can be observed in M_w 6.0 having its source located in the southern part and we can observe higher amplification in NS component as compared to EW component. In general sites located on the right to the surface projection of fault predict lower SAF as compared to those present on the left.

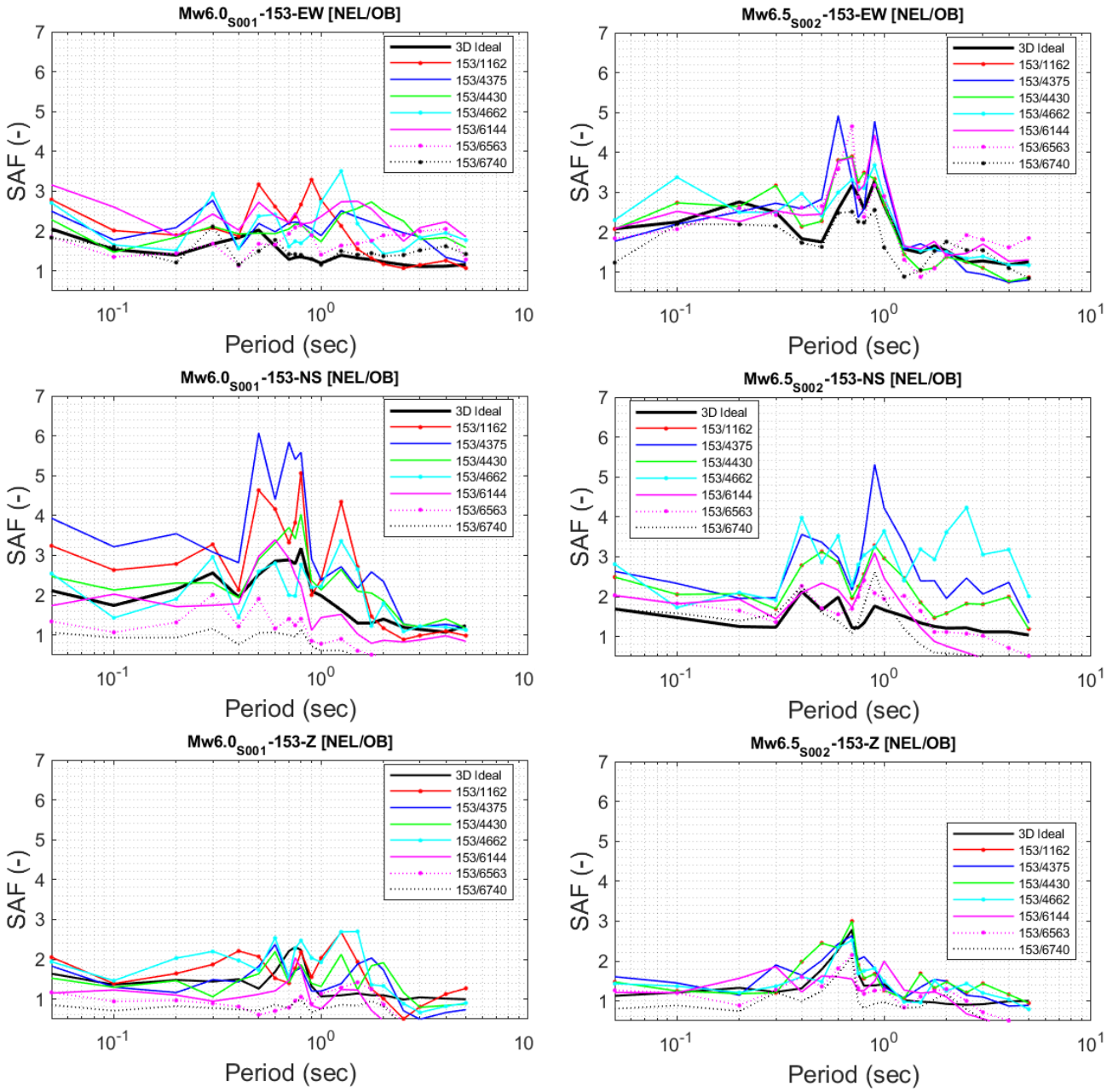

Figure 5-18 SAF dependency on reference site for receiver point 153 in terms of EW, NS and Z components Left: Hypothetical Mw 6.0_S001; Right: Hypothetical Scenario Mw6.5_S002; Top to Bottom: Components EW, NS, Z

5.2.4. Receiver 373

A comparison of different earthquake scenarios to assess the dependency of SAF on the reference bed rock sites have been made in terms of three components named as EW, NS and Z and compared with 3D ideal SAF in Figure 5-19 and Figure 5-20 and It is inferred from the trends that peak response of SAF is observed around 0.7sec-1sec. We can observe shift in the resonance towards higher period this could be due to the fact that it is located near the boundary of the basin and have relatively lower depth of sediments. What has already observed at the other sites can be inferred in this case too that the SAF tends to have higher amplitude

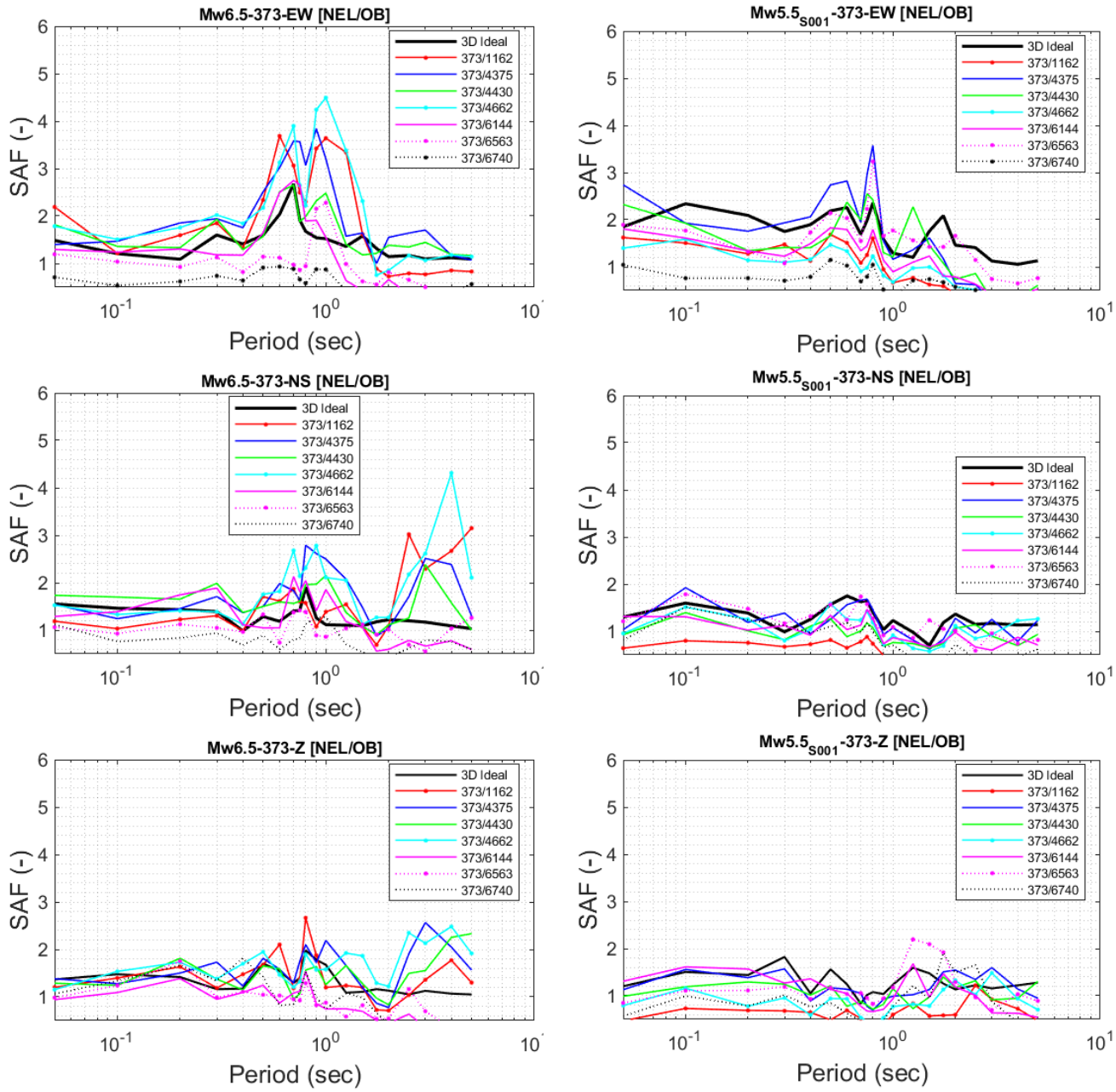

Figure 5-19 SAF dependency on reference site for receiver point 373 in terms of EW, NS and Z components Left: October 30, 2016 Mw 6.5; Right: Hypothetical Scenario Mw5.5; Top to Bottom: Components EW, NS, Z

for the reference located on the left side of surface projection of fault as compared to those on the right side.

5.2.1. Concluding Remarks on SAF Analysis

By taking into consideration the comparison done so far in this section we can reasonably conclude that:

i. Highest amplitude of SAF about 15 is observed in EW component at NRC station and moving toward south we observe are decay in the SAF to a value of 5 and this

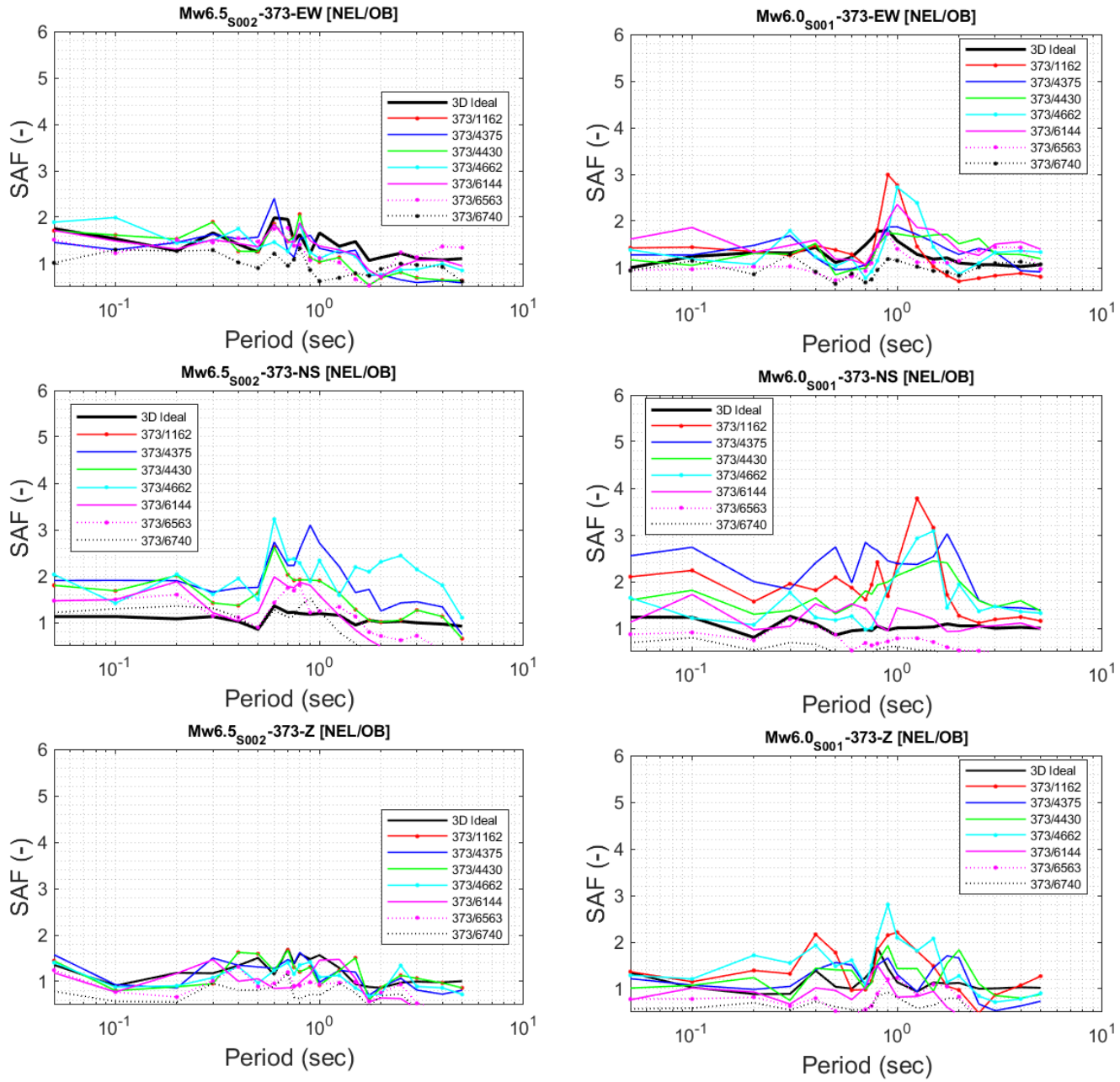

Figure 5-20 SAF dependency on reference site for receiver point 373 in terms of EW, NS and Z components Left: Hypothetical Scenario Mw 6.5_S002; Right: Hypothetical Scenario Mw 6.0_S001; Top to Bottom: Components EW, NS, Z

decrease is in agreement with the depth of sediment which decreases from north to south as shown in Figure 5-7.

ii. We observe resonance in a relatively narrow range of period 0.7sec-1.2sec i.e.(1.43Hz-0.75Hz) and this is highly dependent on the scenario while for period greater than 2sec (0.5Hz) we observe de amplification. The fact that the differences between the spectral ratios are strongly period dependent suggests that not only the

distance of reference site from the source but also a complex wave propagation pattern from the source to the basin may have a prevailing role in affecting ground motions at outcropping bedrock.

iii. We observed that the effect of source is vital in the amplification and it is evident that by changing source from north towards south as it is in M_w 6.0 we observe higher amplification of NS and Z component as compared to EW component.

iv. In general local site response of Norcia basin is governed by the horizontal component of seismic input however, vertical component also shows higher amplification in some cases.

v. Analysis of spatial variability in SAF with respect to reference sites depicts that in a broader sense the reference sites located leftward from the surface projection of fault results in higher amplitude of SAF as compared to those located on the right side in all the earthquake scenarios.

6. Conclusions

In this study 3D physics-based approach, including the ANN technique for the high-frequency part applied to produce broad band time histories to overcome the limit in the numerical resolution of 3D Physics based simulation has proven to be very useful as the results predicted by broadband simulations show a good agreement with the ground motion recorded at recording stations. In chapter 3 a comparison between BB simulated and recorded time histories is shown in terms of Acceleration, Velocity and Displacement for 4 stations named as NRC, NOR, CLO and CNE and we observe that numerical model in a broader sense properly simulates the real response obtained at the recording stations. Furthermore, to assess the validity of numerical model in the frequency domain analyses were performed in terms of FAS (Fourier Amplitude Spectra), RS (Response Spectra) and S_d (Spectra Displacement) and the results can be summarised as follows:

- FAS depicts the enrichment of wave in higher frequencies by keeping the low frequency wave form such as below 1Hz practically invariant and BB predicts almost same amplitude as of recording stations especially at NOR and NRC station which lie within the basin and are more prone towards complex 3D wave propagation effects . This aspect clearly states the validity of BB simulation in the low frequency range. Moreover, peaks in FAS can be seen at around 1.3Hz which corresponds to the fundamental frequency of the basin.
- RS in terms of pseudo spectra acceleration illustrates that BB simulations underpredict real response obtained at recording station however, BB response in the shorted period (below 0.75sec) overcomes the numerical limitation of 3D PBS and the underprediction in response of BB this may be due to the fact that 3D model on outcropping bedrock is too rigid (Vs=1700 m/s) and may underestimate the actual amplitudes.
- From the analysis of displacement waveforms presented in chapter 4 we can reasonably conclude that In a broader sense numerical model is able to preserve permanent displacement as of real recording stations for longer periods.
- Shake maps indicates that BB simulations are in good agreement with recorded peak ground values especially in the near source region and more specifically at NRC and NOR station. Concentration of peak values is in the north eastern part due to up dip directivity effects.

- In general the response in the basin shows higher amplitude in the horizontal components.

In chapter 4 spatial variability of SAF (Spectral Amplification function) is quantified for 2 stations named as NCR and NRC and 2 receiver points such as 153 and 373 for four earthquake scenarios having different slip distribution, hypocentre location and magnitude. In addition to this dependence of 3D ideal SAF on the scenario and spatial location is analysed. In order to better understand response SAF was analysed along the two cross sections named as EW and NS for four different periods such as T=0sec, 0.5sec, 1sec and 2 sec. In the end variability of SAF with respect to reference bedrock is quantified for the selected sites and the results of analysis can be summarised as:

- Highest SAF amplitude of about15 is observed in EW component at NRC station and moving toward south we observe decay in the SAF to a value of 5 and this decrease is in agreement with the depth of sediment which decreases from north to south
- We observed that the effect of source is vital in the amplification and it is evident that by changing source from north towards south as it is in M_w 6.0 we observe higher amplification of NS and Z component as compared to EW component.
- In general local site response of Norcia basin is governed by the horizontal component of seismic input however, vertical component also shows higher amplification in some cases.
- Analysis of spatial variability in SAF with respect to reference sites depicts that in a broader sense the reference sites located leftward from the surface projection of fault results in higher amplitude of SAF as compared to those located on the right side.
- Effect of period on SAF is more relevant in the period range of 0.5sec-1 sec

Appendix I

Comparison between simulated and BB Time histories

Station ACC

EW Component **NS Component** **Z Component**

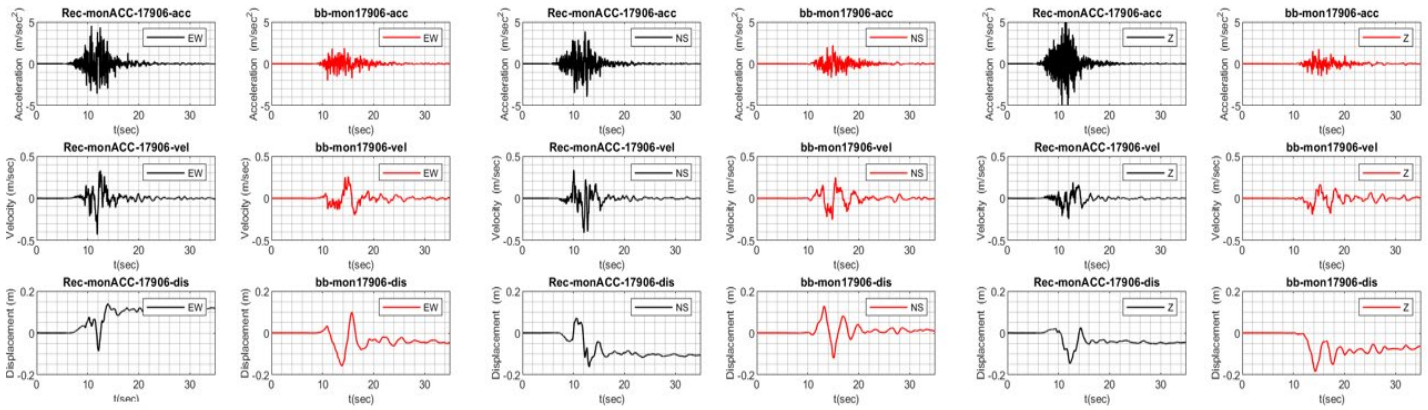

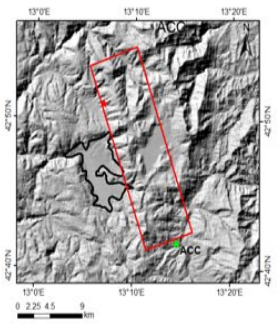

Fourier Amplitude Spectra (FAS)

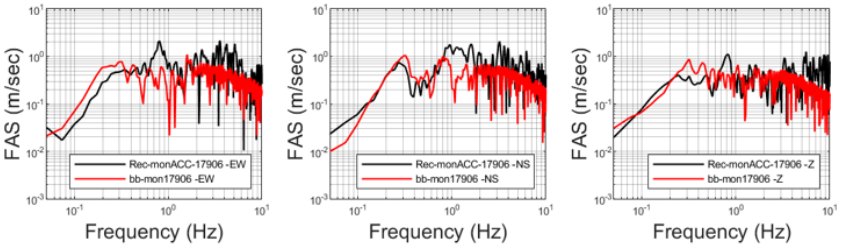

Spectral Displacement (Sd)

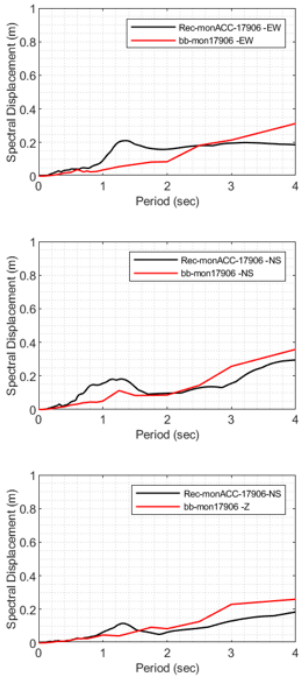

Response Spectra (RS)

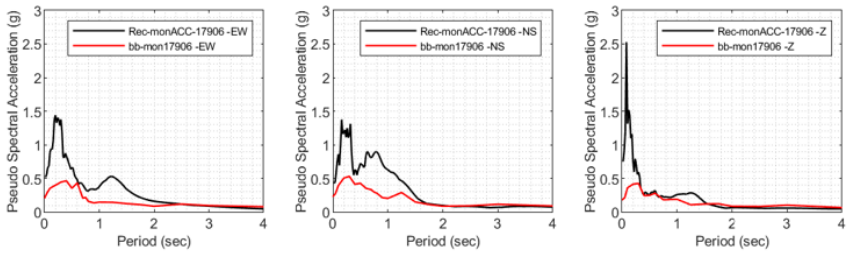

Station AMT

EW Component | **NS Component** | **Z Component**

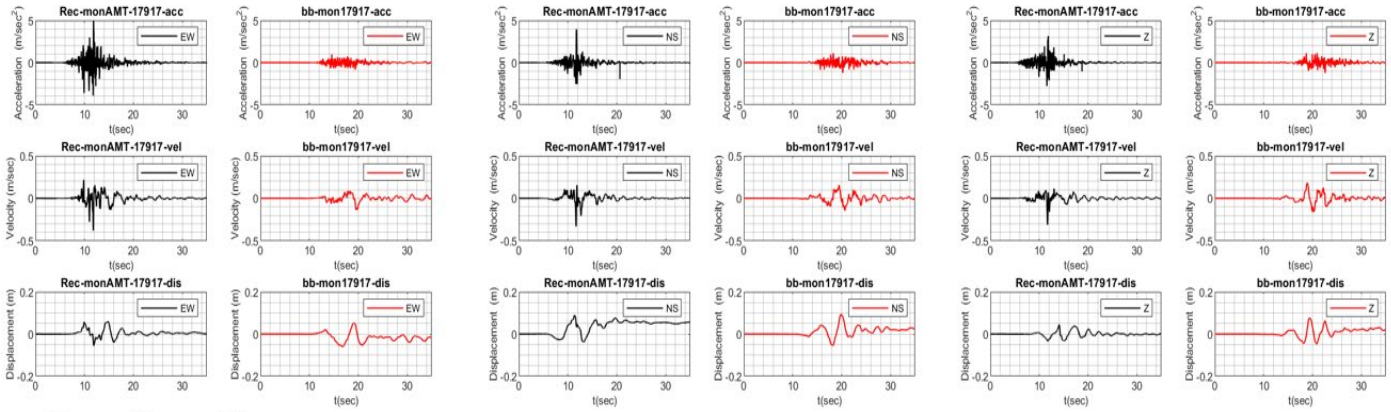

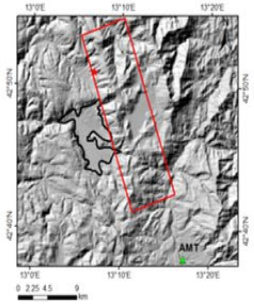

Fourier Amplitude Spectra (FAS)

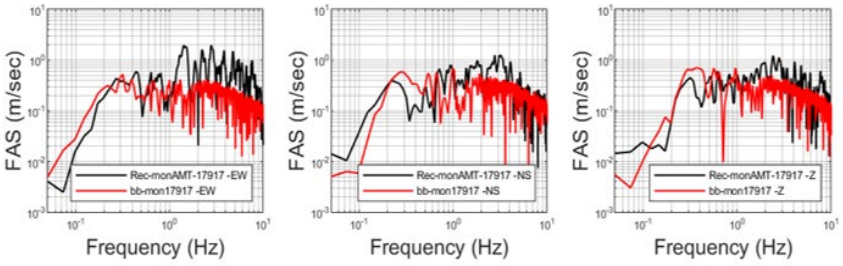

Spectral Displacement (Sd)

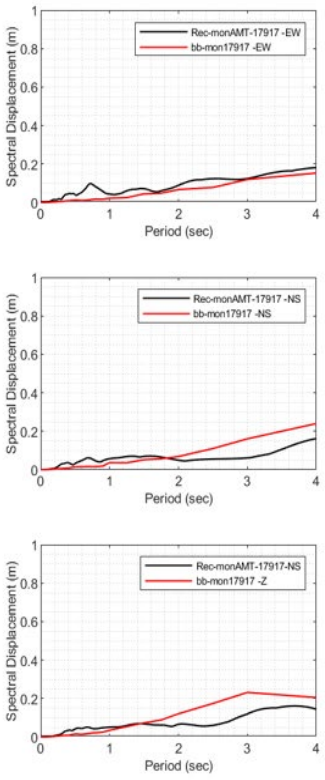

Response Spectra (RS)

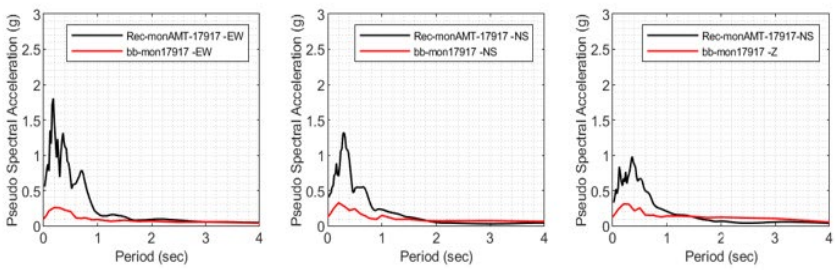

Station ICT

EW Component | **NS Component** | **Z Component**

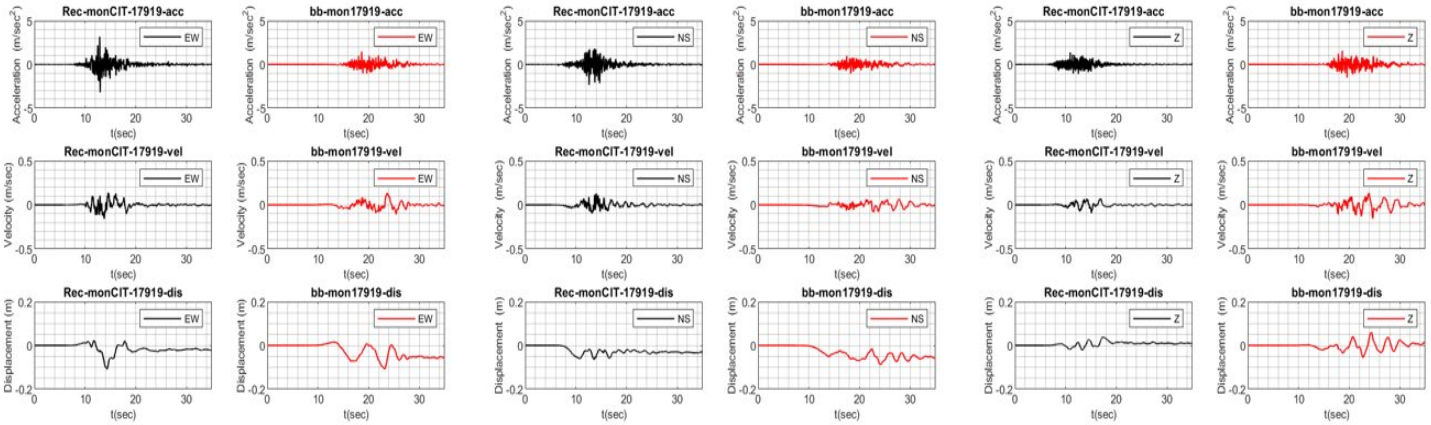

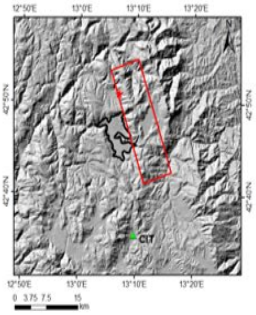

Fourier Amplitude Spectra (FAS)

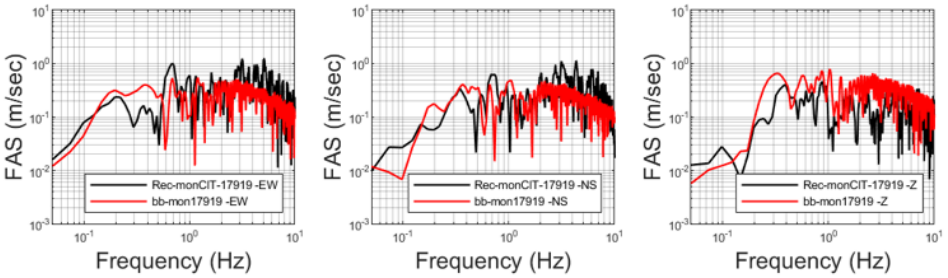

Spectral Displacement (Sd)

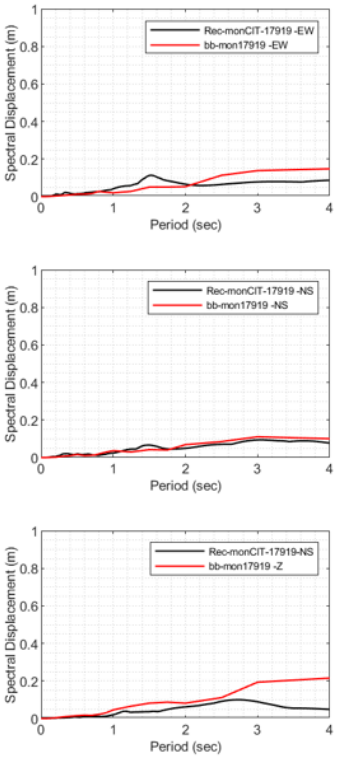

Response Spectra (RS)

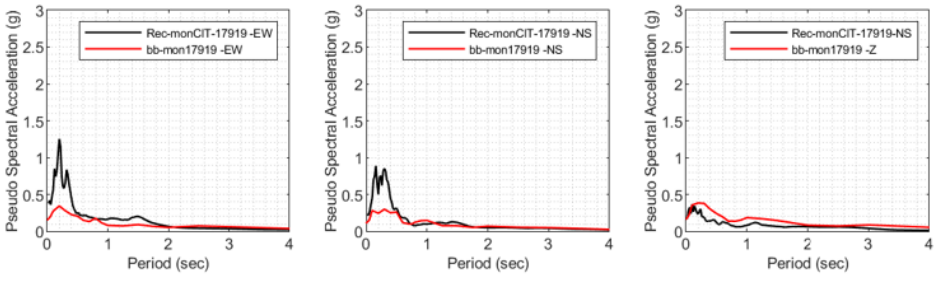

Station CSC

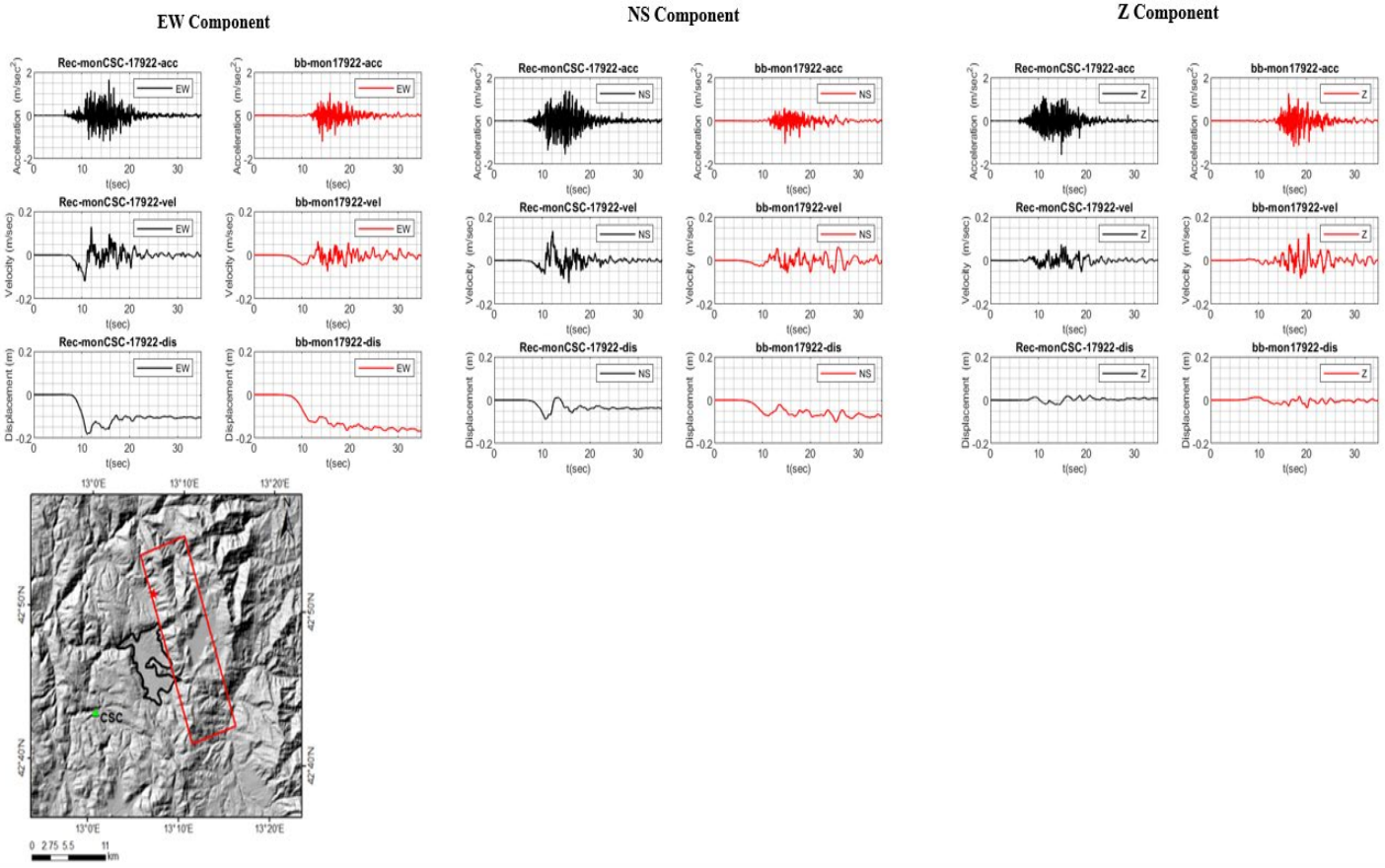
EW Component
NS Component
Z Component
Rec-monCSC-17922-acc
bb-mon17922-acc
Rec-monCSC-17922-vel
bb-mon17922-vel
Rec-monCSC-17922-dis
bb-mon17922-dis
Acceleration (m/sec²)
Velocity (m/sec)
Displacement (m)
t(sec)
EW
NS
Z
CSC
13°0'E
13°10'E
13°20'E
42°50'N
42°40'N
0 2.75 5.5 11
km

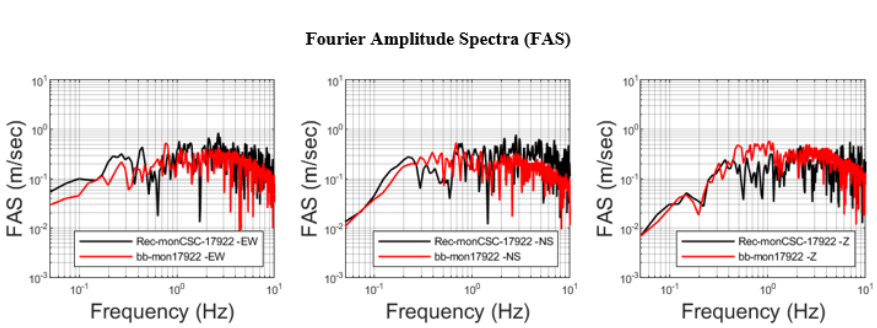
Fourier Amplitude Spectra (FAS)
FAS (m/sec)
Frequency (Hz)
Rec-monCSC-17922 -EW
bb-mon17922 -EW
Rec-monCSC-17922 -NS
bb-mon17922 -NS
Rec-monCSC-17922 -Z
bb-mon17922 -Z

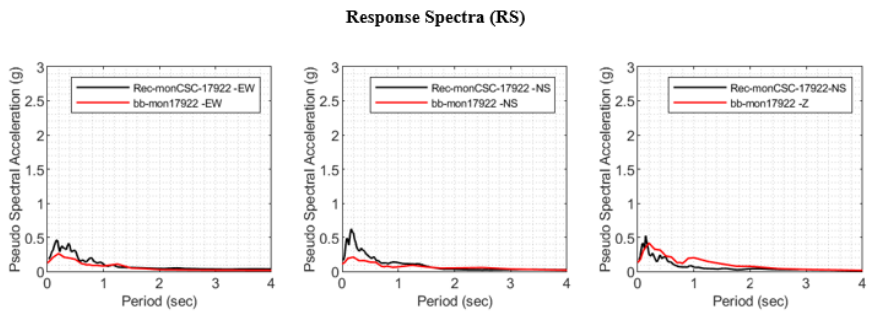
Response Spectra (RS)
Pseudo Spectral Acceleration (g)
Period (sec)
Rec-monCSC-17922 -EW
bb-mon17922 -EW
Rec-monCSC-17922 -NS
bb-mon17922 -NS
Rec-monCSC-17922-NS
bb-mon17922 -Z

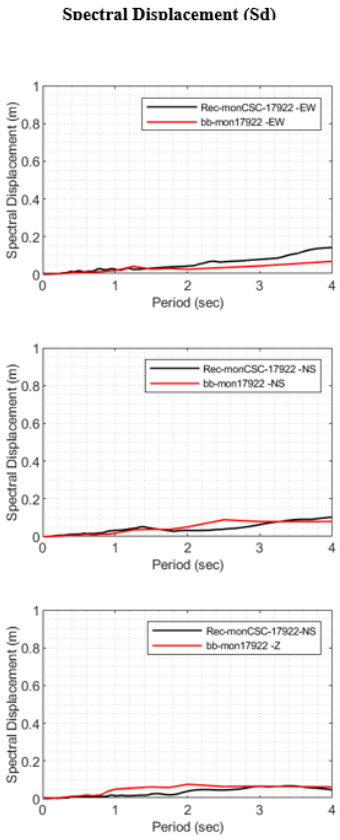
Spectral Displacement (Sd)
Spectral Displacement (m)
Period (sec)
Rec-monCSC-17922 -EW
bb-mon17922 -EW
Rec-monCSC-17922 -NS
bb-mon17922 -NS
Rec-monCSC-17922-NS
bb-mon17922 -Z

Station MCV

EW Component

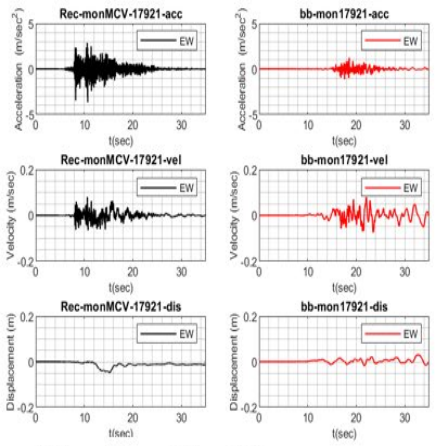

NS Component

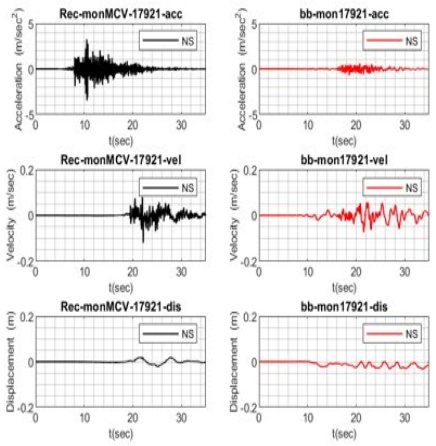

Z Component

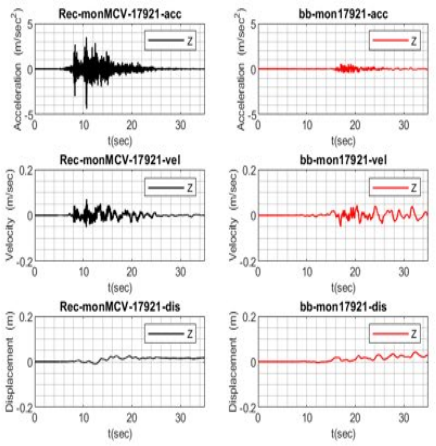

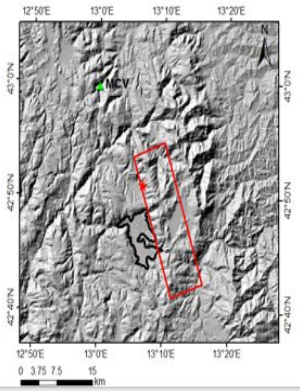

Fourier Amplitude Spectra (FAS)

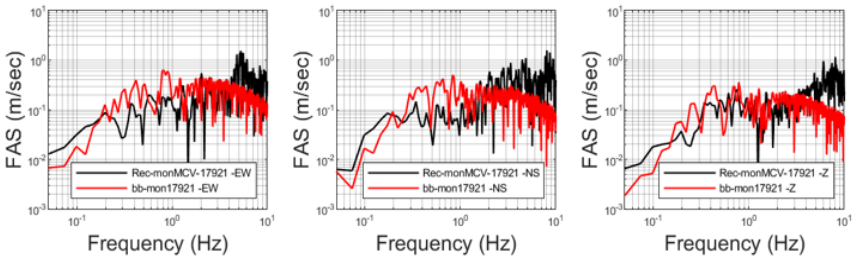

Spectral Displacement (Sd)

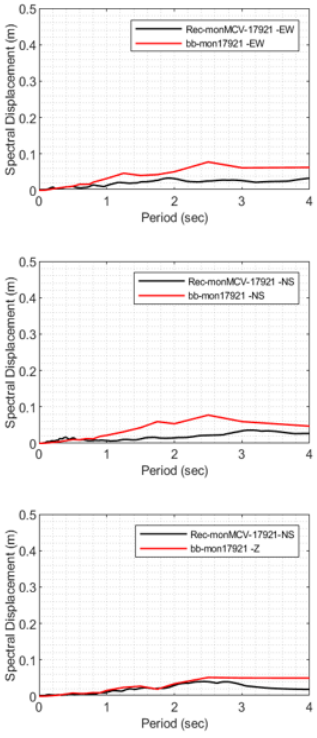

Response Spectra (RS)

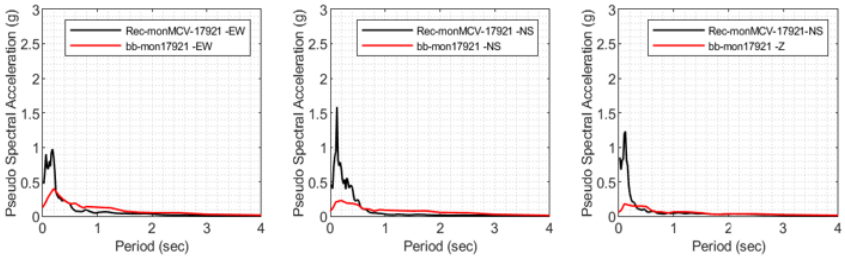

MMO Station

EW Component | **NS Component** | **Z Component**

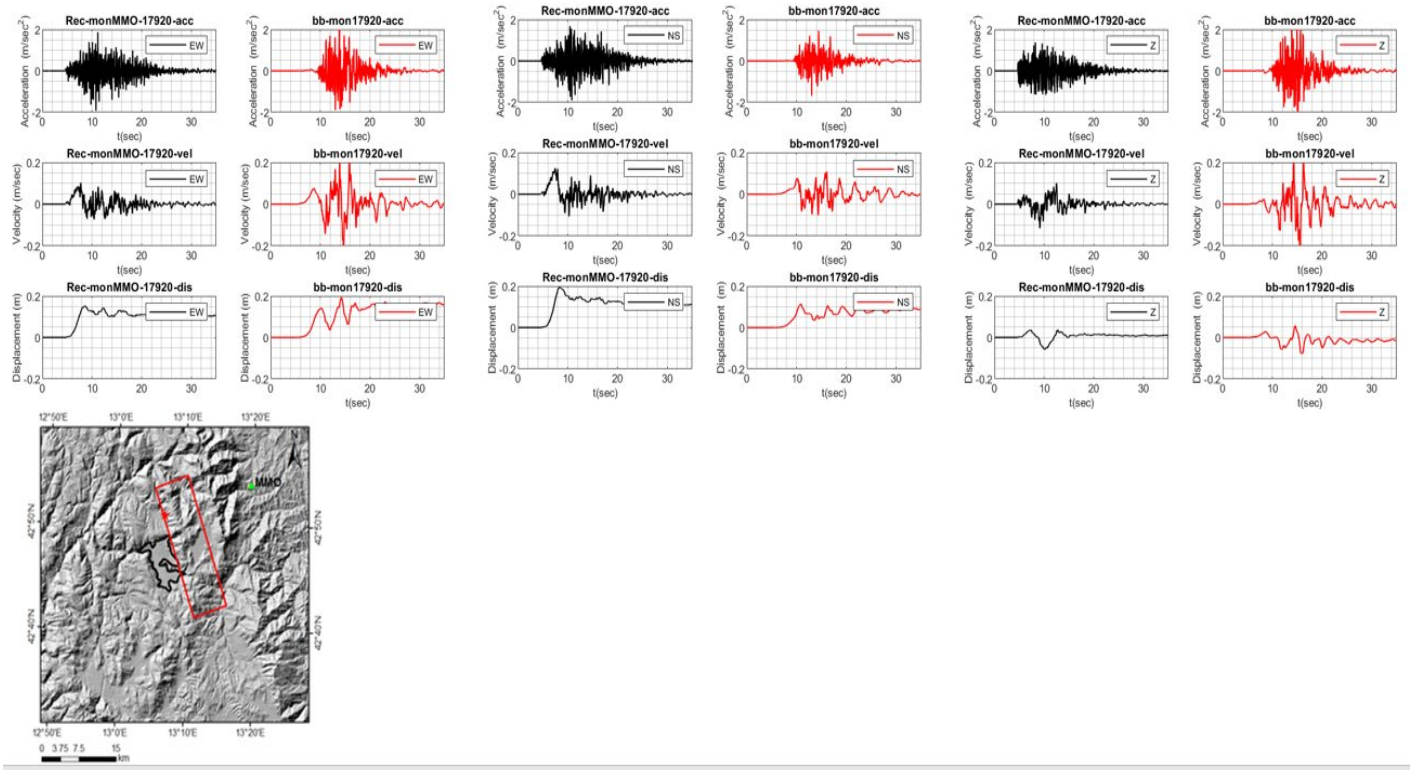

Fourier Amplitude Spectra (FAS)

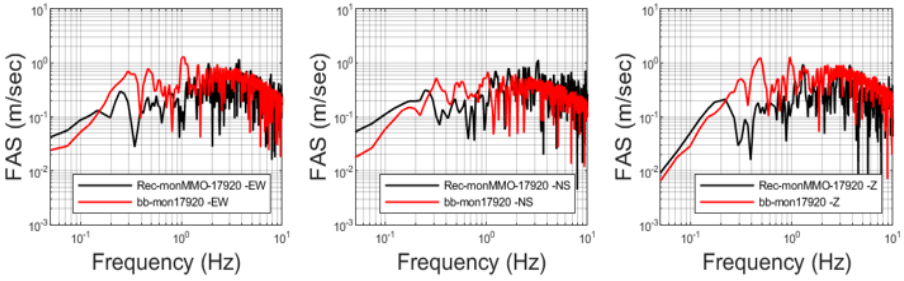

Spectral Displacement (Sd)

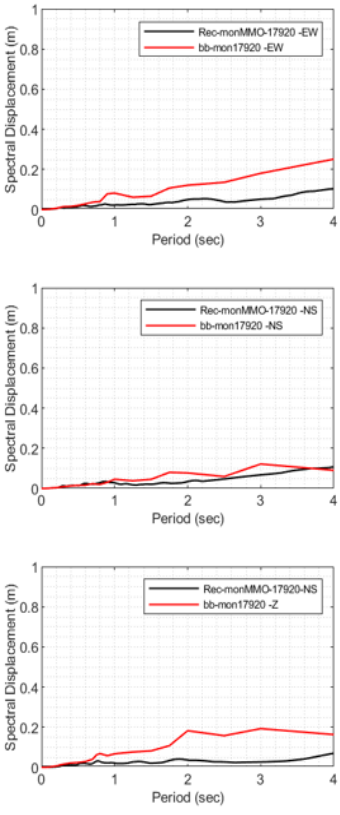

Response Spectra (RS)

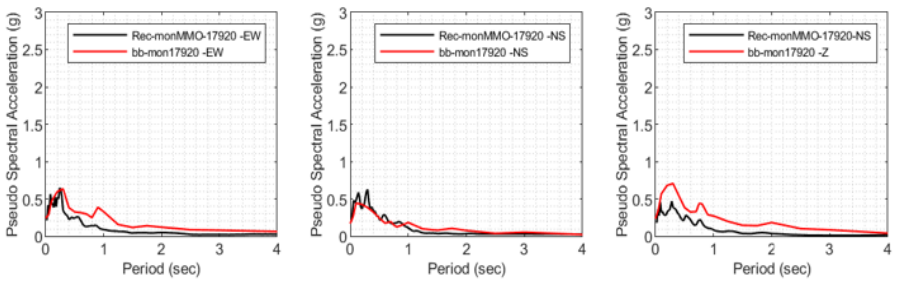

Station PRE

EW Component

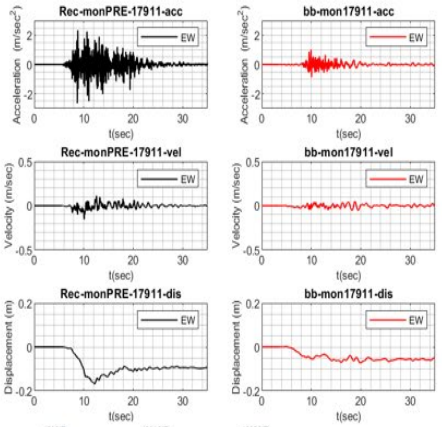

NS Component

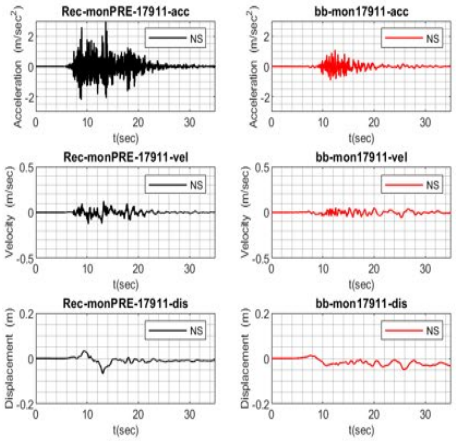

Z Component

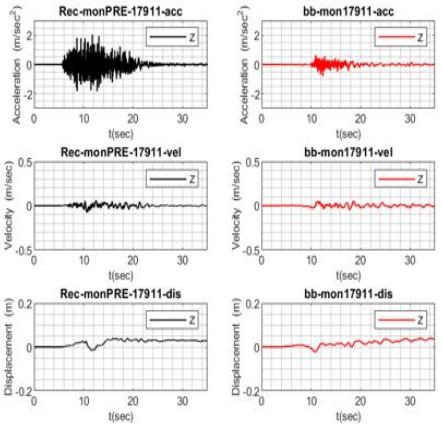

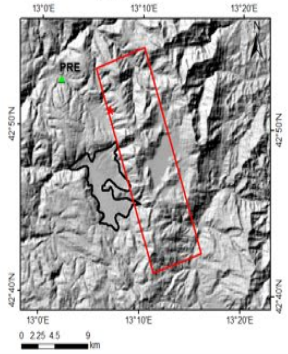

Fourier Amplitude Spectra (FAS)

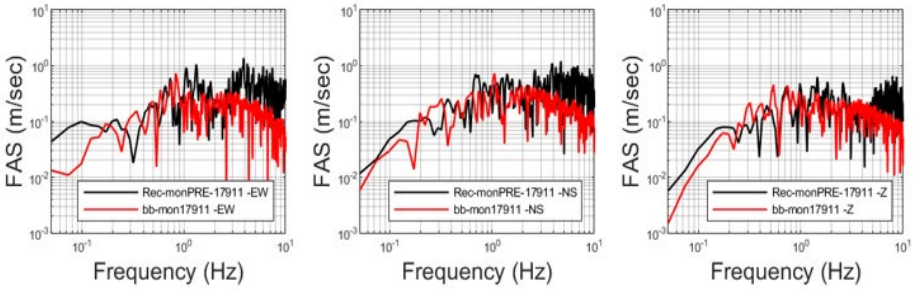

Spectral Displacement (Sd)

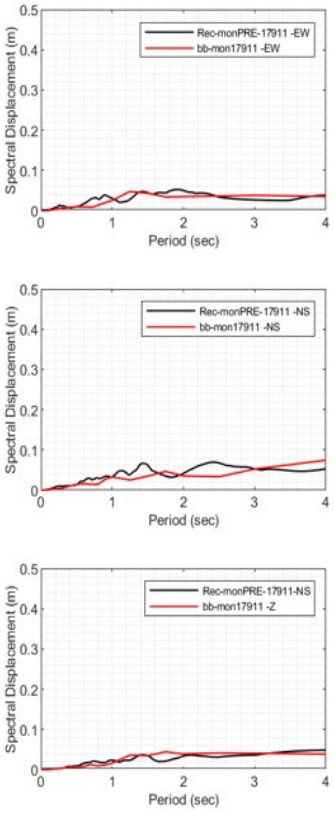

Response Spectra (RS)

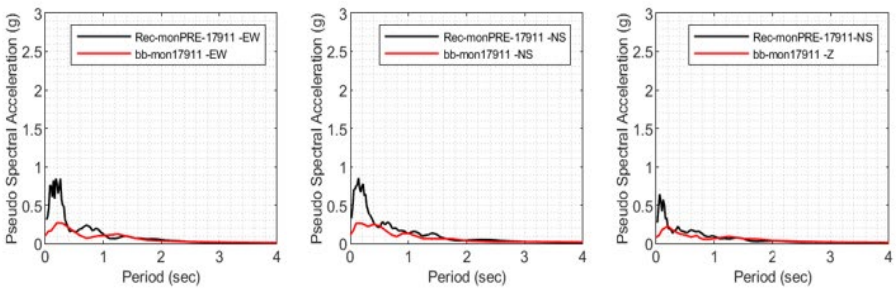

Station T1212

EW Component

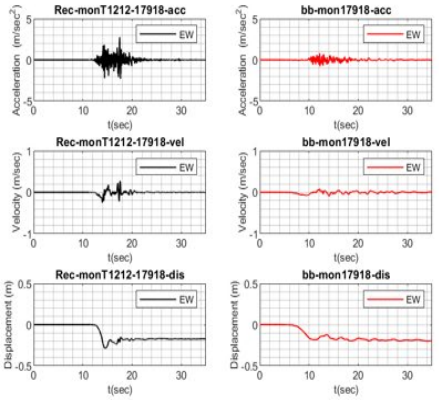

NS Component

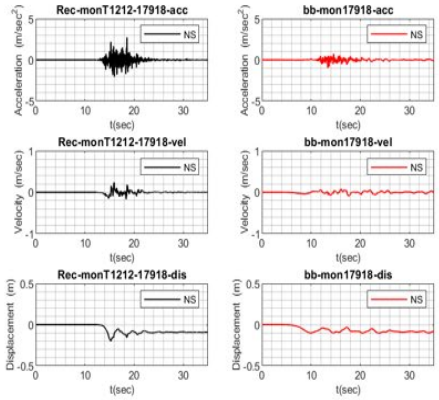

Z Component

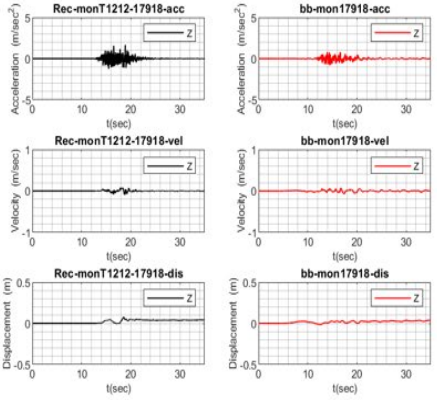

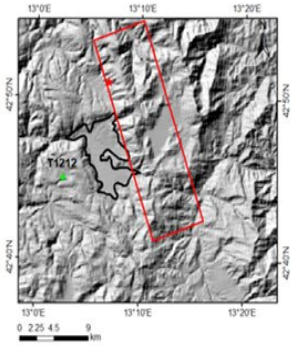

Fourier Amplitude Spectra (FAS)

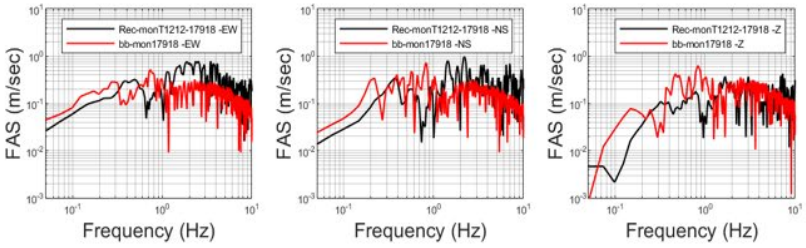

Spectral Displacement (Sd)

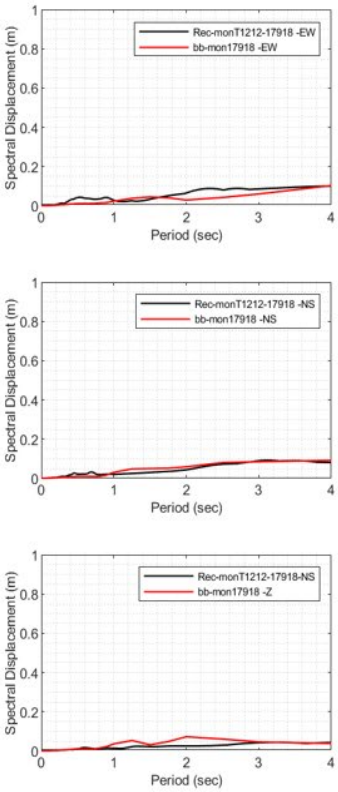

Response Spectra (RS)

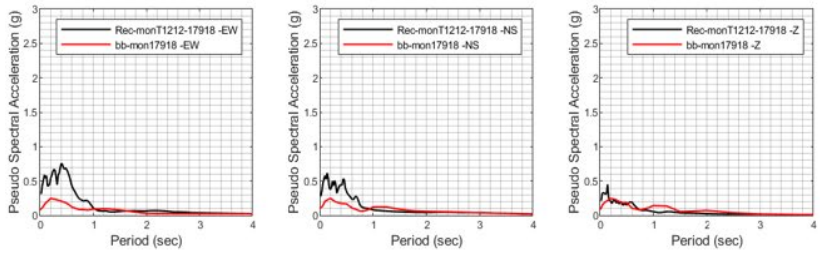

Station T1213

EW Component

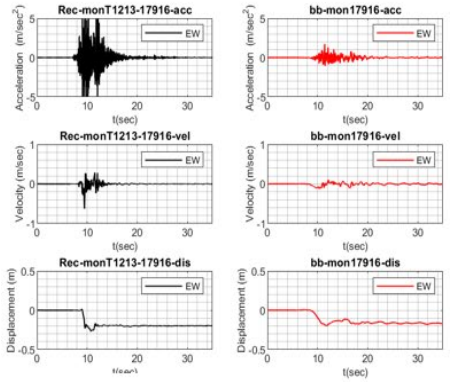

NS Component

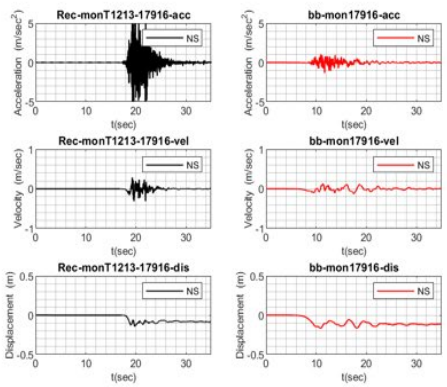

Z Component

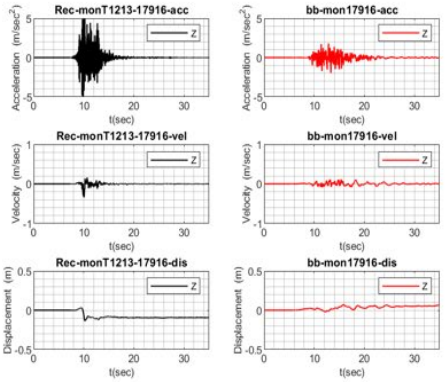

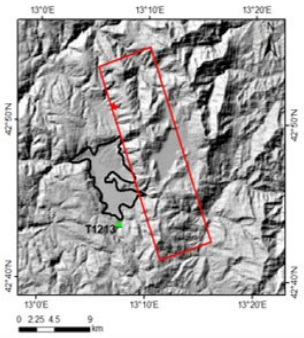

Fourier Amplitude Spectra (FAS)

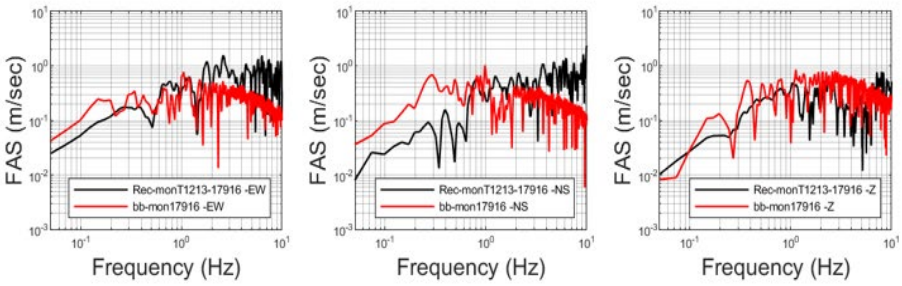

Spectral Displacement (Sd)

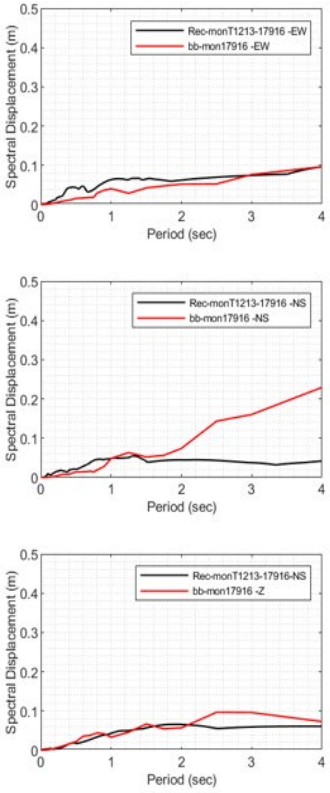

Response Spectra (RS)

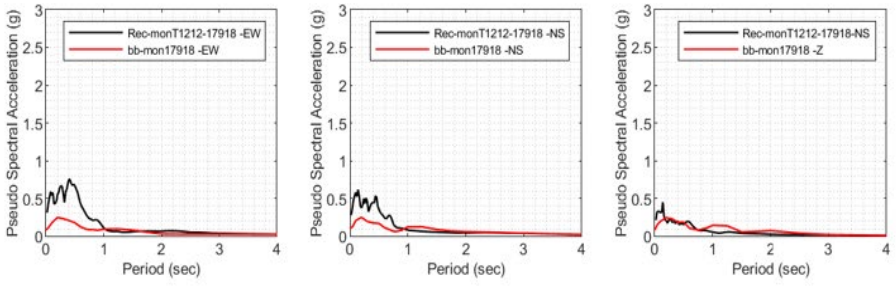

Dependence of SAF on Reference Site

Receiver Point 142

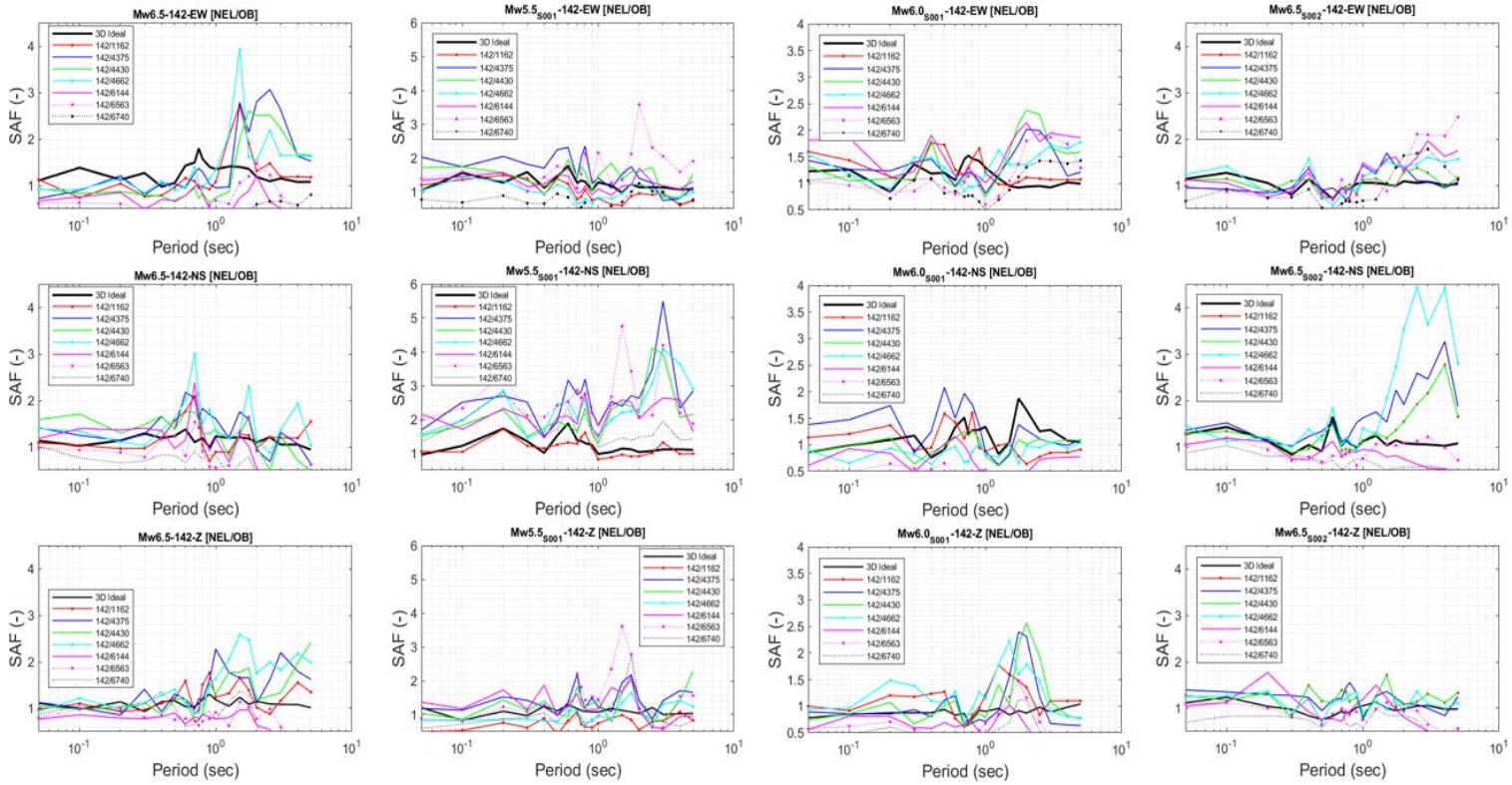

Receiver Point 420

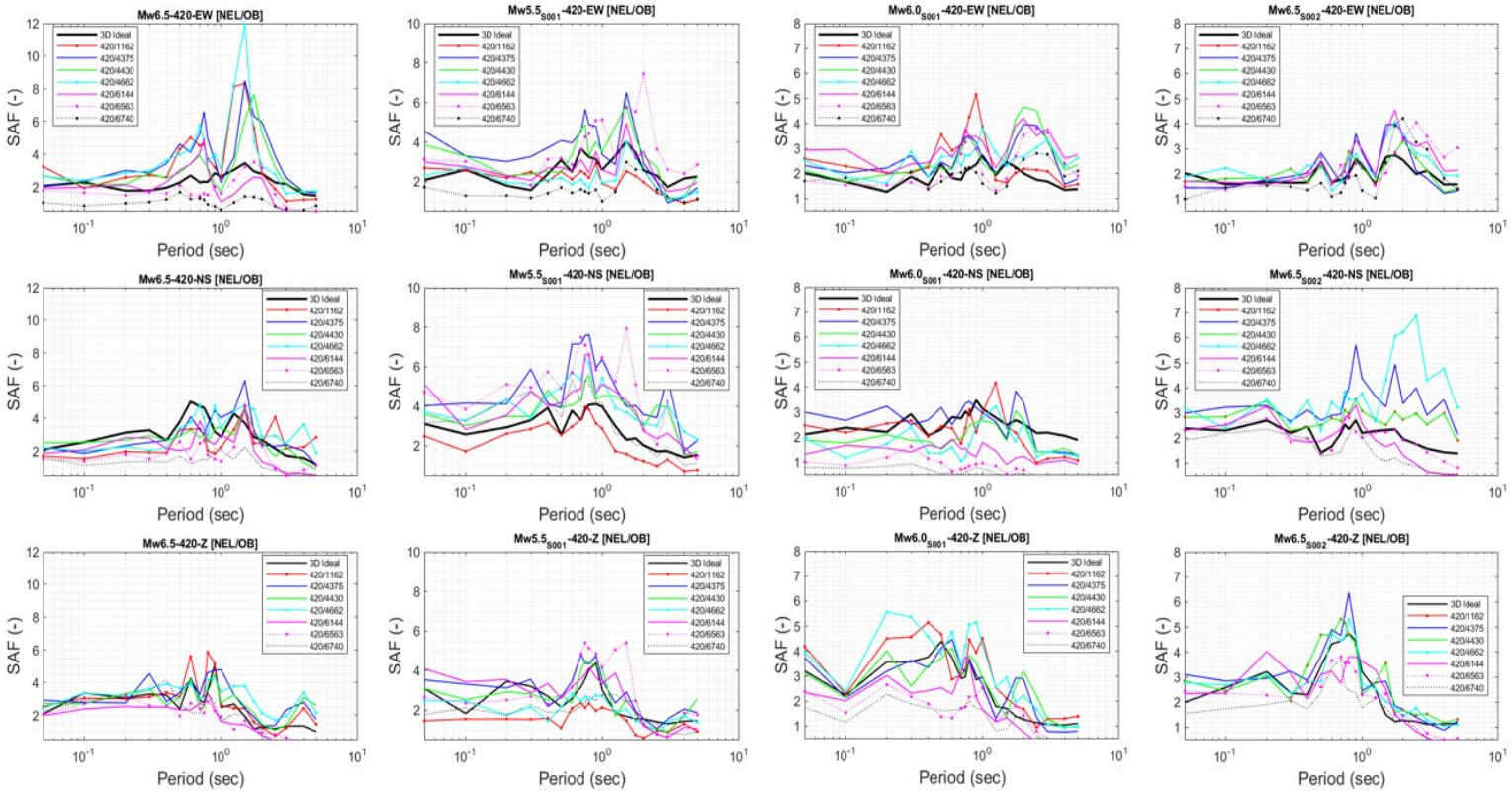

Receiver Point 1174

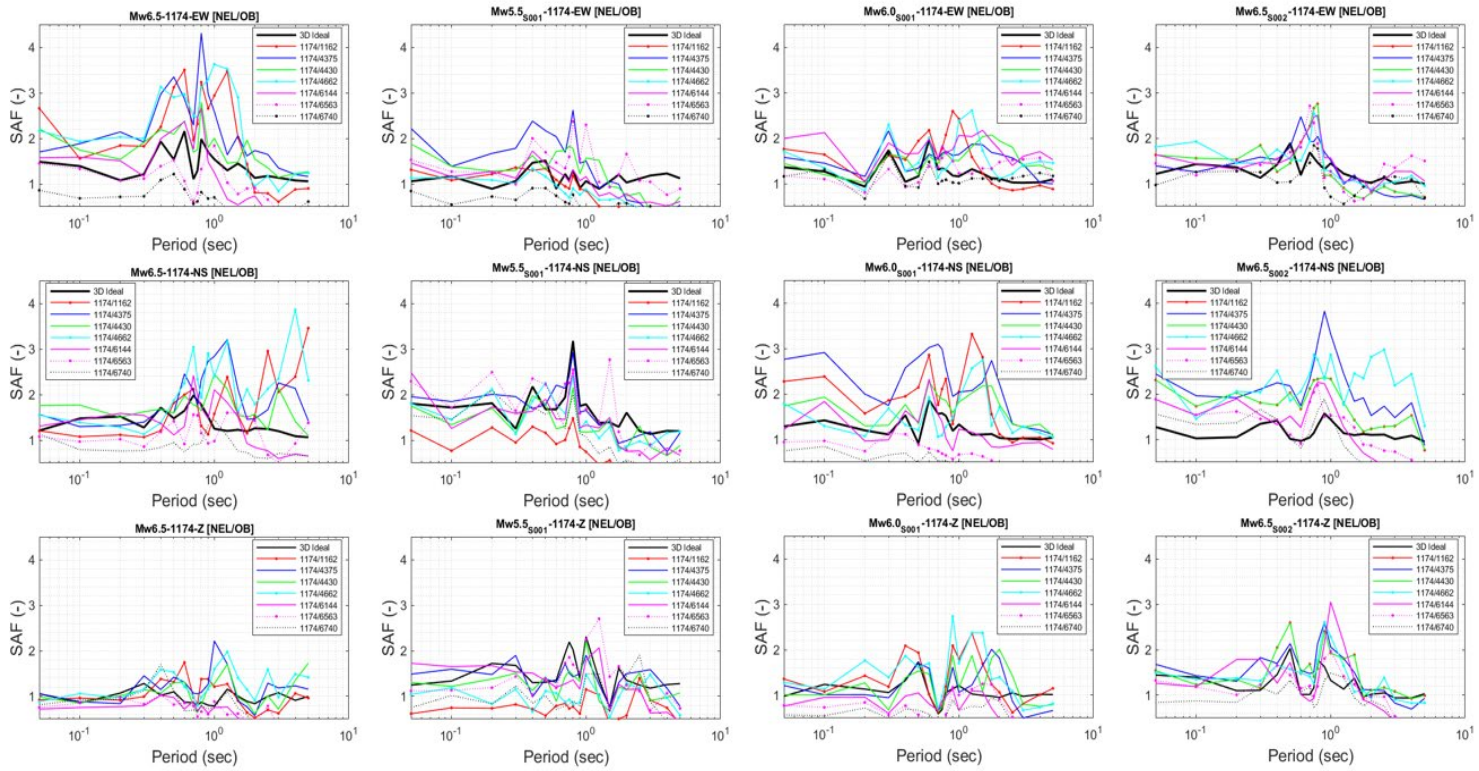

Receiver Point 153

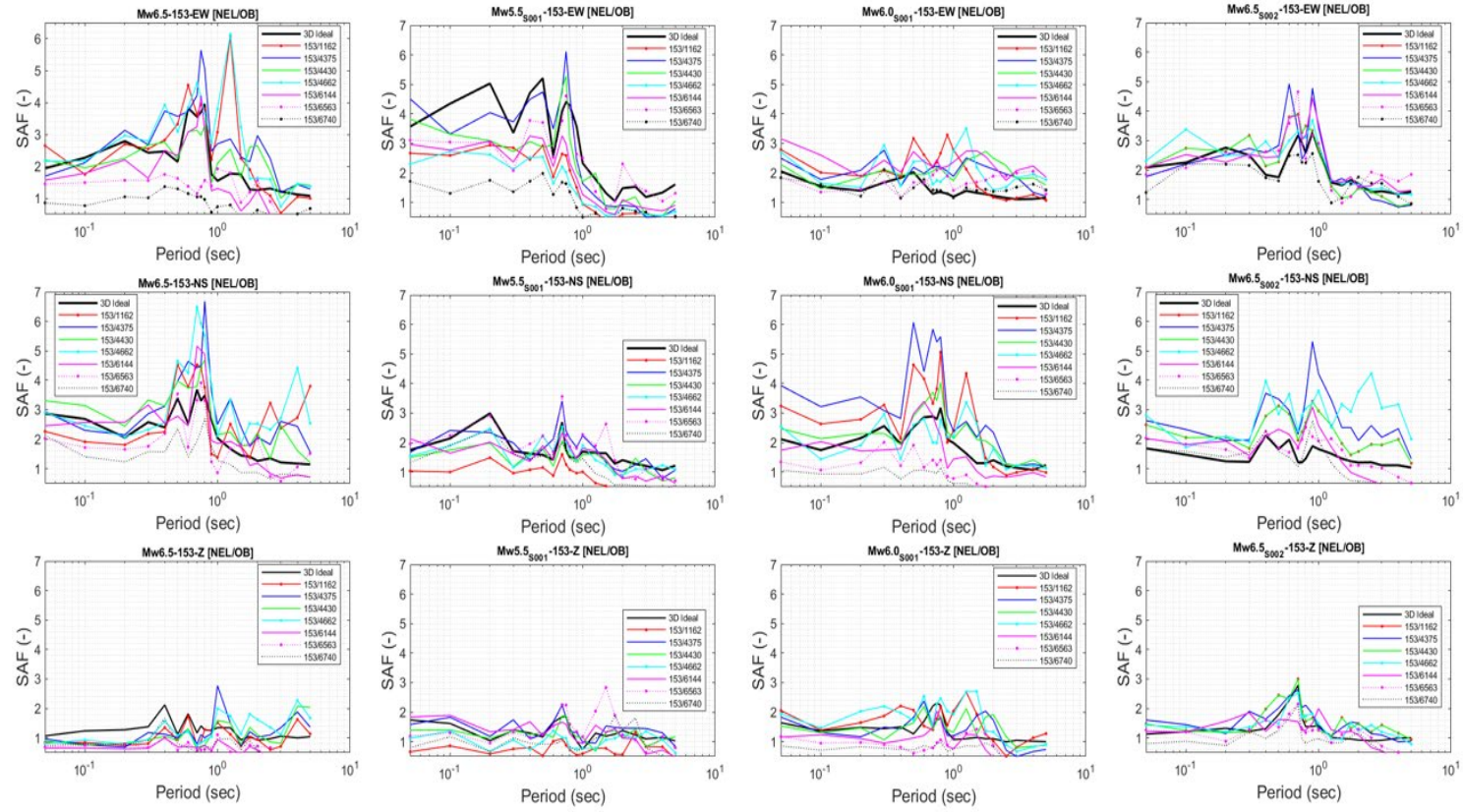

Receiver Point 1989

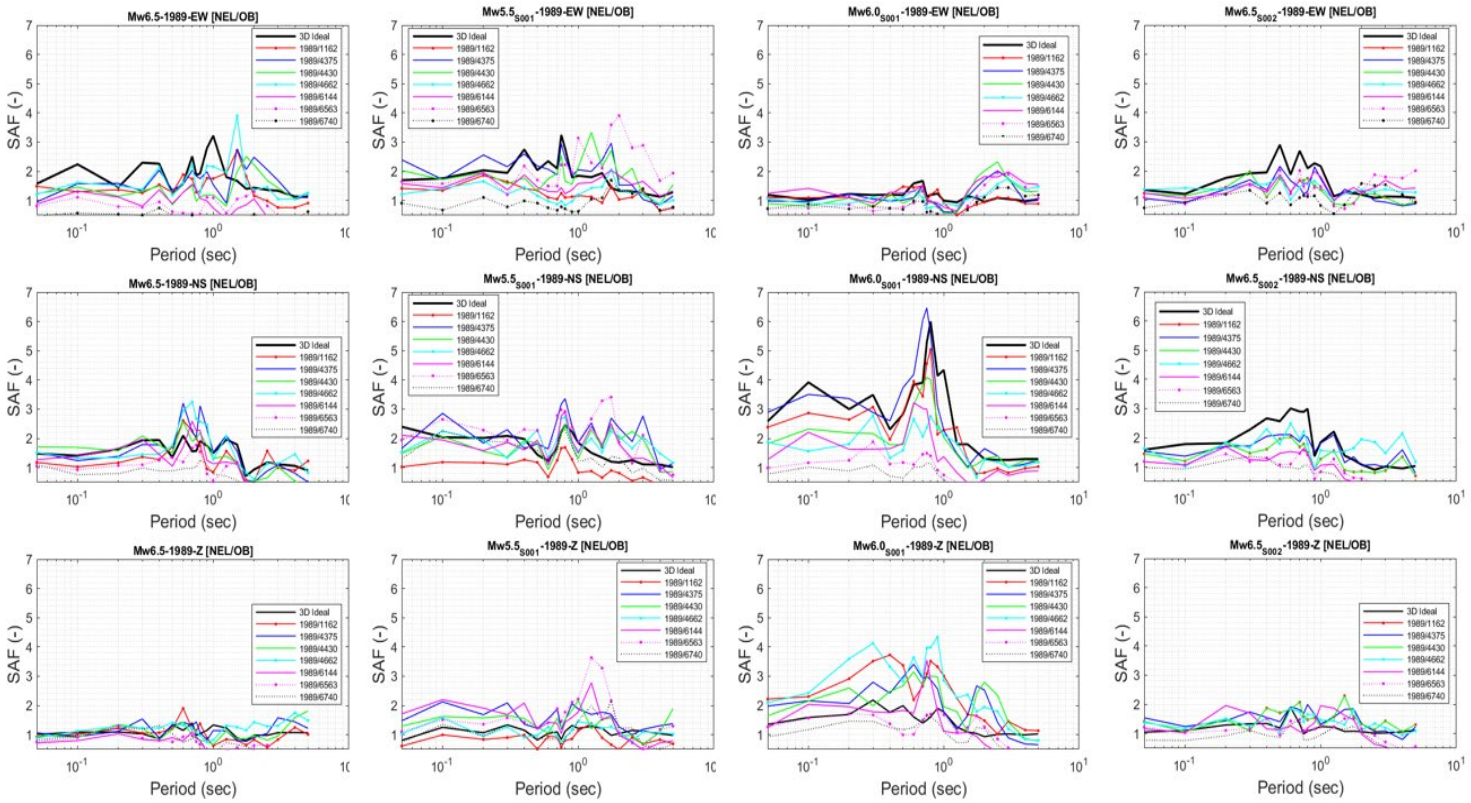

Receiver Point 3091

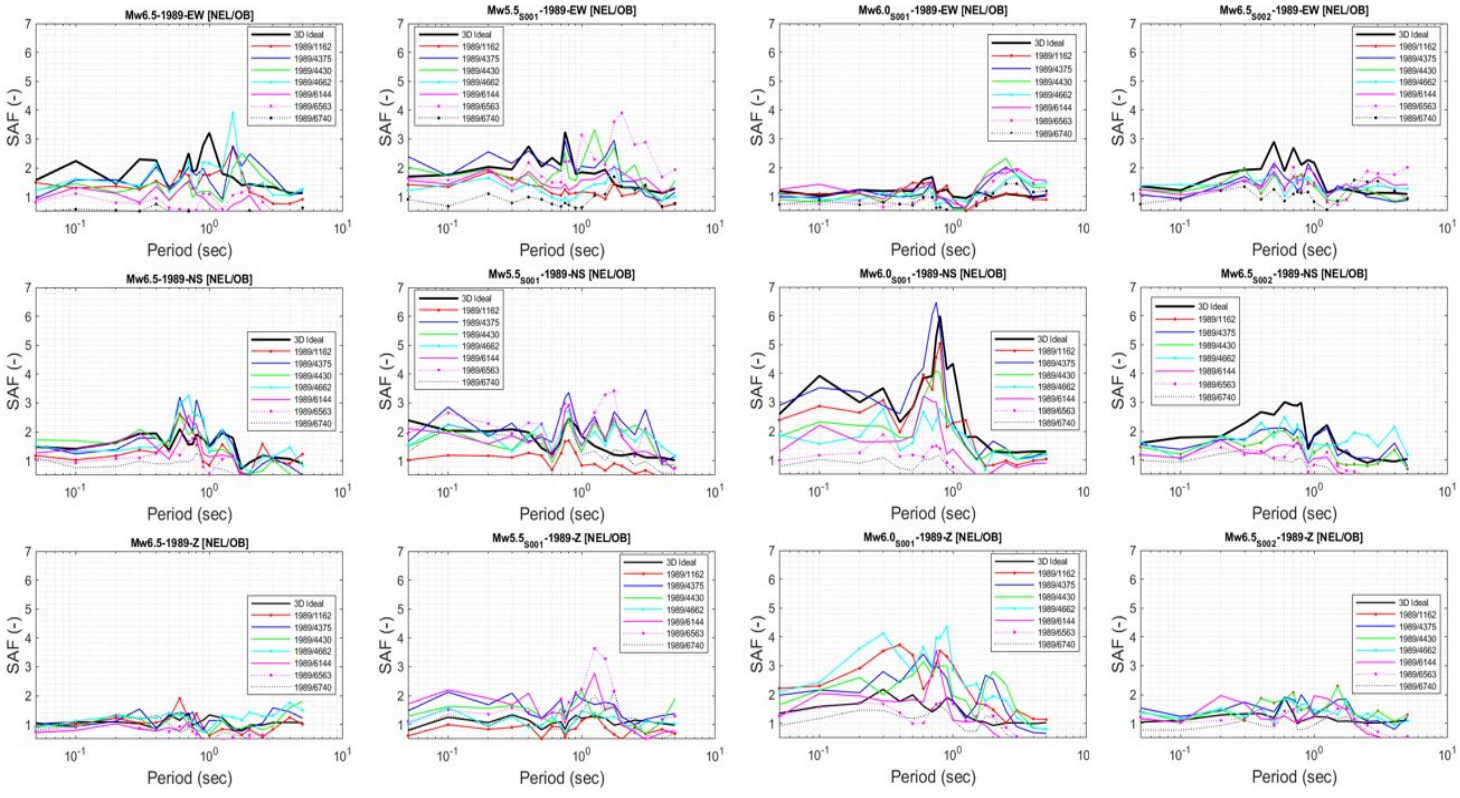

Receiver 412

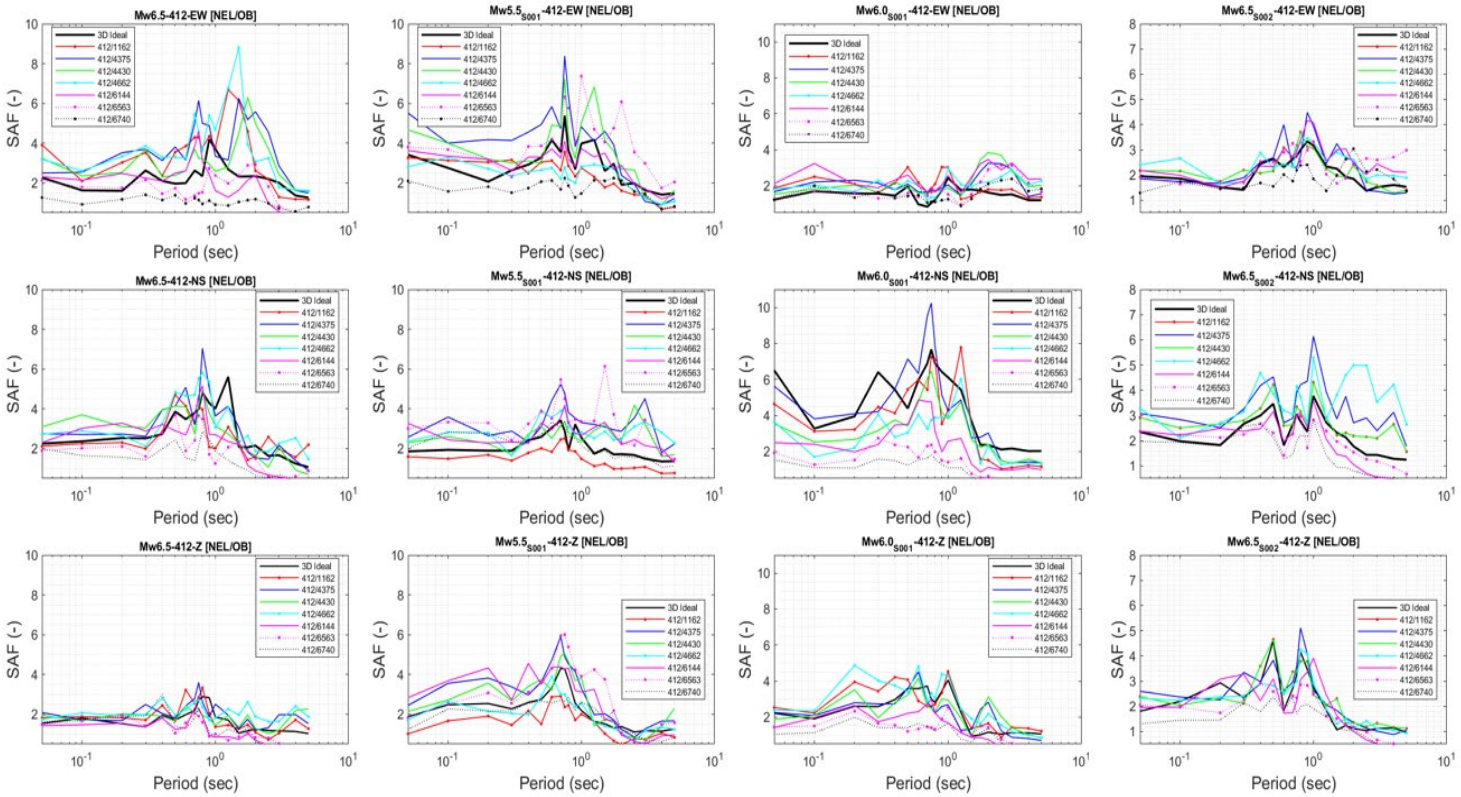

7. References

- Bindi, D., Luzi, L., Parolai, S., Giacomo, D. Di, & Monachesi, G. (2011). Site effects observed in alluvial basins: The case of Norcia (Central Italy). *Bulletin of Earthquake Engineering*, *9*(6), 1941–1959. https://doi.org/10.1007/s10518-011-9273-3
- Brando, G., Pagliaroli, A., Cocco, G., & Di Buccio, F. (2020). Site effects and damage scenarios: The case study of two historic centers following the 2016 Central Italy earthquake. *Engineering Geology*, *272*(August 2019), 105647. https://doi.org/10.1016/j.enggeo.2020.105647
- Civico, R., Pucci, S., Nappi, R., Azzaro, R., Villani, F., Pantosti, D., Cinti, F. R., Pizzimenti, L., Branca, S., Brunori, C. A., Caciagli, M., Cantarero, M., Cucci, L., D'Amico, S., De Beni, E., De Martini, P. M., Mariucci, M. T., Montone, P., Nave, R., … Venuti, A. (2019). Surface ruptures following the 26 December 2018, Mw 4.9, Mt. Etna earthquake, Sicily (Italy): EMERGEO Working Group (Etna 2018). *Journal of Maps*. https://doi.org/10.1080/17445647.2019.1683476
- Cybenko, G. (1989). Approximation by superpositions of a sigmoidal function. *Mathematics of Control, Signals, and Systems*. https://doi.org/10.1007/BF02551274
- Di Giulio, G., Ercoli, M., Vassallo, M., & Porreca, M. (2020). Investigation of the Norcia basin (Central Italy) through ambient vibration measurements and geological surveys. *Engineering Geology*, *267*(June 2019), 105501. https://doi.org/10.1016/j.enggeo.2020.105501
- Evangelista, L., del Gaudio, S., Smerzini, C., d'Onofrio, A., Festa, G., Iervolino, I., Landolfi, L., Paolucci, R., Santo, A., & Silvestri, F. (2017). Physics-based seismic input for engineering applications: a case study in the Aterno river valley, Central Italy. *Bulletin of Earthquake Engineering*, *15*(7), 2645–2671. https://doi.org/10.1007/s10518-017-0089-7
- Infantino, M., Paolucci, R., Smerzini, C., & Stupazzini, M. (2018). Study of the Spatial Correlation of Earthquake Ground Motion By Means of Physics-Based Numerical Scenarios. *16th European Conference on Earthquake Engineering, 16ECEE, June 18-21, Thessaloniki, Greek*, *June*, 12.
- Messina, P., Galadini, F., Galli, P., & Sposato, A. (2002). Quaternary basin evolution and present tectonic regime in the area of the 1997-1998 Umbria-Marche seismic sequence (Central Italy). *Geomorphology*. https://doi.org/10.1016/S0169-555X(01)00077-0
- Paolucci, R., Evangelista, L., Mazzieri, I., & Schiappapietra, E. (2016). The 3D

numerical simulation of near-source ground motion during the Marsica earthquake, central Italy, 100 years later. *Soil Dynamics and Earthquake Engineering*, *91*(September), 39–52. https://doi.org/10.1016/j.soildyn.2016.09.023

- Paolucci, Roberto, Gatti, F., Infantino, M., Smerzini, C., Özcebe, A. G., & Stupazzini, M. (2018). Broadband ground motions from 3D physics-based numerical simulations using artificial neural networks. *Bulletin of the Seismological Society of America*, *108*(3), 1272–1286. https://doi.org/10.1785/0120170293
- Paolucci, Roberto, Infantino, M., Mazzieri, I., Özcebe, A. G., Smerzini, C., & Stupazzini, M. (2018). 3D physics-based numerical simulations: Advantages and current limitations of a new frontier to earthquake ground motion prediction. The Istanbul case study. *Geotechnical, Geological and Earthquake Engineering*, *46*, 203–223. https://doi.org/10.1007/978-3-319-75741-4_8
- Pierantoni, P., Deiana, G., & Galdenzi, S. (2013). Stratigraphic and structural features of the sibillini mountains(Umbria- Marche Apennines, Italy). *Italian Journal of Geosciences*. https://doi.org/10.3301/IJG.2013.08
- Pizzi, A., Di Domenica, A., Gallovič, F., Luzi, L., and Puglia, R. (2017). Fault segmentation as constraint to the occurrence of the main shocks of the 2016 Central Italy seismic sequence. Tectonics, 36(11), 2370-2387.
- Smerzini, C. (2018). Spatial Variability of Near-Fault Earthquake Ground Motion From 3D Physics-Based Numerical Simulations. *16th European Conference on Earthquake Engineering, 16ECEE, June 18-21, Thessaloniki, Greek.*
- Smerzini, C., Galasso, C., Iervolino, I., & Paolucci, R. (2014). Ground motion record selection based on broadband spectral compatibility. *Earthquake Spectra*, *30*(4), 1427–1448. https://doi.org/10.1193/052312EQS197M
- Smerzini, C., Paolucci, R., & Stupazzini, M. (2011). Comparison of 3D, 2D and 1D numerical approaches to predict long period earthquake ground motion in the Gubbio plain, Central Italy. *Bulletin of Earthquake Engineering*, *9*(6), 2007–2029. https://doi.org/10.1007/s10518-011-9289-8.
- Data of Earthquake in Central Italy available at: http://terremoti.ingv.it/en
- SPEED : http://speed.mox.polimi.it/.